SYNTHESIS AND CHARACTERIZATION OF

COVALENTLY-LINKED DENDRIMER BIOCONJUGATES

AND THE NON-COVALENT SELF-ASSEMBLY

OF STREPTAVIDIN-BASED MEGAMERS

A Dissertation

by

MEGAN E. MCLEAN

Submitted to the Office of Graduate Studies of
Texas A&M University
in partial fulfillment of the requirements for the degree of

DOCTOR OF PHILOSOPHY

December 2004

Major Subject: Chemistry

SYNTHESIS AND CHARACTERIZATION OF

COVALENTLY-LINKED DENDRIMER BIOCONJUGATES

AND THE NON-COVALENT SELF-ASSEMBLY

OF STREPTAVIDIN-BASED MEGAMERS

A Dissertation

by

MEGAN E. MCLEAN

Submitted to the Office of Graduate Studies of
Texas A&M University
in partial fulfillment of the requirements for the degree of

DOCTOR OF PHILOSOPHY

Approved as to style and content by:

_____	_____
Eric E. Simanek	Gary A. Sulikowski
(Chair of Committee)	(Member)
_____	_____
Richard M. Crooks	Alan E. Pepper
(Member)	(Member)

_____
Emile A Schweikert
(Head of Department)

December 2004

Major Subject: Chemistry

ABSTRACT

Synthesis and Characterization of Covalently-Linked Dendrimer Bioconjugates and the

Non-Covalent Self-Assembly of Streptavidin-Based Megamers. (December 2004)

Megan E. McLean, B.S., State University of New York College at Fredonia

Chair of Advisory Committee: Dr. Eric E. Simanek

This work details the attachment of dendrimers to proteins, peptides and single stranded DNA (ssDNA). Dendrimers based on melamine satisfy many of the synthetic demands in the field of bioconjugate chemistry including: monodispersity, synthetic flexibility and scalability. The solution-phase syntheses of both ssDNA-dendrimer and peptide-dendrimer bioconjugates is described, and thorough characterization by matrix-assisted laser desorption ionization/ time-of-flight (MALDI-TOF) mass spectrometry, UV-vis spectroscopy, fluorescence spectroscopy, and polyacrylamide gel electrophoresis is discussed.

Non-covalent DNA-dendrimer complexes have been shown to facilitate antisense gene delivery, but are vulnerable to dissociation and subsequent enzymatic degradation within the cell. In an effort to prepare biocompatible antisense agents capable of effectively shielding ssDNA from intracellular nuclease digestion, disulfide-linked ssDNA-dendrimers were prepared and rigorously characterized to rule out the possibility of an electrostatic-based interaction.

Hybridization assays were performed to determine if the covalently-attached dendrimer affected the ability of the attached ssDNA strand to anneal with a

complementary sequence to form double-stranded DNA (dsDNA)-dendrimers. Results indicate that ssDNA-dendrimer conjugates readily anneal to complementary ssDNA strands either in solution or attached to gold surfaces. Nuclease digestions of conjugates in solution suggested that enzymatic manipulation of dsDNA-dendrimers is possible, offering promise for DNA-based computation and other fields of DNA-nanotechnology.

Much larger bioconjugates consisting of dendrimers, proteins and peptides were prepared with the goal of obtaining molecular weights sufficient for enhanced permeability and retention (EPR) in tumors. While the dendrimer provides the advantages of a purely synthetic route for drug delivery, the protein portion of the bioconjugate provides a monodisperse, macromolecular scaffold for the non-covalent self-assembly of the dendrimers. The strategy presented herein is based on the strong interaction between biotin and the 60 kD tetrameric protein streptavidin. Each monomer of streptavidin is capable of binding 1 biotin molecule, thus when biotin functionalized peptide-dendrimers are added to streptavidin they bind to form a cluster of dendrimers, or a megamer.

The biotinylated peptides that link the dendrimers to the streptavidin core provide a way to actively target specific cell types for drug delivery. Megamer formation through the addition of tetrameric streptavidin was successful as indicated by MALDI-TOF, UV-vis titration and gel electrophoresis assays.

To Mom and Dad:

Thank you for your extra dose of fight that I could not have gotten through graduate school without. More importantly, thank you for lovingly guiding me into the awareness and peace that comes with being grateful for what we have and counting our many blessings each and every day. It is this awareness that saw me through the toughest days.

ACKNOWLEDGEMENTS

I thank Dr. Eric Simanek, my mentor, who five years ago assured me that even a turtle can earn a Ph.D. as long as she has passion and determination. Thanks to my committee members: Dr. Gary Sulikowski, Dr. Richard Crooks, Dr. Alan Pepper, and former member and mentor Dr. Frank Raushel for their guidance and support. Much thanks to the entire Simanek group. The new grads: Dr. Mackay Steffensen (who could always make me laugh, yes even on a Monday) and Dr. Alona Umali (my sponsor and fellow July-sixer – thank you for sharing your home when I was in need of one). Current graduate students: Sergio Gonzalez (our source of musical entertainment and amusing stories), Susan Hatfield (my fellow MK partygoer), Michael Neerman (my fellow DMB fan), and Karlos Moreno (my fellow Aggie Catholic). Current postdocs: Dr. Emily Hollink (my favorite Canadian) and Dr. Hui Ting Chen (our spirited source of smiles and candy). Former group members: Dr. Wen Zhang (who made us all look lazy), Dr. Steve Bell (my Wisconsin crew comrade), Dr. Erick Acosta (the nicest guy I've ever knocked out in a boxing ring), and Kiran Bhattarai (a pal through my rough NY to TX transition). I am also grateful to a couple of other 5th floorers: Eman Ghanem for her friendship and frequent coffee invites, and Brian Reedy for teaching me the importance of viewing all situations with a *carpe diem* attitude. I feel so blessed to have met and learned from such extraordinary people throughout my graduate school years. I am forever indebted to my ultimate inspiration and unending source of love, without who my last year of graduate school might very well have caused me to go bald (as a result of ripping out my hair). September cannot come soon enough Shane, I love you.

TABLE OF CONTENTS

LIST OF TABLES

LIST OF FIGURES

CHAPTER I

INTRODUCTION

BACKGROUND

Dendrimer background. The first known dendrimers, initially called *cascade molecules* were reported by Vögtle and coworkers in 1978.[1] Since then, the prevalence of dendrimers in the literature has reached over 4,000 research articles and reviews (up from only a small handful in 1996), and the impact they will make in nanobiotechnology and pharmaceutics is just beginning to be realized. Dendritic molecules have made significant contributions in many fields including but not limited to: drug delivery,[2-7] protein mimicry,[8,9] gene transfection,[10-13] materials and coatings,[14-20] sensors and detectors,[21-25] patterning and templating,[26-29] adhesives,[30,31] image contrast agents,[32-34] optics and optical films,[35-38] quantum dots and nano dots,[39-42] catalysis,[43-47] and separations.[48-50]

Structurally, dendrimers are globular synthetic macromolecules that branch out from a central core. They are synthesized in layers, in a stepwise fashion, to yield a monodisperse (or nearly monodisperse, depending on the chemical nature of the peripheral functional groups) polymer with a high degree of symmetry and a well defined size. Dendrimers consist of three structural units: (1) the core, (2) branching units and (3) peripheral groups. There are two general synthetic routes toward dendrimers: (A) divergent and (B) convergent. As shown in Scheme 1-1, either method allows for some level of control over the number and type of functional groups along the periphery, or

outermost layer, such that the peripheral functional groups may be chemically distinct from the interior groups.

Scheme 1-1

A

B

= core

= branching group

= peripheral group
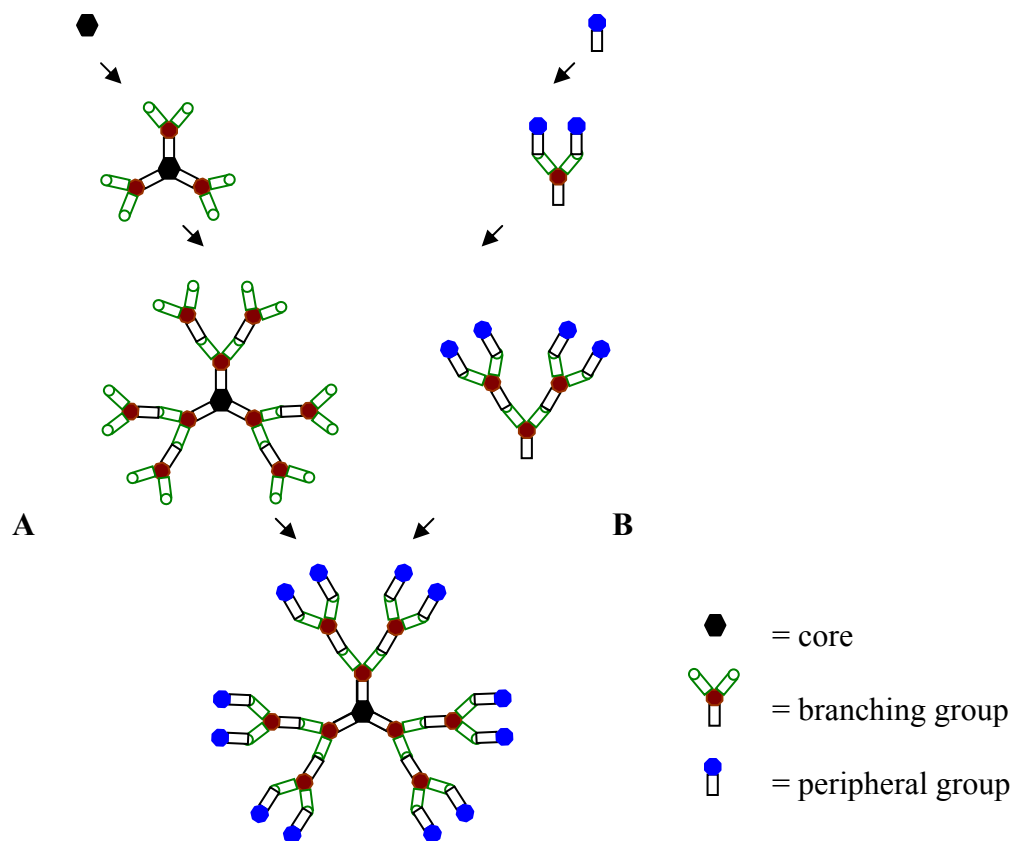
Starburst dendrimers, introduced by Tomalia,[51,52] are prepared using a divergent synthetic strategy. Scheme 1-2 shows the layer-by-layer branching pattern of a starburst polyamidoamine (PAMAM) dendrimer. Each layer (or generation) of a dendrimer is noted by GX, where X is the number of chemical layers, or branching groups, counting out from the core, which in this case is ethylenediamine.

Scheme 1-2
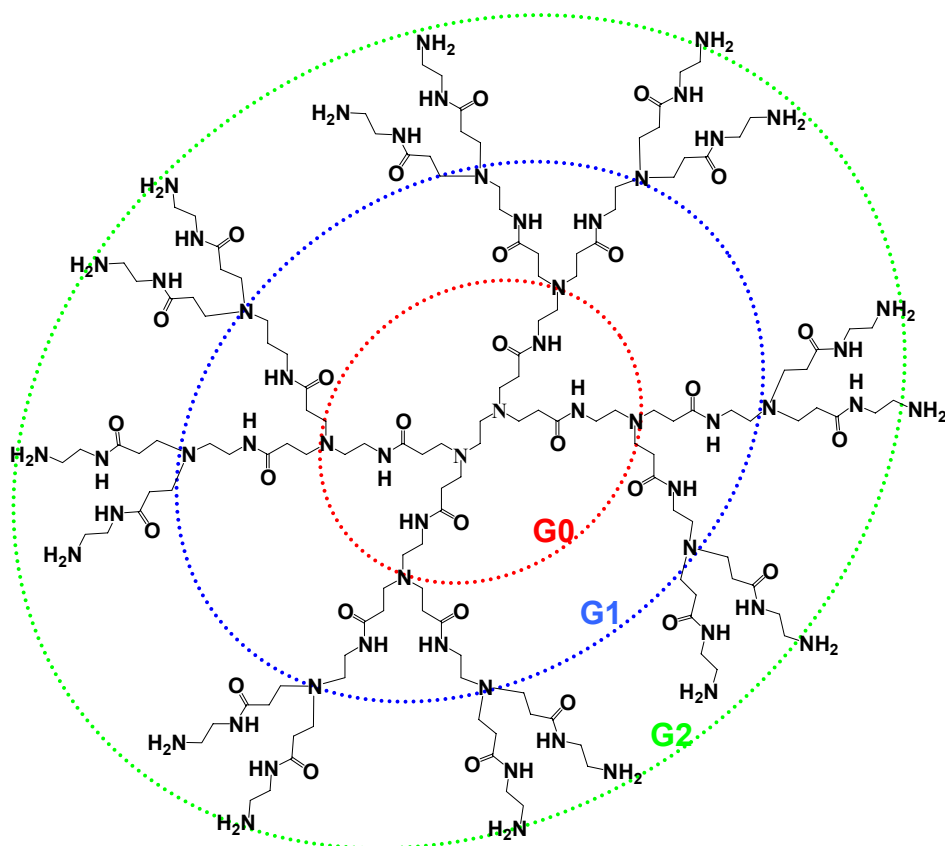
Benefits of convergent synthesis. Fréchet and coworkers[53] introduced the convergent approach to dendrimer synthesis. The convergent approach, though less popular in industry, allows for greater control over the regiospecific display of the peripheral groups. Due to the differential reactivity of the core molecule, asymmetrical dendrimers are more readily prepared by using a convergent approach, than when building from the inside out, or divergently. The convergent synthesis of a dendrimer is compared to that of a divergent approach in Scheme 1-1. In the convergent approach, a multifunctional core molecule is reacted with peripheral functional groups or *dendrons* (the term *dendron* is loosely designated for an incomplete dendrimer). The product is purified if necessary, and a new core molecule is used to link together the newly formed intermediate dendrons. The process is repeated until the desired target has been synthesized. Depending on the valency of the core molecule, a dendron could structurally comprise of half of a dendrimer, one forth, and so on.

The number of reactions per growth step is constant in the convergent approach, whereas in the divergent approach, the number of reactions per growth step increases with the increasing number of peripheral groups per generation. It is also generally easier to separate out the intermediate byproducts at each growth step when using the convergent approach. To illustrate this generalization, one possible byproduct arising from an incomplete reaction during (A) divergent synthesis and (B) convergent synthesis of a dendrimer are shown in Scheme 1-3. Given the simplest scenario where all of the peripheral groups are the same, it is easier to achieve chromatographic separation solely based on the retention factor of the desired intermediate compared to that of the byproduct in (B) using the convergent approach than in (A) using the divergent approach.

When some peripheral groups are different creating a heterogeneous outermost layer, it becomes increasingly difficult to separate out the many possible side products formed in a divergent approach.

Scheme 1-3

A   B
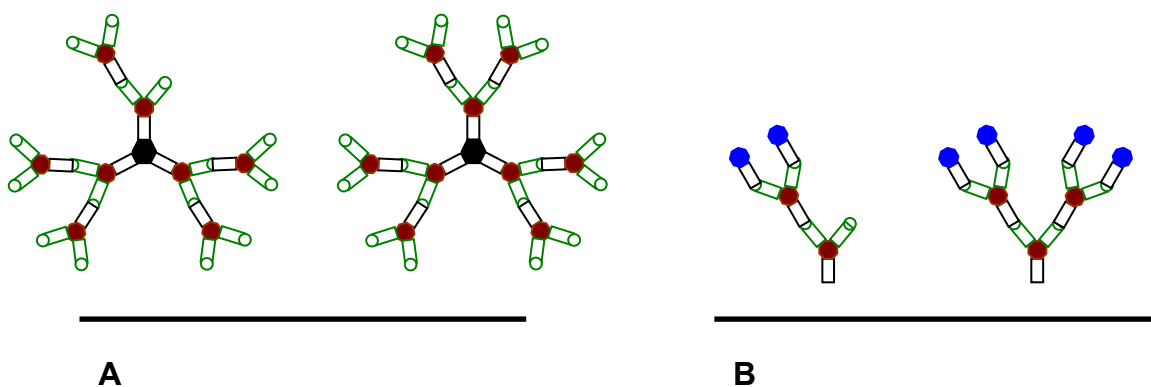
Dendrimers based on melamine. Dendrimers based on melamine are ideally suited for the convergent approach since the core molecule, triazine trichloride (cyanuric chloride), offers differential control of nucleophilic aromatic substitution at each of the three reactive sites.[54] The phrase "dendrimers based on melamine" is derived from the melamine core that is formed when all three chlorides of the triazine are displaced with amine groups. Scheme 1-4 demonstrates how three chemically unique amines may be added to cyanuric chloride. Differential reactivity is manipulated in two ways, temperature and nucleophilicity. The differential reactivity of cyanuric chloride with various amines has been demonstrated by Steffensen and Simanek.[55]

Scheme 1-4
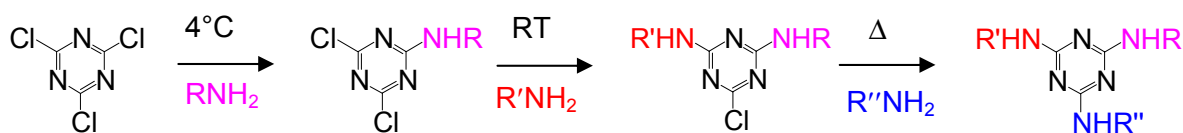
Synthetically, the advantage of using dendrimers based on melamine lies in the ability to diversify the chemical functionality not only from one generation to the next, but also site-specifically within the layers without having to rely on elaborate and strategic protecting group manipulations. The temperature-controlled addition of primary or secondary amines to cyanuric chloride allows for the attachment of three chemically unique substituents around the triazine core. For primary amines, the first addition occurs at 4 °C on ice, the second adduct forms at room temperature, and the third addition requires a degree of heat dependent upon the reactivity of the amine (usually ~ 70º C). Diamines permit branch elongation and stepwise growth through subsequent reactions with cyanuric chloride. Precautions must be taken, however, to avoid the dimerization of two core molecules via the diamine. The addition of diamines with differential reactivity toward substitution on the triazine ring allows for orthogonal assembly and prevents dimerization events. Scheme 1-5 illustrates how the reactivity of a benzylic amine relative to aniline (benzyl amine >> aniline) can be utilized in the convergent approach to prevent the formation of dendrimeric byproducts wherein both amines on the newly introduced diamine react with 2 equivalents (eq.) of monochloride triazine, forming a dimer. This synthetic route also demonstrates how both temperature and amine reactivity

can be used to place different R groups along the periphery in a regiospecific manner without the use of protecting group strategies.

Scheme 1-5
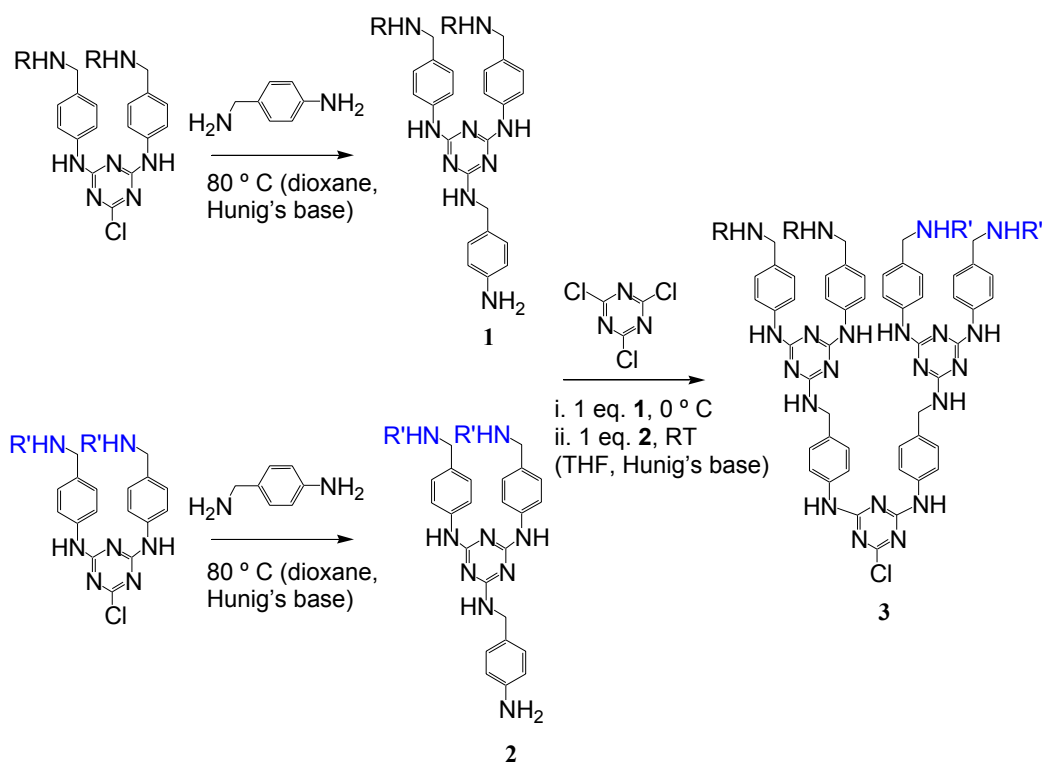
Polymeric drug delivery.   In the mid-1970s, just prior to Vögtle's first dendrimeric structures, Ringsdorf[56] introduced the concept (that was unrelated at the time) of a macromolecular prodrug. Ringsdorf proposed that a water-soluble polymer could be attached to a drug through a selected linker molecule as shown in Scheme 1-6. The polymer was used to encapsulate the drug, artificially enhance the molecular weight

and restrict cellular uptake to an endocytosis-mediated pathway. Since macromolecules are unable to diffuse passively into cells, they are instead engulfed as membrane-encircled sacs (vesicles). The increased size of the drug-polymer conjugate decreases clearance through the kidneys, so the polymer-drug conjugate should circulate longer. Ringsdorf hypothesized that with the appropriate biodegradable linker and/or a cell-specific targeting group, it would be possible to deliver the drug directly to the targeted site avoiding the toxic side-effects associated with many drugs.

Over the last 25 years many advances in the field of responsive polymers have been reported,[57-59] and polymers that respond to: magnetic, electric, or ultrasound stimuli, temperature, pH, ionic strength, or even glucose levels have been reported.[60] Despite significant advances in time-controlled polymeric drug release, the synthetic challenges involved in engineering polymers with a high therapeutic index, low toxicity, and low immunogenicity have proven difficult to overcome.[61]

Scheme 1-6
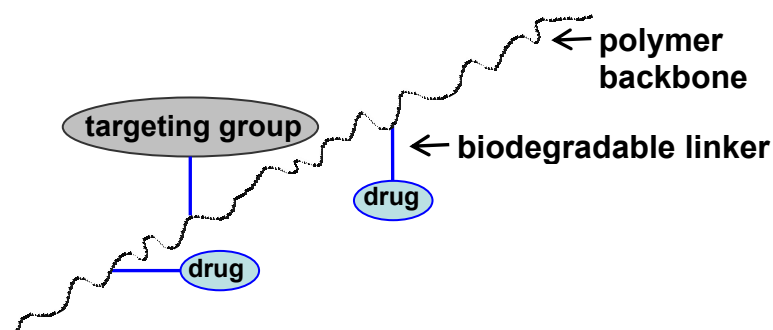
Dendrimers are ideally suited to satisfy Ringsdorf's idea. Indeed, the synthetic focus in polymeric therapeutics has broadened from using linear polymers to control drug release and prolong the drug's lifetime through lengthened circulation to include three other important properties: (1) monodispersity, (2) size, and (3) presentation of several different reactive sites for the conjugation of targeting and transport groups.

Importance of monodispersity. Currently, all polymeric drug delivery systems in clinical trials and on the market are polydisperse systems.[61] A polydisperse polymer system is one in which there is a distribution of molecular weights present. A monodisperse system would have only one molecular weight present. Polydispersity can be defined as the ratio of weight average molecular weight (M_w) to number average molecular weight (M_n), or M_w/M_n, where $M_w/M_n \geq 1$. M_n is determined by counting the number of species with a particular molecular weight (MW) and multiplying by the MW. The values are then summed and divided by the total number of polymer species present in the sample. M_w can be obtained by recording the weights of the species present in the sample, summing these weights, and dividing by the total weight of the sample. Low polydispersity of a drug carrier system allows for more predictable pharmacokinetic properties since there are fewer versions of the molecule rather than a range, and their fates can be more easily tracked *in vivo*. As early as 1976, Breslow pointed out that each distinct molecular weight in a polymeric range produced a unique biological response.[62] Although recent advances in atom transfer radical polymerization techniques have allowed for *nearly* monodisperse product formation,[63] enzymatic breakdown or other biologically-mediated polymer degradation can result in the release of various molecular weight polymers with potential for producing an immunological response.[64] Thus the

synthesis of a monodisperse polymer for use in drug delivery, while essential for evaluation of drug metabolism and pharmacokinetics (DMPK), may not necessarily afford biocompatibility. The polymer and subsequent degradation products must also be biologically inert. Even with well-accepted polymer-drug delivery systems such as polyethylene glycol (PEG)-grafted liposome delivery agents, immunotoxicity and fatalities through anaphylactic shock have been reported.[65] From a synthetic standpoint, another benefit of monodispersity is that the products may be more rigorously characterized. Current separation techniques do not allow for the isolation of a monodisperse polymers from standard polymerization protocols.

Importance of size. The size of the drug carrier is an important factor when considering the delivery of therapeutics for the treatment of cancer. Expression and secretion of Vascular Endothelial Growth Factor-A (VEGF-A) by tumor cells induces leakiness and dilation of tumor blood vessels resulting in a phenomenon known as enhanced permeability and retention, or the EPR effect.[66] As a result, tumor tissue tends to take up larger molecules at a faster rate than normal tissue, and due to poor lymphatic drainage, molecules that are taken up are also retained. Scheme 1-7 represents how the EPR effect works. The leaky vasculature of blood vessels in cancerous tissue causes the polymer-drug conjugates to seep out into the tumor tissue. Poor lymphatic drainage traps the polymer-drugs within the tumor tissue while the intact vasculature of blood vessels found in healthy tissue precludes the conjugates from seeping into non-cancerous tissue. Molecules that are at least 40 kDa demonstrate enhanced permeability and retention in tumors. Various polymeric drug delivery systems have been designed that take advantage of the hyperpermeable vasculature of solid tumors.[67]

Scheme 1-7
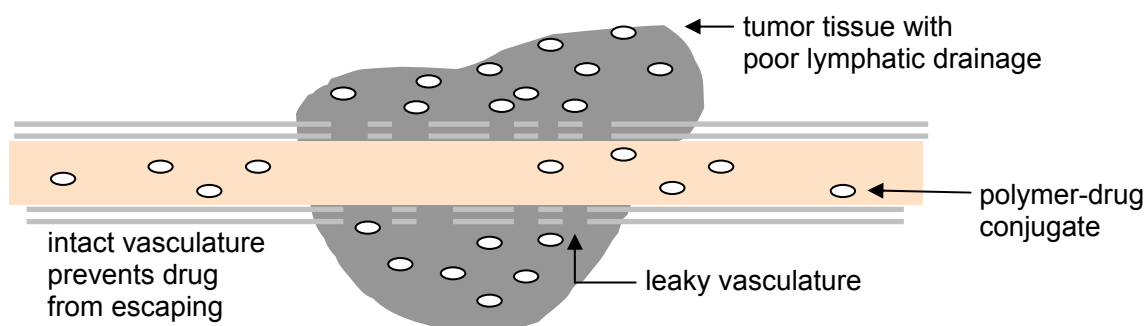
Importance of targeting and transport groups. Cancer cells can be differentiated from healthy cells by the receptors that are displayed on the periphery. For example, tumors are known to overexpress receptors for various growth hormones, lipids, and vitamins, many of which bind to specific ligands. Folate has been used to target the overexpressed folate receptor on tumor cells, for example.[68] Roughly 30% of cancerous cells including ovarian, kidney, most brain, some types of lung, and many breast cancer cells overexpress folate receptors, but most colon cancers and prostate cancers do not. Thus the need for a synthetically flexible drug carrier is clear, as there will never be one magic bullet for all cancers. Most drugs are selective for a particular signaling pathway that may or may not predominate in all cancer types at all stages of cancer development. Thus, there is an emerging interest in combination drug therapy to target several different proteins in a particular signaling pathway, and/or aim for different cell types in cancer development as a way to produce more effective anti-cancer agents.[69] This strategy provokes interest in expanding upon Ringsdorf's model by adding several different types of targeting or drug agents on a single macromolecular, monodisperse carrier.

Dendrimer-drug delivery. Dendrimers represent an interesting solution to the collective challenges of monodispersity, size, and specific targeting ability, especially since *in vivo* studies suggest they are relatively non-toxic and demonstrate low immunogenicity.[70] Most current dendrimer-drug conjugates focus on host-guest interactions of the drug which is encapsulated within the gaps on the interior of the dendrimer. The micellar character of dendrimers with amphiphilic moieties permit entrapment of drugs without the instability of traditional micelles which fall apart at concentrations below the critical micellar concentration (cmc).[71] Hawker *et al.*[72] reported the solubilization of pyrene in water using poly(aryl ether) dendrimers with carboxylic acid peripheral groups, and Liu *et al.* used poly(ethylene glycol) (PEG) coated dendrimers with a hydrophobic core to solubilize pyrene.[73] Meijer and coworkers presented the "dendritic box" in 1994[74] and later reported the shape selective release of the entrapped guests.[75] Examples of covalently linked dendrimer-drugs conjugates and bioconjugates, however, are increasingly popular. Scheme 1-8 compares the "dendritic box" or micellar strategy of drug delivery to the covalent strategy wherein drugs are covalently attached to the surface groups of the dendrimer.[76] Scheme 1-8 (A) shows entrapment of drug molecules within the interior gaps, and (B) shows covalent attachment of drug molecules to the periphery.

Scheme 1-8

A   B
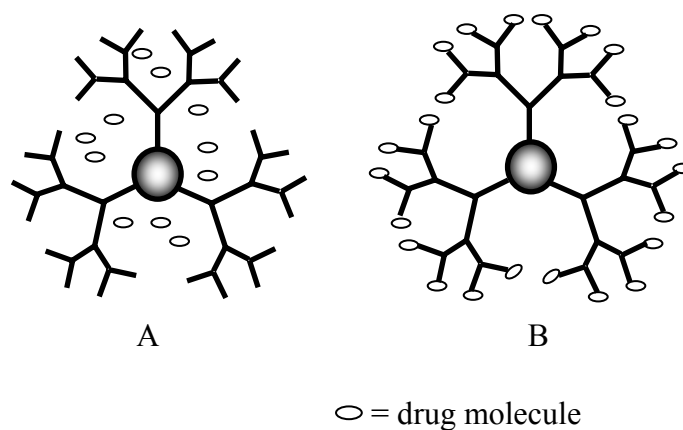
⬭ = drug molecule

Fréchet and coworkers proposed a model for dendrimer-mediated drug delivery similar to the one shown in Scheme 1-9. Ideally, the dendrimer would have solubilizing groups attached to the majority of the surface with several drug molecules and a targeting agent such as an antibody or antigen-specific peptide.

Scheme 1-9

⬡ = solubilizing agent

▼ = targeting agent

◢ = drug

— = cleavable linker
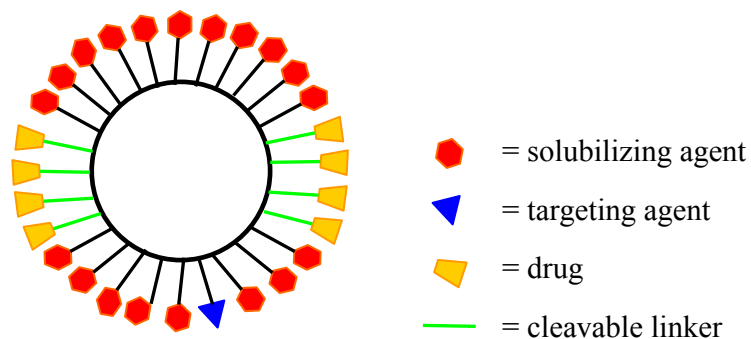
The synthesis required for the preparation of dendrimers that are large enough to demonstrate EPR in tumors still represents a significant burden. Appending polyethylene glycol (PEG) chains to increase the size of smaller dendrimers represents a covalent solution to this burden. Since PEG chains are polydisperse, however, any clinical and/or synthetic benefits that may be reaped from using a monodisperse drug delivery agent could be lost by adding PEG chains.

DNA-dendrimer bioconjugates. Modern molecular biology techniques allow us to both program intreractions between DNA strands according to Watson-Crick base-pair complementarity and manipulate DNA using a number of different sequence specific enzymes. These techniques have brought oligonucleotides to the forefront of nanotechnology.[77] DNA has been used to construct: templates for computation,[78,79] self-assembled two-dimensional crystals[80,81] and three dimensional objects,[82] nano-devices,[83,84] nano-motors,[85-87] biosensors[88] and electrical circuits.[89,90] Dendritic DNA nanostructures have been constructed to expand the capabilities of DNA nanotechnology through polyvalent oligonucleotide display.[91] The use of DNA constructs in the aforementioned DNA-machines, DNA-computing, antisense therapy, and biosensors has fueled intense research into suitable methods for immobilizing DNA on surfaces and preparing soluble DNA-nanoparticle assemblies. Multiple ssDNA oligonucleotides have been attached to soluble organic polymers and gold nanoparticles, but methods for the covalent attachment of individual ssDNA oligonucleotides to soluble nanoparticles are surprisingly rare.[92] Dendrimers based on melamine provide a tractable scaffold for controlled covalent functionalization of dendrimers with ssDNA.

Disulfide-linked DNA-dendrimer conjugates, introduced in Chapter II, establish an inexpensive, chemically flexible DNA-dendrimer synthetic strategy based on the temperature controlled reactivity of cyanuric chloride as shown in Schemes 1-2 and 1-3. An unparalleled level of synthetic diversity exists with these systems in which some specified number of unique oligonucleotide sequences may be covalently and site-specifically linked to various chemically unique dendrimers. Control over the chemoselective addition and cleavage of application-specific chemical handles like fluorophores or polypeptides to and from the dendrimer may be further accomplished through strategic protecting group manipulations. This work presents the first example of a strategy that simultaneously offers a high degree of control over charge, size, solubility, interior composition and peripheral attachment chemistry.

Focusing on biosensors and diagnostics, methods for the rapid and accurate detection of biological targets (in the identification of biological warfare agents, for example) are in high demand. Previous signal enhancement methods for ssDNA detection have relied on expensive labels, radiological tags, or secondary signal enhancement such as rolling circle amplification. Nanoparticle-based probes for solution-phase and surface array ssDNA detection have made progress in this field, but usually require gold surfaces or self-assembled monolayers as the support.

Of particular interest is the ability of cationic dendrimers to charge neutralize anionic DNA, allowing for cellular uptake for gene therapy.[93] Covalent, reversible DNA-dendrimer linkages such as disulfides could prove to shelter the antisense strand from intracellular enzymatic degradation without compromising biocompatability. A general representation of how antisense gene therapy works to prevent the biological synthesis of

disease-related proteins is shown in Scheme 1-10. Typically the antisense agent binds to the messenger RNA (mRNA) preventing it from associating with the ribosome during translation thereby halting the biosynthesis of the deleterious protein. Other mechanisms of gene therapy exist, for example in the formation of a triple helix prior to transcription preventing formation of the corresponding mRNA strand. Regardless of the exact mechanism of action, however, all antisense delivery agents must be able to transfer the therapeutic DNA strand (or antisense drug) across the cell membrane and protect the attached oligonucleotide from enzymatic degradation within the cell. When targeting the disease-related gene at the transcriptional level, the agent must also afford passage through the nuclear membrane and stability within the nucleus.

Scheme 1-10
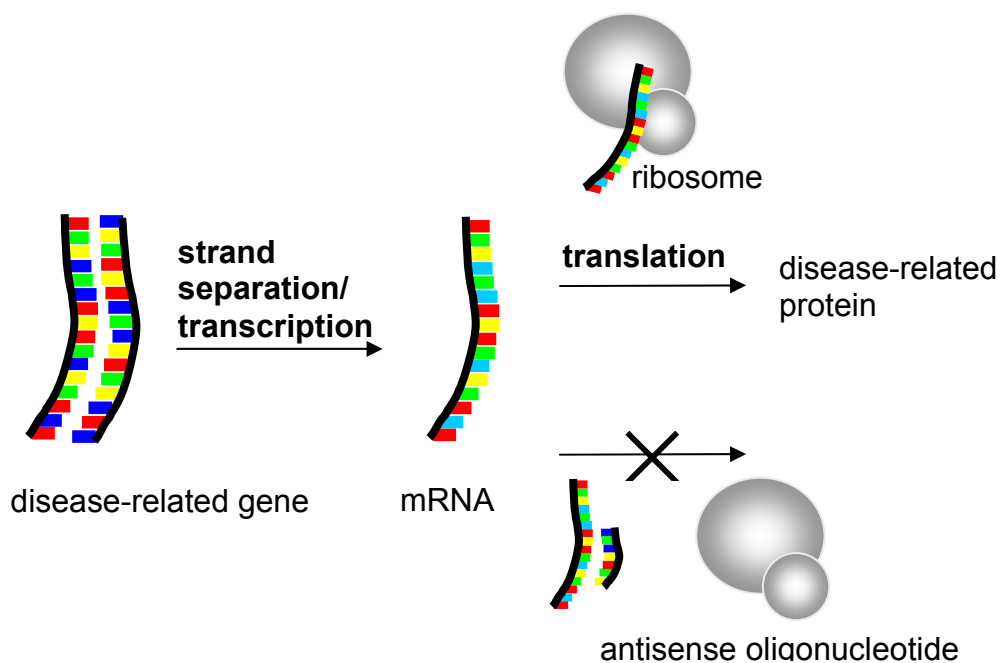
Plasmid DNA is too large and negatively charged to penetrate the cell membrane in naked form,[94] and internalized plasmid DNA is quickly degraded by intracellular enzymes.[95,96] Symmetrical, polycationic dendrimers such as polyamidoamine (PAMAM) dendrimers have been extensively studied for their ability to transport therapeutic DNA across biological membranes.[97] The ability of "polyplexes" or electrostatically-linked polycation-DNA conjugates to dissociate, however, could be one explanation for their limited usefulness in antisense gene delivery.

Peptide-dendrimer bioconjugates. A review of peptide dendrimers, written by Sadler and Tam,[98] summarizes several proposed uses for peptide-dendrimer bioconjugates and discusses the three general classes: (1) grafted peptide dendrimers with unnatural amino acid-based or organic-based cores and peptide or protein-based surface functional groups, (2) branching polyamino acids (usually lysine) with terminal amino acids acting as surface groups, and (3) amino acid branching units with surface peptidyl chains. The most common example of the last type of peptide dendrimer is the multiple antigen peptide (MAP) which has been used extensively to stimulate an immune response or probe antigen-antibody interactions.

The primary reasons for creating peptide-dendrimer bioconjugates are for drug delivery and biomedical applications such as MRI contrasting agents.[25] While peptides can act as therapeutic agents in their own right, they may also be used to target specific cell types[99,100] or aid in transport through the cell membrane. Wender and coworkers have determined the most efficient peptide sequences for use as cell penetrating carriers to attach cargo for intracellular delivery. Several researchers have since incorporated the arginine-rich sequence referred to as "TAT" (transactivator of transcription) into their

drug delivery vehicles. Protein transduction domains like TAT have been either genetically or chemically linked to proteins, antibodies, nucleic acids, liposomes, nanoparticles and small molecules to affect their transfer into cells. The TAT peptide is a protein transduction domain from HIV-1 that aids in the translocation of viral genetic material across the cell membrane. Although the mechanism of this transport remains unknown, the portion of the TAT protein required for translocation consists of residues 49-57 (RKKRRQRRR). This highly basic domain facilitates cell surface recognition and protects the transferred material from lysosomal degradation. TAT has also been used to carry attached cargo into the nucleus.

Biotin serves as a natural ligand for the tetrameric, 60 kDa protein streptavidin with a dissociation constant of 10^{-15} M. Upon addition of streptavidin to a biotinylated macromolecular drug delivery agent, each streptavidin monomer would theoretically bind one biotin such that four biotinylated molecules would self assemble around each streptavidin tetramer. The additional bulk provided by the streptavidin would increase the molecular weight of the drug carrier system into the required size range to observe an EPR effect in tumor tissue. Since proteins are in essence monodisperse polymers, the resulting bioconjugates formed through the highly specific and robust biotin-streptavidin interaction would provide a promising route toward anti-cancer drug delivery.

Supramolecular dendrimers and megamers. Naturally existing biological macromolecules often provide inspiration for synthetic supramolecular architectures. Dendrimers are especially useful as building blocks for functional materials and as mimics of globular proteins.[101,102] Percec and coworkers prepared insulated, self-assembled electrical wires resembling the DNA double helix where electrically

conducting small molecules take the place of the base pairs, and dendrimers take the place of the sugar-phosphate backbone.[103] Dendrimers have been used as cages to produce coenzyme B12 mimics[104] and as capping agents to produce spatially encumbered models of non-heme iron proteins.[9] Balzani and coworkers have used coordination chemistry to produce complex redox-active, luminescent, and fluorescent architectures using dendrimers.[105,106] Dendritic building blocks that assemble due to hydrogen-bonding interaction have been described by Zimmerman and coworkers.[107] Hydrogen-bonding-based molecular recognition has been used to prepare a dendritic framework for use in site-specific molecular recognition, guest(s) encapsulation and solubilization.[108]

The generic term megamer was first used by Tomalia and coworkers to describe a cationic dendrimer core surrounded by excess anionic shell dendrimers to form a charge neutral "core-shell (tecto)dendrimer".[109] A "sphere upon sphere" model of a megamer is shown in Scheme 1-11. Megamers, as presented by Tomalia are *nearly* monodisperse assemblies that are held together covalently.

Scheme 1-11
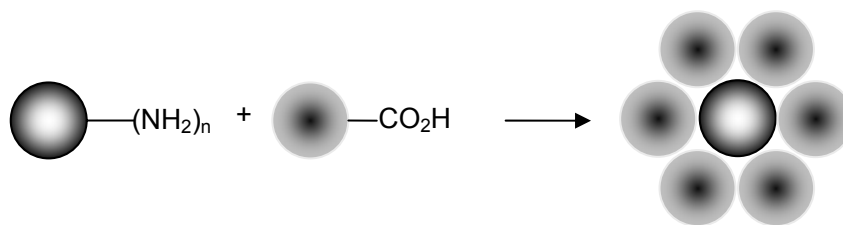
Other examples of noncovalent macromolecular synthesis rely on naturally occurring biopolymers. A notable example is the preparation of DNA-based architectures

that assemble into polyhedra of predetermined shape.[110] Whitesides and coworkers reported the synthesis of monodisperse polymers from proteins.[111] Padilla and coworkers have reported self assembling protein cages, layers, crystals and filaments.[112]

Proteins offer a monodisperse scaffold for macromolecular syntheses that bypasses the need to attach chemically synthesized polymers to drug carrier systems in order to achieve EPR in tumors. The ability of proteins to bind natural ligands, for example streptavidin to biotin, leads us to explore the preparation of self-assembling megamers. Megamers based on the streptavidin-biotin interaction, unlike Tomalia's core-shell megamers, would be *monodisperse* and held together *non*-covalently.

In closing, the important issues of monodispersity, size, and targeting of macromolecular drug delivery systems may be addressed using various macromolecular bioconjugates of dendrimers based on melamine. The chemical flexibility of dendrimers based on melamine lends itself to bioconjugate formation with drug molecules such as antisense genes, targeting moieties such as peptides, and proteins as macromolecular scaffolds.

CHAPTER II

SOLUTION-PHASE SYNTHESIS AND CHARACTERIZATION OF DISULFIDE-

LINKED DNA-DENDRIMER BIOCONJUGATES

BACKGROUND

Using thiol/disulfide exchange chemistry, thiol-terminated 12-base single stranded DNA sequences with or without an Oregon Green fluorophore attached (purchased in C_{18} HPLC-purified form from Trilink Biotechnologies, Inc.) were added to second- and third-generation triazine-based dendrimers. The synthesis permits either one or two single-stranded DNA (ssDNA) oligonucleotides to be covalently attached to the dendrimer at the core, the periphery, or both as depicted in Table 2-1.

DNA-dendrimer conjugates from Table 2-1 will be referred to as **AI, AII, AIII, BI, BII,** and **BIII**, for convenience. A method for HPLC purification of **AII** is presented with subsequent peak assignments by MALDI-TOF. Further structure elucidation of **BII** was made possible through labeling analysis using Ellman's reagent, and degradation analysis with a reducing agent. Proof of structure for all other architectures was derived primarily from mass spectrometry and polyacrylamide gel electrophoresis was performed whenever yields permitted.

Most of the conjugates in Chapter II were prepared from 12-mer ssDNA. Two of the conjugates, **AI** and **BIII**, consisted of 31-mer ssDNA and 22-mer ssDNA,

respectively. These longer conjugates were prepared in order to study the hybridization behavior of these conjugates with surface bound probe ssDNA in Chapter III.

Table 2-1. Targets arising from disulfide exchange between ssDNA and dendrimer.
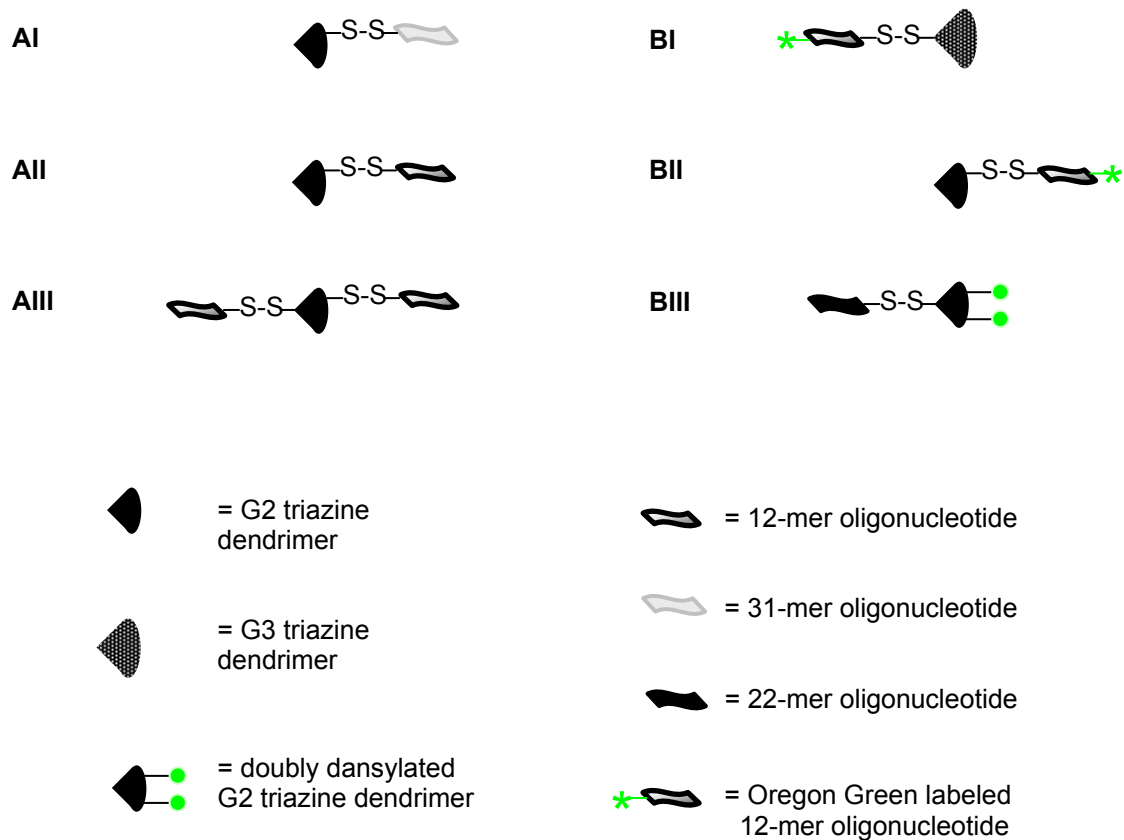
EXPERIMENTAL PROCEDURES

Materials. Reagent grade chloroform, methylene chloride, methanol, and ethyl acetate were used without further purification during synthesis. THF was dried over 4Å molecular sieves prior to use in synthesis. All deuterated solvents used were purified in the same manner as the non-deuterated equivalent after being received from Cambridge Isotope Laboratories (Cambridge, MA). Cyanuric chloride (98%), DIPEA (99%), and piperazine (99+%) were used as supplied by Acros (Pittsburgh, PA). Dansyl chloride (98+%) was used as supplied by Aldrich (Milwaukee, WI). Sulfosuccinimidyl 4-(N-maleimidomethyl)cyclohexane-1-carboxylate (SSMCC, Pierce), tris(2-carboxyethyl)phosphine, HCl (TCEP-HCl, Pierce), triethanolamine (TEA, 98%, Aldrich Chemical Co.), NaH_2PO_4 (99%, Mallinckrodt AR), ethylenediaminetetra acetic acid (EDTA, 100%, Sigma), sodium dodecylsulfate (SDS, 99%, Fluka Chemie AG), and NaCl (EM Science) were used as received. Ultrapure 18 MΩ·cm Milli-Q water was used to prepare buffer solutions and to rinse. Immobilized tris(carboxyethyl)phosphine (TCEP) and succinimidyl 3-(2-pyridylthio)propionate (SPDP) were used as purchased from Pierce Chemical (Rockford, IL). Electrophoresis grade acrylamide:bisacrylamide (29:1), ethidium bromide (1% solution), and coomassie blue R250 were used as received from FisherBiotech (Pittsburgh, PA).

Trisborate EDTA (0.45 M) and 10× DNA gel loading buffer were purchased from Eppendorf (Hamburg, Germany). Disulfide-modified oligonucleotides were purchased from Trilink Biotechnologies (San Diego, CA). Nuclear magnetic resonance (NMR) spectra (^{1}H and ^{13}C) were recorded on a Varian 300 NMR spectrometer.

Dendrimer synthesis. Syntheses of the dendrimers discussed in this chapter were aided by post doctoral group members Dr. Steven Bell and Dr. Wen Zhang. The synthesis of dendrimer 5, from Scheme 2-1, is reported below. Steps b, c, and d in Scheme 2-1 describe the substitution of cyanuric chloride with three chemically unique amines. Experimental details for the preparation of dendrimer 5 are found below Scheme 2-1, and they clearly demonstrate the methodology behind the synthesis of dendrimers based on melamine. All other dendrimer syntheses for this work have been published.[113,114]

Scheme 2-1*
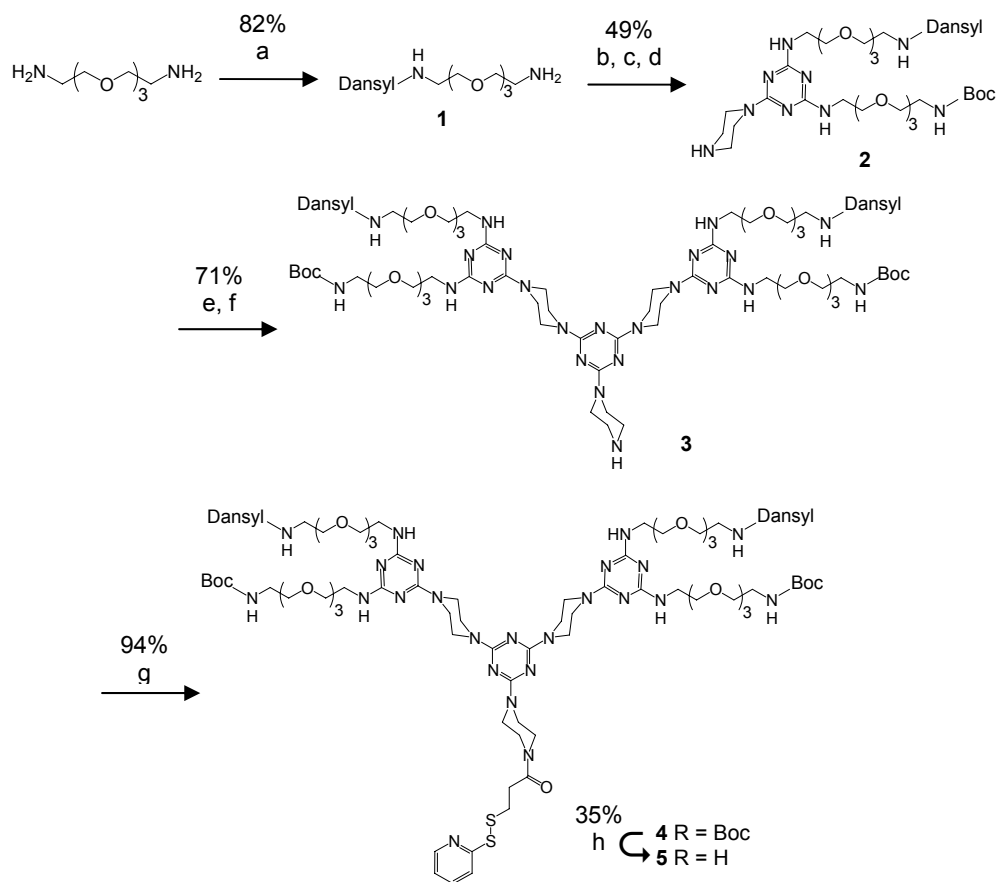
*a) 1 eq. NH₂CH₂(CH₂OCH₂)₃CH₂NH₂, 1 eq. dansyl chloride, DIPEA, dioxane, RT, 14 h.; b) C₃N₃Cl₃, DIPEA, THF, -6 ºC; c) BocNHCH₂(CH₂OCH₂)₃CH₂NH₂, DIPEA, THF, RT, 14 h.; d) Piperazine, DIPEA, THF, 70 ºC, 14 h.; e) C₃N₃Cl₃, DIPEA, THF, RT, 14 h.; f) Piperazine, DIPEA, THF, 70 ºC, 14 h.; g) SPDP, DIPEA, THF, RT, 24 h.; h) Trifluoroacetic acid:CH₂Cl₂ (1:1), RT, 10 h.

Synthesis of 1. Dansyl chloride (1.306 g, 4.84 mmol) was added to a solution of

$NH_2CH_2(CH_2OCH_2)_3CH_2NH_2$ (5.58 g , 29.0 mmol) and DIPEA (1.7 mL, 5.03 mmol) in

THF (100 mL). The resulting mixture was dried by centrifugal evaporation (*in vacuo*)

and then partitioned between CH_2Cl_2 and water. The organic phases were dried *in vacuo*,

and concentrated *in vacuo* to yield a bright green oil which was purified via silica gel

column chromatography (100:8, CH_2Cl_2:MeOH eluent). A bright green oil was obtained

(1.260 g, 61.1 %). ^{1}H NMR (300 MHz, CD_3OD) δ3.72 (tr, 4H, NCH_2), 3.62 (m, 24H,

CH_2OCH_2), 3.49 (tr, 4H,-C(O)NHCH_2CH_2$), 3.20 (tr, 4H, NHC$H_2CH_2), 2.79 (br, 4H,

HNCH_2), 1.42 (s, 18H, OC(CH_3)$_3$). ^{13}C NMR (75 MHz, CD_3OD) δ166.2, 165.0, 157.1,

78.9, 70.4, 53.9, 43.7, 43.0, 40.4, 27.8; MALDI-TOF (*m/z*): $[M + H]^+$ calcd. for

$C_{33}H_{63}N_9O_{10}$, 746.5; found, 746.8.

Synthesis of 2. Compound **1**, (0.906 g, 2.13 mmol) in THF (10 mL) was added

drop-wise to a cooled (-6 °C), solution of cyanuric chloride (0.404 g, 2.13 mmol) and

DIPEA (1.7 mL, 5.03 mmol) in THF (30 mL) while stirring. After 2 h the reaction

mixture was warmed to room temperature and more DIPEA (1.5 mL, 4.84 mmol) was

added, followed by a THF solution (15 mL) of BOC-NHCH$_2$(CH$_2$OCH$_2$)$_3$CH$_2$NH$_2$

(0.622 g, 4.95 mmol). After stirring for 14 h at room temperature a pale green/yellow

solution with white precipitate formed, yielding a single TLC spot (R_f = 0.78;

DCM:MeOH, 5:1). A six-fold excess of piperazine (1.50 g, 12.8 mmol) and DIPEA (1.5

mL, 4.84 mmol) was added, and the mixture was stirred for 14 h at room temperature.

After concentrating the sample by vacuum centrifugation, the residue was partitioned

between CH_2Cl_2 and water. The organic phases were concentrated *in vacuo* to yield a

bright green oil which was purified via silica gel column chromatography (100:5,

CH$_2$Cl$_2$:MeOH eluent). A pale green oil was obtained (1.10 g, 58.7 %). ^{1}H NMR (300 MHz, CD$_3$OD) δ8.2 (tr, 1H, *o*-C*H*), 7.75 (m, 2H, *m*-C*H*), 7.2 (tr, 1H, *p*-C*H*), 3.75 (br, 4H, NC*H*$_2$) 3.63 (m, 12H, C*H*$_2$OC*H*$_2$), 3.50 (tr, 4H, C(O)NHC*H*$_2$CH$_2$ and NC*H*$_2$CH$_2$S), 3.21 (tr, 2H, NHC*H*$_2$CH$_2$), 3.02 (tr, 2H, NCH$_2$C*H*$_2$S), 2.82 (br, 4H, NHC*H*$_2$), 1.43 (s, 9H, OC(C*H*$_3$)$_3$). ^{13}C NMR (75 MHz, CD$_3$OD) δ167.6, 166.1, 161.2, 150.1, 139.2, 122.6, 121.2, 80.2, 71.4, 49.9, 46.3, 44.5, 41.4, 40.8, 39.6, 28.9; MALDI-TOF (*m/z*): [M + H]$^+$ calcd for C$_{27}$H$_{45}$N$_9$O$_5$S$_2$, 640.3; found, 640.4.

Synthesis of 3. Dendrimer **2** (0.453 g, 0.516 mmol) was dissolved in THF (25 mL), and added drop-wise to a cooled (-6 °C), THF solution (30 mL) of cyanuric chloride (0.046 g, 0.258 mmol) and DIPEA (0.75 mL, 2.42 mmol) while stirring. After 2 h the reaction mixture was warmed to room temperature. After stirring for 14 h at room temperature a pale green/yellow solution with white precipitate formed. After removal of solvent, the residue was partitioned between CH$_2$Cl$_2$ and water. The organic phases were concentrated *in vacuo* to yield a pale green/yellow oil which was purified via silica gel column chromatography (100:4, CH$_2$Cl$_2$: MeOH eluent). A green oil was obtained (0.251 g, 50.7 % yield). ^{1}H NMR (300 MHz, CD$_3$OD) δ8.2 (m, 1H, *o*-C*H*), 7.78 (m, 2H, *m*-C*H*), 7.19 (tr, 1H, *p*-C*H*), 3.75 (br, 16H, NC*H*$_2$), 3.62 (m, 36H, CH$_2$OC*H*$_2$), 3.50 (br, 8H, C(O)NHC*H*$_2$CH$_2$ and NC*H*$_2$CH$_2$S), 3.22 (m, 6H, NC*H*$_2$) 3.04 (tr, 2H, NCH$_2$C*H*$_2$S), 1.43 (s, 27H, OC(C*H*$_3$)$_3$); ^{13}C NMR (75 MHz, CD$_3$OD) δ169.5, 166.1, 165.0, 164.4, 160.0 157.0, 150.0, 137.8, 121.1, 119.8, 78.9, 71.2, 70.2, 43.5, 42.9, 40.3, 27.9. MALDI-TOF (*m/z*): [M + H]$^+$ calcd for C$_{63}$H$_{10}$N$_{21}$O$_9$S$_2$, 1495.5; found, 1495.8.

Synthesis of 4. Dendrimer **3** (0.040 g, 0.021 mmol) was reacted with N-Succinimidyl 3-[2-pyridyldithio]-propionamidoSPDP (0.066 g, 0.021 mmol) for 14 h at

RT in THF (10 mL). A green/yellow oil was obtained after solvent evaporation (0.032 g, 72.0 %). ^{1}H NMR (300 MHz, CD$_3$OD) δ8.12 (m, 1H, *o*-C*H*), 7.82 (m, 2H, *m*-C*H*), 7.45 (tr, 1H, *p*-C*H*), 3.84 (br, 14H, NC*H$_2$*), 3.78 (br, 6H, NH$_2$C*H$_2$*CH$_2$), 3.65 (m, 36H, CH$_2$OC*H$_2$*), 3.22 (m, 6H, N-C*H$_2$*), 3.04 (tr, 2H, NHCH$_2$C*H$_2$*S); ^{13}C NMR (75 MHz, CD$_3$OD) δ166.1, 165.0, 164.4, 157.0, 150.0, 137.8, 121.1, 119.8, 71.2, 70.2, 43.5, 42.9, 40.3. NMR Spectra are in Supporting Information. MALDI-TOF (*m/z*): [M + H]$^+$ calcd for C$_{48}$H$_{82}$ClN$_{21}$O$_9$S$_2$, 1196.6; found, 1196.6.

Synthesis of 5. Dendrimer **4** (0.028 g, 0.013 mmol) was reacted with 85% trifluoroacetic acid (TFA, 1.5 mL) for 14 h (1:1 TFA:CH$_2$Cl$_2$). A yellow oil was obtained after solvent evaporation (0.025 g, 98.3 %). ^{1}H NMR (300 MHz, CD$_3$OD) δ8.37 (m, 2H, *o*-C*H*), 7.77 (m, 4H, *meta*-C*H*), 7.16 (tr, 2H, *p*-C*H*), 3.68 (br, 24H, NC*H$_2$*), 3.59 (m, 48H, C*H$_2$*OCH$_2$), 3.48 (tr, 2H, C(O)NHC*H$_2$*CH$_2$S), 3.21 (tr, 10H, NHC*H$_2$*), 3.04 (tr, 2H, C(O)NHC*H$_2$*CH$_2$S), 1.41 (s, 27H, OC(C*H$_3$*)$_3$). ^{13}C NMR (75 MHz, CD$_3$OD) δ171.2, 166.2, 165.9, 161.6, 158.0, 149.8, 122.1, 120.9, 119.2, 80.1, 71.5, 71.2, 71.1 44.2, 41.3, 36.2, 33.8, 31.9, 28.9. MALDI-TOF (*m/z*): [M + H]$^+$ calcd for C$_{75}$H$_{122}$N$_{24}$O$_{16}$S$_4$, 1743.7; found, 1743.7.

ssDNA handling. Oligonucleotides can be custom-synthesized by various companies for different research demands, but two standard modifiers prevail as the most synthetically and economically feasible options: amino modifiers and thiol modifiers. The oligonucleotides can be modified on either the 5′ or 3′ terminus. For this work, both 5′ and 3′ thiol-modified oligonucleotides were used to form disulfide linkages with various dendrimers. Oligonucleotides (0.1 OD/ μL) were deprotected on immobilized TCEP (2-carboxyethylphosphine) for 15 min at room temperature and eluted with two

volumes of TBE (45 mM tris(hydroxymethyl) aminomethane (Tris)-borate, 1 mM EDTA) pH 8.3 buffer. The use of other buffers including Tris buffer at pH 6.0 and 7.4, did not elute the DNA from the resin.

ssDNA-dendrimer conjugation. The synthesis and characterization of all covalently-linked DNA-dendrimer conjugates was carried out in solution phase. Thiol-terminated oligonucleotides were added to second- and third-generation triazine-based dendrimers via thiol/disulfide exchange chemistry as shown in Scheme 2-2. In a typical conjugation, deprotected ssDNA [2.5 OD, 25 μL H_2O] was incubated with thiopyridyl-containing dendrimer (41.8 nmol). After 12 h at room temperature the reaction was dried *in vacuo*, yielding the disulfide conjugated ssDNA-dendrimer. Scheme 2-2 shows the structure of the dendrimer used to make conjugates **AI**, **AII**, and **BII**.

MALDI-TOF. An overlayer preparation was used with a 2,4,6-trihydroxyacetophenone (THAP) matrix (*22*). A 1:1:1 mixture of 1 μM aqueous reaction mixture, 10 mg/mL THAP matrix in methanol, and 15 mg/mL aqueous ammonium citrate was spotted in 1 μL aliquots on a bed of THAP matrix. The analyte-doped matrix crystals were washed repeatedly (~5-15 times) with 5 μL of cold water to remove alkali metals. MALDI-TOF mass spectra were acquired in positive- and negative-ion mode on a Voyager-DE STR mass spectrometer (Applied Biosystems, Framingham, MA) equipped with a pulsed nitrogen laser emitting at 337 nm. Samples were analyzed in linear mode using a delayed extraction time of 550 ns and an accelerating voltage of 20 kV. The laser light intensity was adjusted to provide the optimal signal-to-noise ratio. All spectra were the result of signal averaging 50-100 laser shots. Positive-ion mass calibrations were performed internally with the $[M + 2H]^{2+}$, $[M + H]^{+}$, and $[2M + H]^{+}$ ions of insulin

(bovine). Negative-ion calibrations were performed externally with the [M - H]⁻ and the

[2M - H]⁻ ions of a standard single stranded 12-mer oligonucleotide.

Scheme 2-2
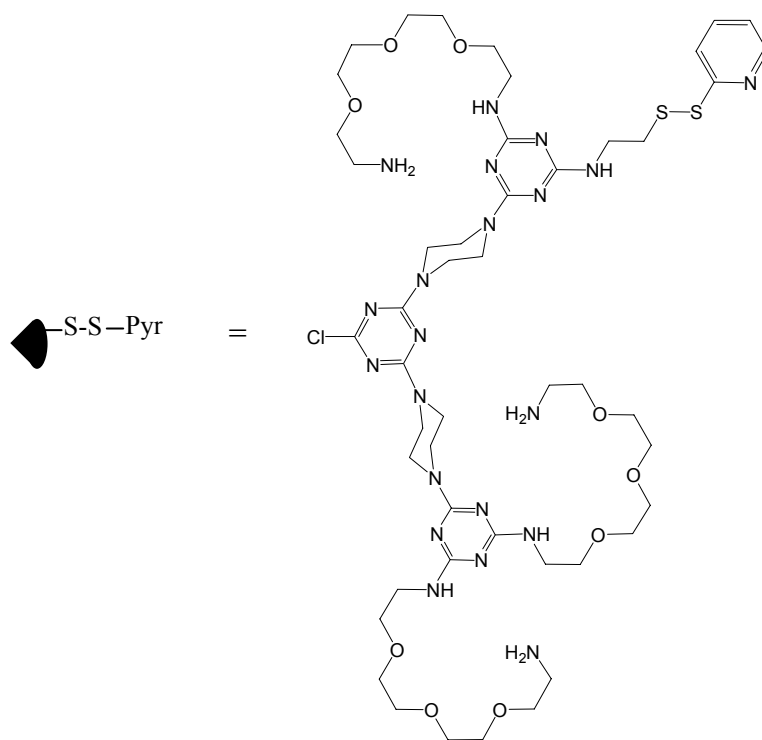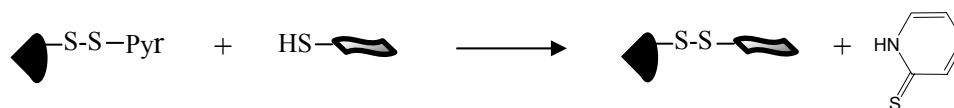
$$C_{48}H_{82}ClN_{21}O_9S_2$$
Exact Mass: 1195.57
Mol. Wt.: 1196.89

31

Scheme 2-3

C₃₅₅H₄₈₂ClN₁₁₀O₂₁₁P₃₁S₂
Exact Mass: 10720.14
Mol. Wt.: 10726.01

$C_{355}H_{482}ClN_{110}O_{211}P_{31}S_2$
Exact Mass: 10720.14
Mol. Wt.: 10726.01
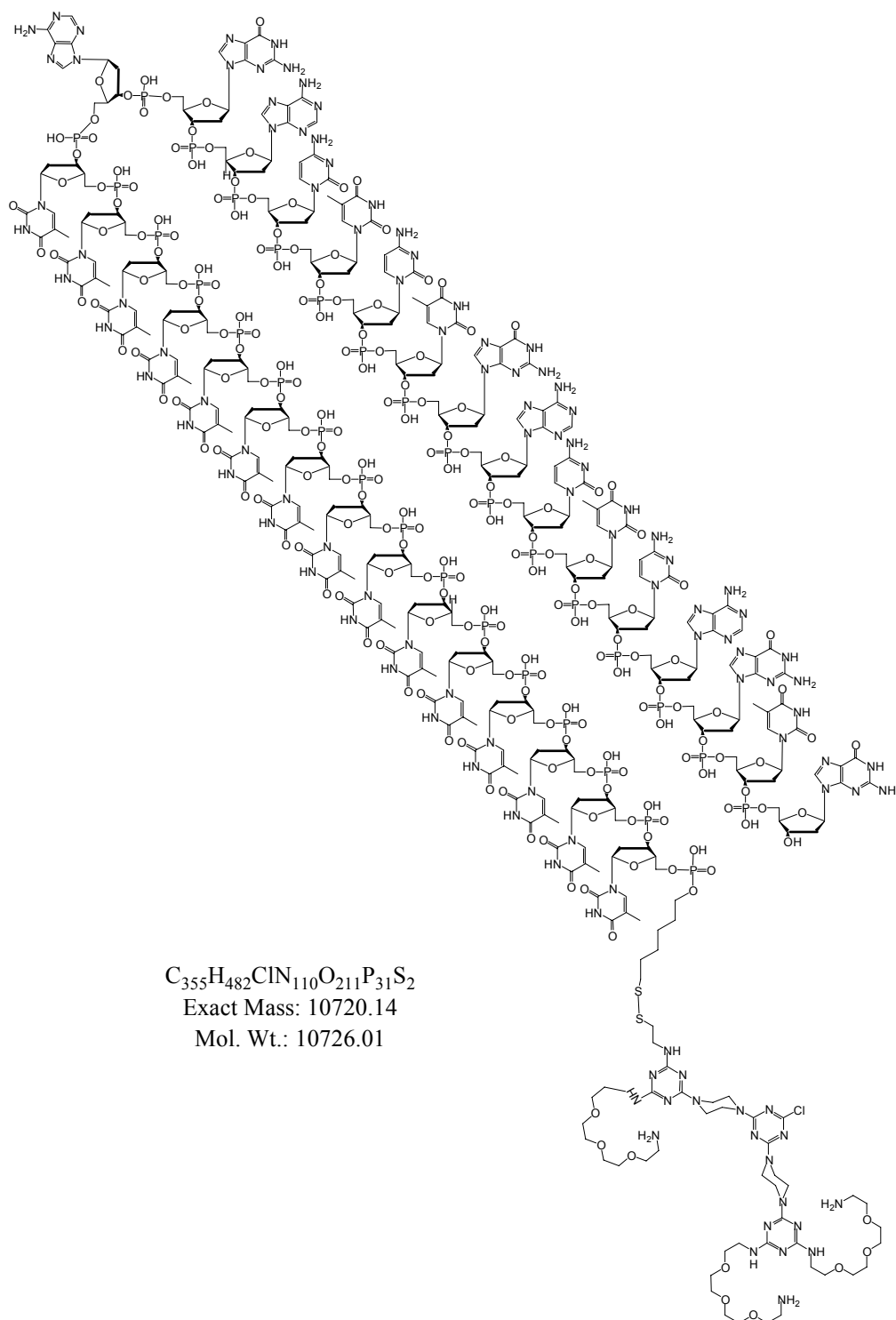
A1(a): 5′ G2 dendrimer-S-S-(CH₂)₆-TTTTTTTTTTTTTTTAGACTCTGACTCAGTG 3′

Scheme 2-4

C$_{355}$H$_{482}$ClN$_{110}$O$_{211}$P$_{31}$S$_{2}$
Exact Mass: 10720.14
Mol. Wt.: 10726.01
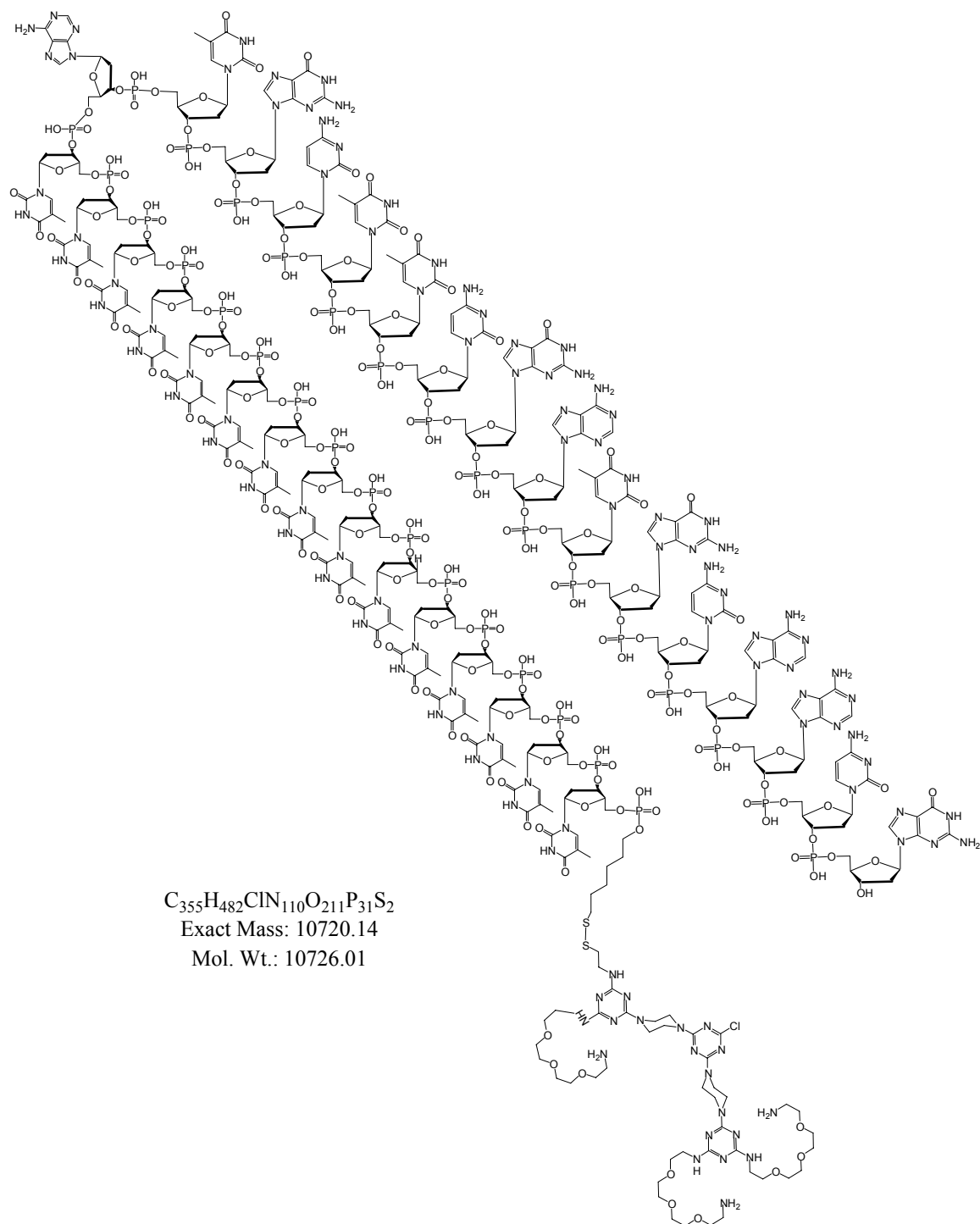
AI (b): 5′ G2 dendrimer-S-S-(CH$_2$)$_6$-TTTTTTTTTTTTTTTATGCTTCGATGCAACG 3′

Scheme 2-5
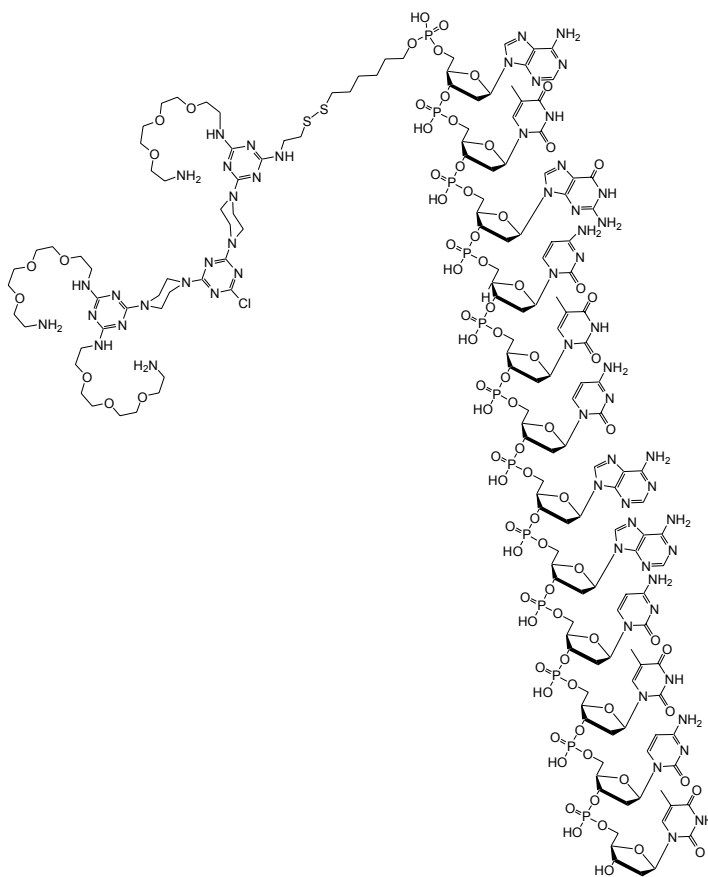
$C_{165}H_{239}ClN_{60}O_{83}P_{12}S_2$
Exact Mass: 4859.23
Mol. Wt.: 4862.29

AII: 5′ G2 dendrimer-S-S-(CH$_2$)$_6$-ATGCTCAACTCT 3′

Scheme 2-6

$C_{352}H_{446}F_{10}N_{108}O_{174}P_{26}S_6$
Exact Mass: 10156.07
Mol. Wt.: 10161.63
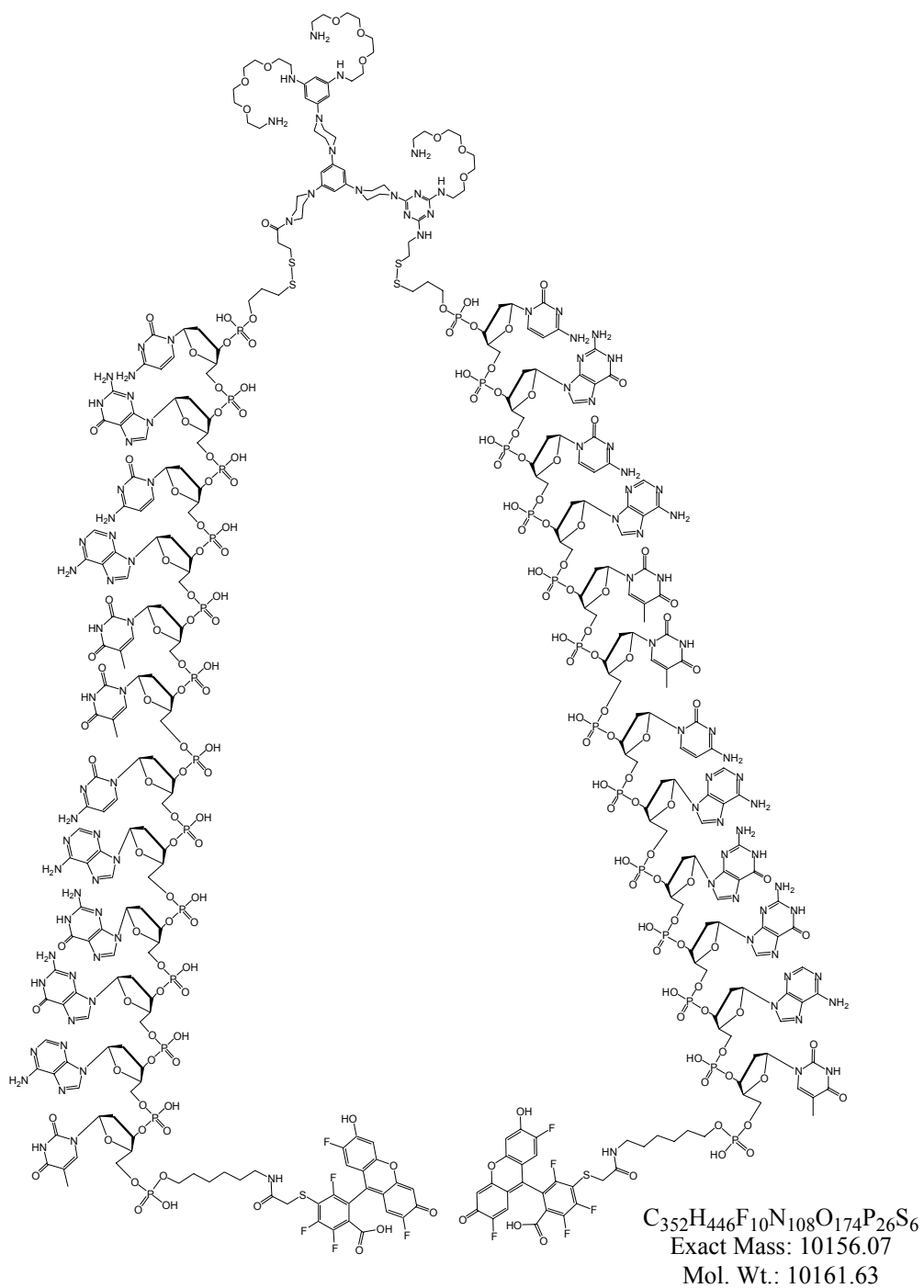
AIII: [5′ Oregon Green-(CH$_2$)$_6$-TAGGACTTACGC-S-S-(CH$_2$)$_3$]$_2$-G2 dendrimer 3′

Scheme 2-7
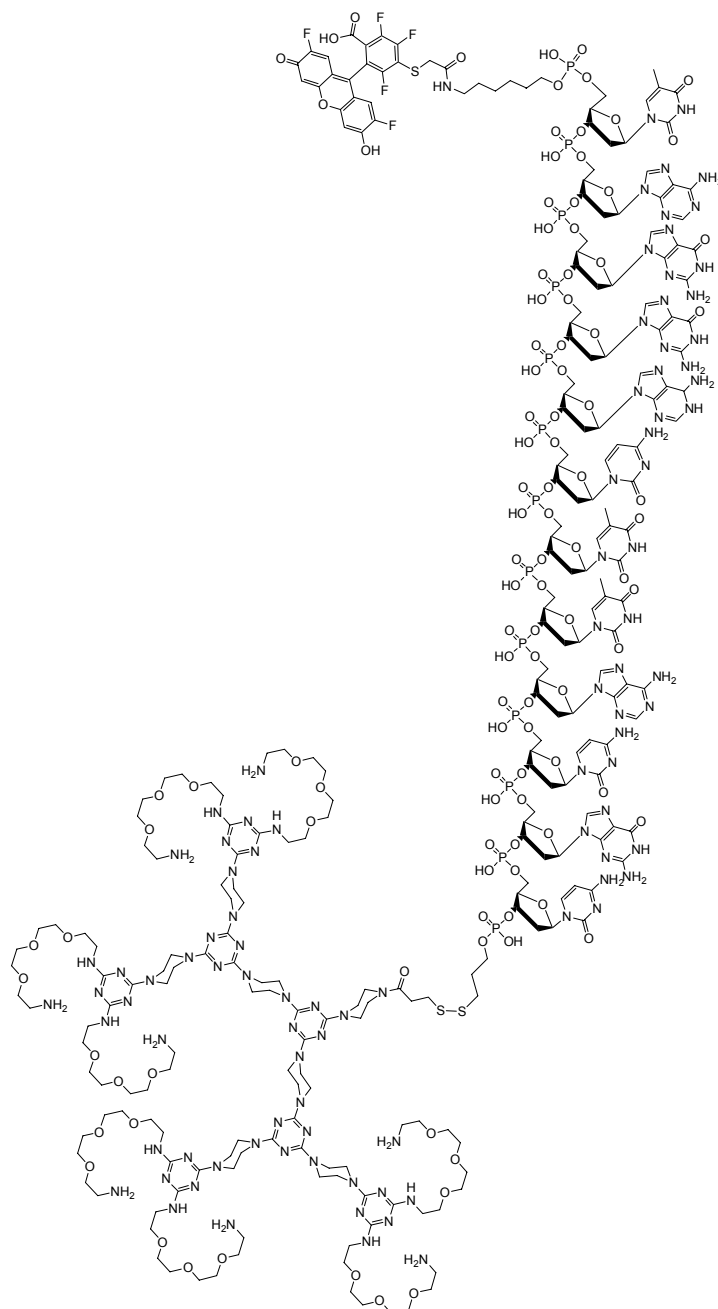
$C_{264}H_{389}F_5N_{97}O_{107}P_{13}S_3$
Exact Mass: 7223.37
Mol. Wt.: 7227.35

BI: 5′ Oregon Green (CH$_2$)$_6$-TAGGACTTACGC-(CH$_2$)$_3$ -S-S-G3 dendrimer 3′

Scheme 2-8

$C_{191}H_{255}ClF_5N_{66}O_{91}P_{13}S_3$
Exact Mass: 5557.27
Mol. Wt.: 5560.76
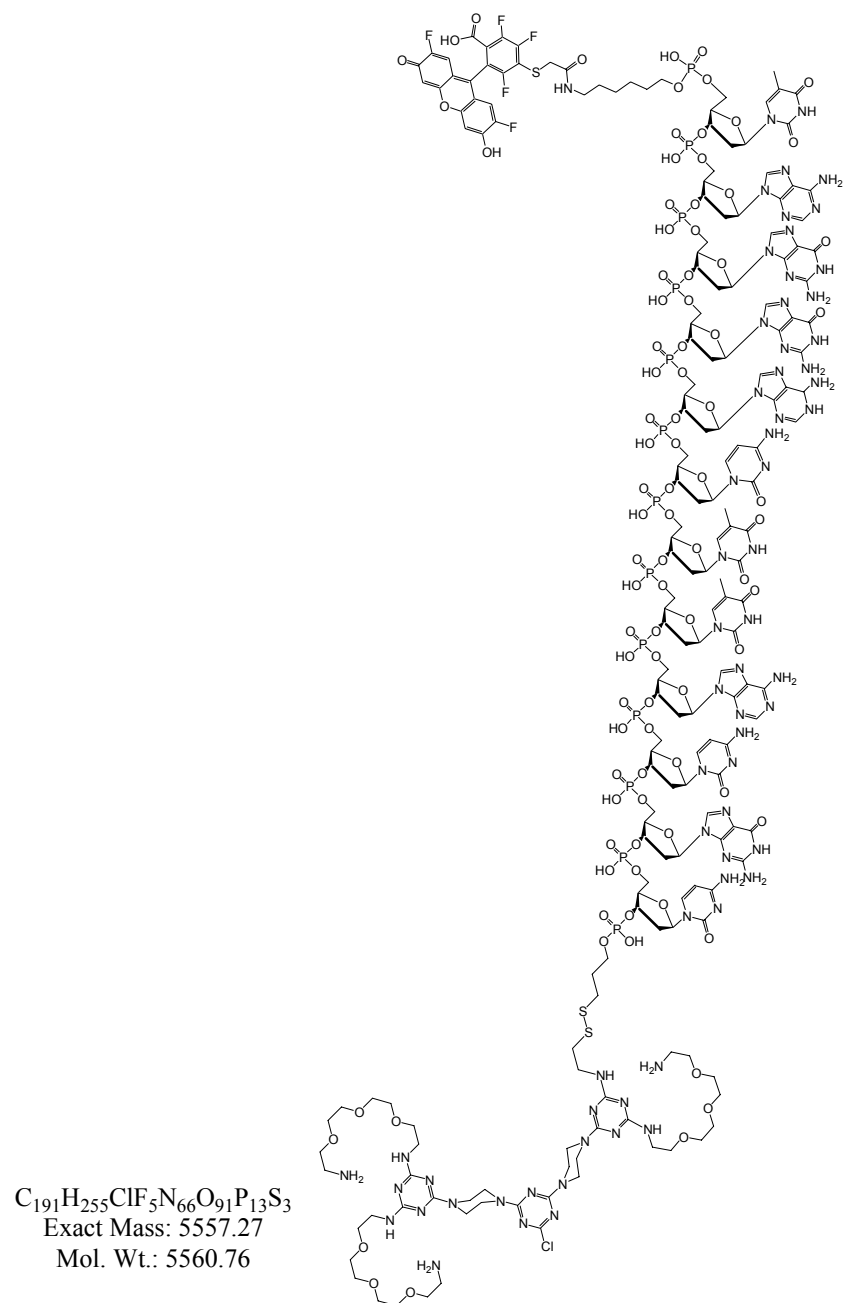
BII: 5′ Oregon Green [CH$_2$]$_6$-TAGGACTTACGC-[CH$_2$]$_3$-S-S-G2 dendrimer 3′

Scheme 2-9

C$_{306}$H$_{416}$N$_{84}$O$_{160}$P$_{22}$S$_{4}$
Exact Mass: 8636.01
Mol. Wt.: 8640.73
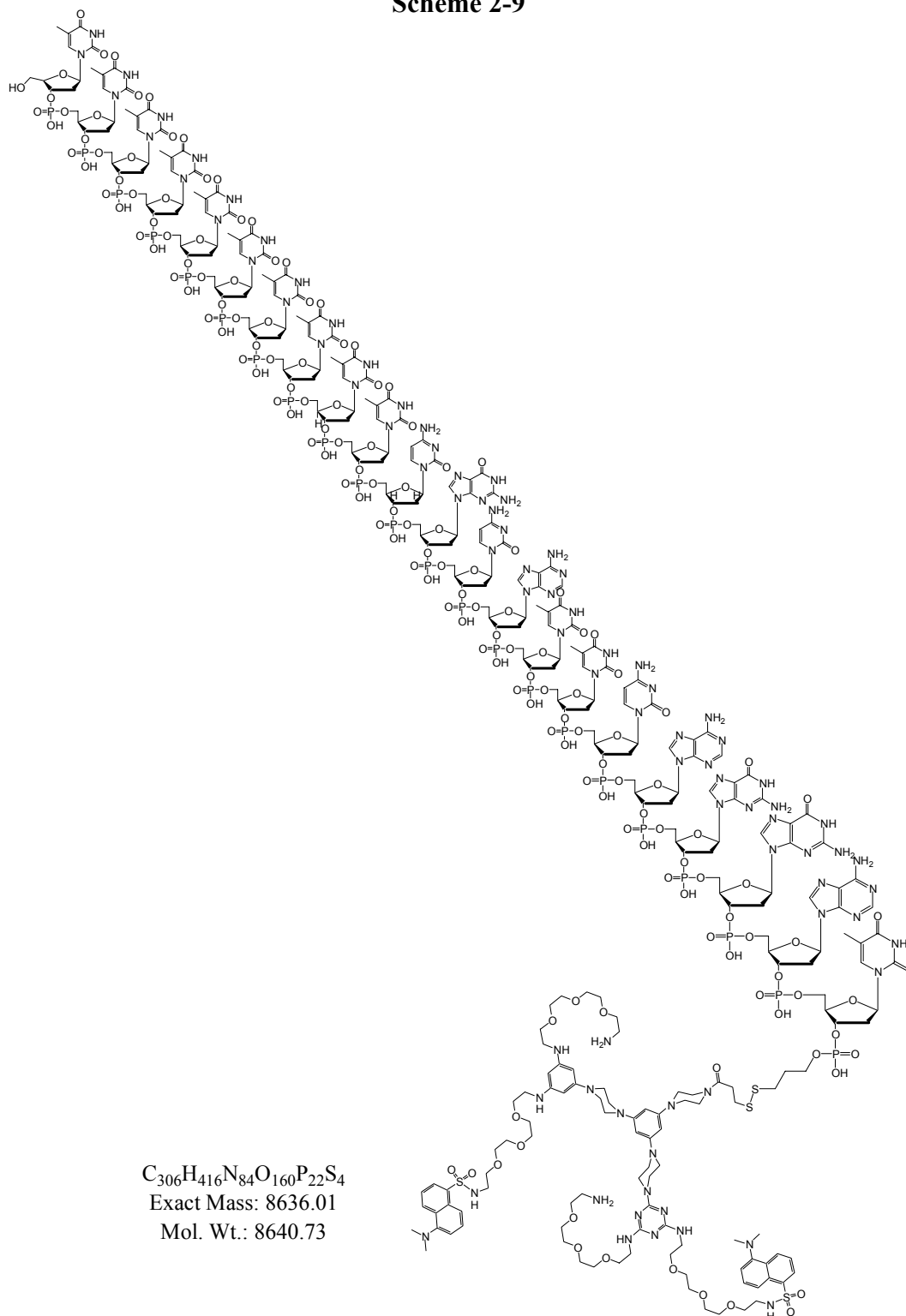
BIII: 5′ TTTTTTTTTTCGCATTCAGGAT-(CH$_2$)$_3$ -S-S-G2 dansyl-dendrimer 3′

Gel electrophoresis. Polyacrylamide gels (20%) were run in TBE (90 mM Tris-Borate, 2 mM EDTA) at 75 V for 2-3 hours using 0.25% bromophenol blue and 40% (w/v) sucrose in water as a sample buffer. Samples were prepared by adding 0.1 volume of sample buffer to each dendrimer and conjugate solution. Gels were soaked in ethidium bromide (4 μL per 100 mL running buffer) while gently rotating, for 20 minutes. After removing the excess ethidium bromide by incubating the gel for 2 minutes, 3 times, in running buffer, bands containing DNA were visualized on a UV transilluminator. The gel was stained with Coomassie Brilliant Blue R250 on a rotator for 1 hour, and destained in 40% methanol, 10% acetic acid in water, until bands were clear. The destaining process sometimes took up to 12 hours to remove enough background to clearly see blue bands corresponding to dendrimer. Gels were visualized on a transilluminator, and all pictures were recorded on a CCD camera.

HPLC purification. A model 600 Waters HPLC workstation equipped with a model 2487 dual absorbance detector and XTerra MS C18 2.5 μm, 4.6X50 mm column was used for the purification of all DNA-dendrimers. An example of a typical solvent gradient is described for a 12-mer oligonucleotide attached *via* disulfide linkage to the periphery of a G2 dendrimer. Parameters must be optimized, however, for DNA-dendrimers of differing sizes and charge ratios. Buffer A, 100% acetonitrile, was increased from 0% to 50% with respect to Buffer B, 0.1 M TEAA pH 7.5 containing 15% acetonitrile, at a rate of 1 mL/min over 15 minutes. Samples were dried *in vacuo*, dissolved in 0.1 M TEAA pH 7.5 containing 15% acetonitrile to a final concentration of approximately 1 μg/μL, and loaded onto a 20 μL sample loop at about 20 μg per injection. Absorbance was monitored at wavelengths 254 and 260 nm.

RESULTS AND DISCUSSION

Single-stranded DNA oligonucleotides were successfully attached to dendrimers at the core, the periphery, and both sites. To distinguish between covalent attachment and electrostatic association, conjugate **AII** from Scheme 2-5 was rigorously characterized using polyacrylamide gel electrophoresis (PAGE), high-performance liquid chromatography (HPLC), and matrix-assisted laser desorption ionization time-of-flight (MALDI-TOF) mass spectrometry. All other conjugates were analyzed by MALDI-TOF. Whenever sufficient material was available, further analysis was carried out by gel electrophoresis.

Evidence for AI from MALDI-TOF. Two different 5′ thiol modified 31-mer oligonucleotides were used to prepare **AI**-type conjugates. The reason for preparing two conjugates with the same molecular weight will become clear in Chapter III. Briefly, the conjugates contain the exact same nucleotide (G, C, A and T) content, but different sequences, in order to study their hybridization by surface plasmon resonance (SPR) analysis. Hybridization efficiencies increase with increased GC base pair content, so strands with the same GC base pair content were designed. Sequences used for **AI** conjugates were:

5′ DMT-C6-S-S-C6-TTT TTT TTT TTT TTT AGA CTC TGA CTC AGT G 3′

and

5′ DMT-C6-S-S-C6-TTT TTT TTT TTT TTT ATG CTT CGA TGC AAC G 3′

for 31-mer (a) and 31-mer (b), respectively. Conjugation of 31-mer (a) with G2

dendrimer *via* disulfide bond formation afforded **AI (a)**. Likewise, Conjugation of 31-

mer (b) with G2 dendrimer *via* disulfide bond formation afforded **AI (b)**. The mass to

charge ratio (*m/z*) for negative ion mode [M-H]⁻ MALDI-TOF was calculated for

conjugates **A1 (a)** and **A1 (b)** to be 10,725.01 and 10,724.79, respectively. The observed

m/z for **AI (a)** and for **AI (b)** was 10,724.83 (Figures 2-1 and 2-2 respectively). Doubly

charged species ([M-2H]²⁻) were also observed. The calculated [M-2H]²⁻ **AI (a)** and **AI**

(b) was 5362.51, and the observed signal was found at 5361.78 for **AI (a)** and 5361.72

for **AI (b)** (Figures 2-1 and 2-2 respectively). Some unreacted oligonucleotide thiol

remained in the sample after filtration. The (*m/z*) [M - H]⁻ calculated for excess thiol was

9639.29, and the observed signal was found at 9638.79 for the thiol corresponding to **AI**

(a), and 9638.89 for the thiol corresponding to **AI (b)** (Figures 2-1 and 2-2 respectively).
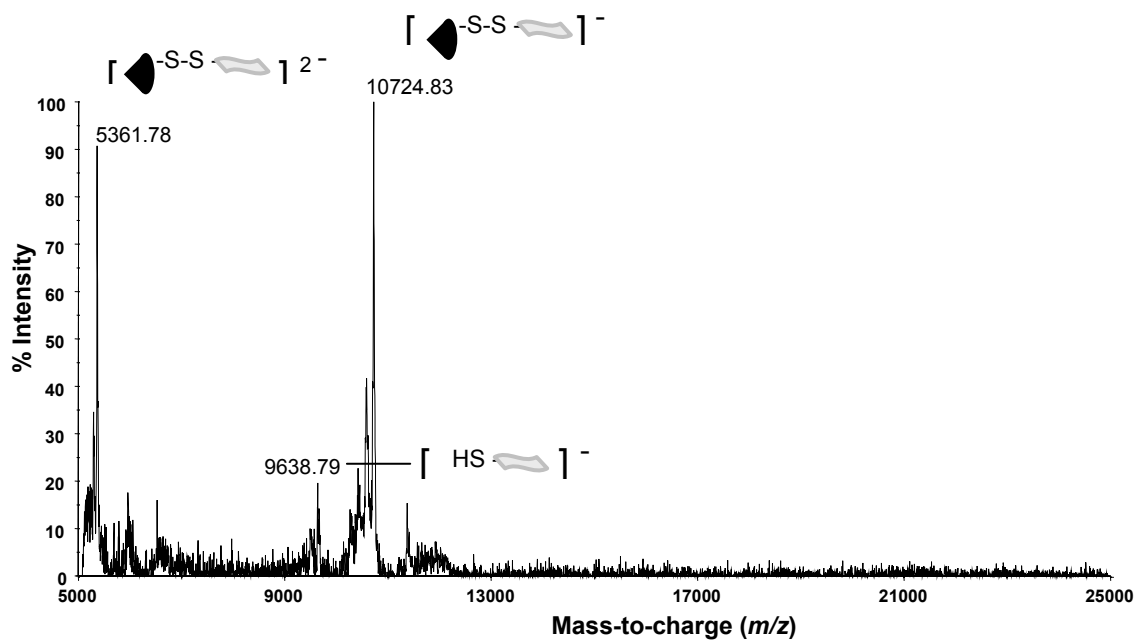
Figure 2-1. MALDI-TOF spectrum corresponding to dendrimer-bound 31-mer, **A1 (a)**
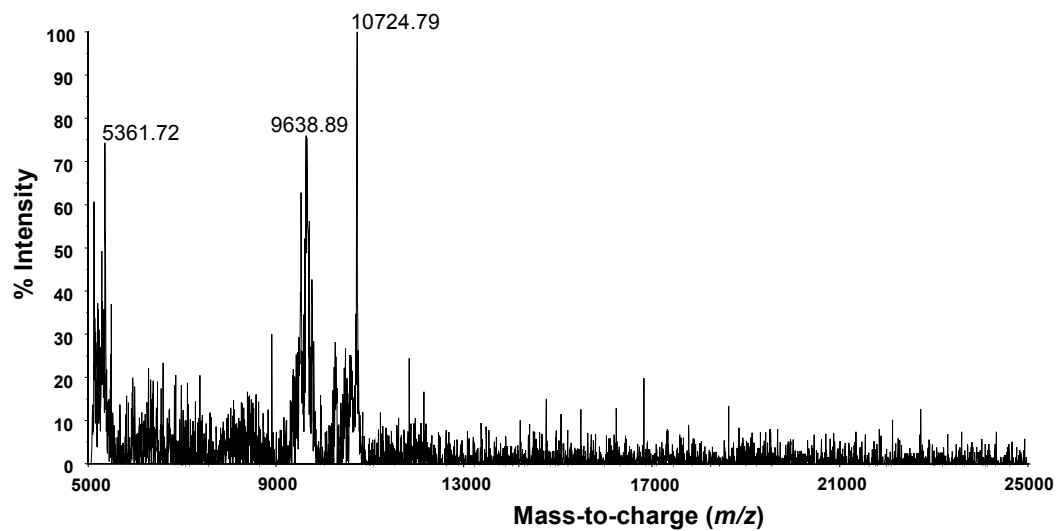
Figure 2-2. MALDI-TOF spectrum corresponding to dendrimer-bound 31-mer, **AI (b)**.

Evidence for AI from gel electrophoresis. To verify covalency, conjugate **AI (b)** was visualized by polyacrylamide gel electrophoresis. Two lanes on the 20% polyacrylamide gel shown in Figure 2-3, compare free thiol oligonucleotide, in lane 1, with the dendrimer-bound conjugate **AI (b)**, in lane 2. Ethidium bromide staining (gel A) allowed for the detection of oligonucleotide present in the sample, and a consequent coomassie stain (gel B) revealed the presence of dendrimer. The two bands present in lane 1 correspond to oligonucleotide disulfide formed during sample preparation, at the top, and the free thiol at the bottom. Lane 2 confirms the presence of the free thiol seen in **AI (a)** and **AI (b)** by MALDI-TOF, in the bottom lane, and the corresponding disulfide appears at the top, directly adjacent to the starting material shown in lane A. A third, faint band is observed in the middle of lane 2, corresponding to **AI (b)**. A coomassie stain of the same gel, shown to the right, confirms the presence of dendrimer in lane 2, as only dendrimer will stain by coomassie.[115] Accordingly, there were no bands observed in lane 1. The faintness of the band corresponding to conjugate might be a result of photo-quenching by the dendrimer. HPLC has proven to be the only effective method to remove all of the un-conjugated oligonucleotide, which as presented for **AII** has been successfully implemented. HPLC purification of **AI (a)** and **AI (b)**, however, was not necessary for the non-quantitative, proof-of-concept comparison analysis presented for this work.
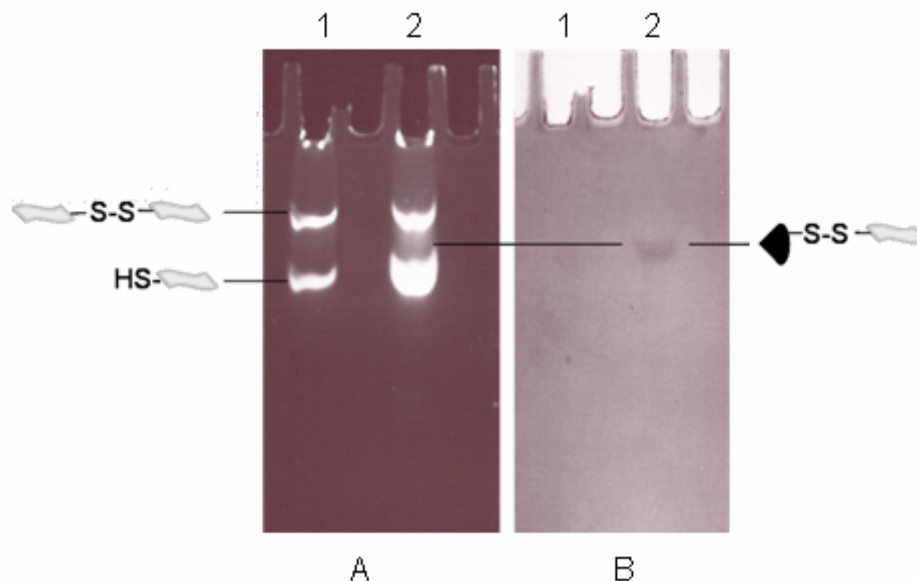
Figure 2-3. 20% polyacrylamide gel of **AI (b)** visualized by differential staining with (A) ethidium bromide and (B) Coomassie Brilliant Blue R-250.

Evidence for AII from HPLC. The oligonucleotide used in this work was: 12-mer (HS-C6)5'-ATGCTCAACTCT-3'. For the 12-mer-G2 DNA-dendrimer (**AII**), three major peaks were observed at 254 nm with retention times of 6.4, 8.4, and 10.4 minutes, as shown in Figure 2-4. Peaks A, B, and C correspond to 12-mer thiol, 12-mer disulfide starting material (a result of both incomplete reduction to the thiol and reformation of the disulfide starting material by oxidation), and AII, respectively. Like peaks were pooled, concentrated on a rotory evaporator, and analyzed by non-denaturing 20% polyacrylamide gel electrophoresis (PAGE) and MALDI-TOF.
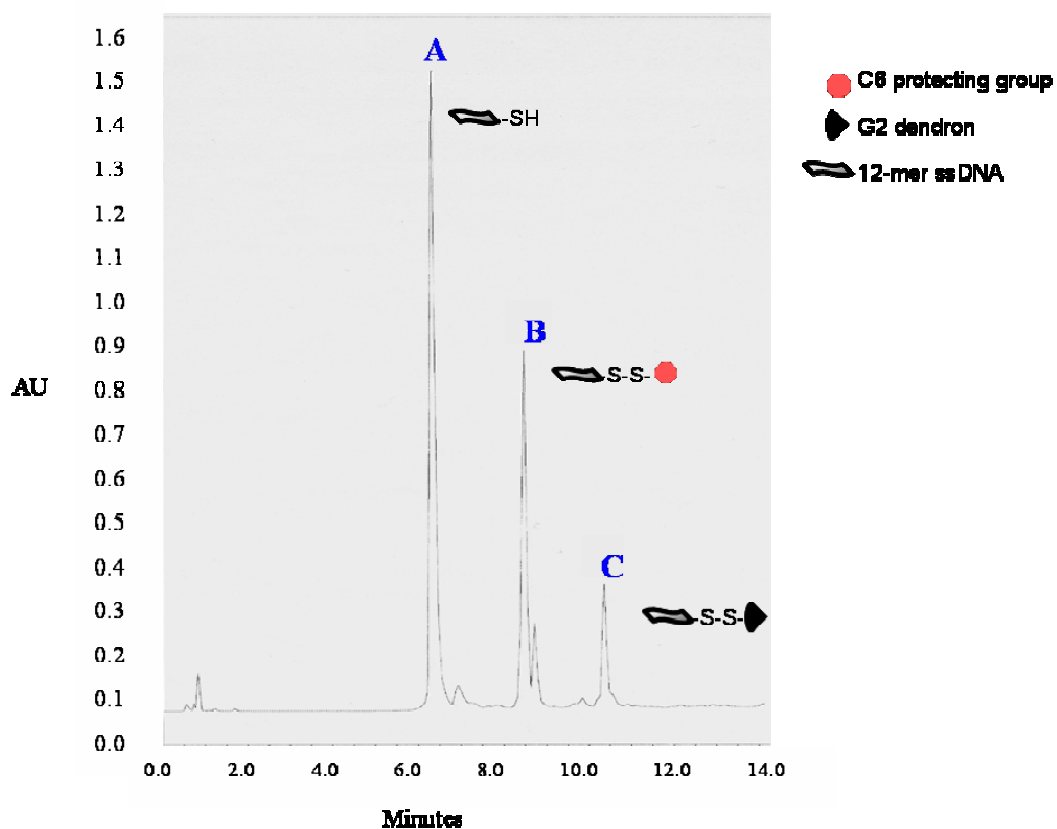
Figure 2-4. HPLC trace of crude **AII** reaction mixture after conjugation reaction.

Evidence for AII from MALDI-TOF. Figure 2-5 contains four separate MALDI spectra. The mass spectrum corresponding to the crude reaction material is compared to mass spectra corresponding to the three fractions (A, B, and C) pooled from eight separate HPLC injections (HPLC shown in Figure 2-4). The structure and molecular formula information for **AII** is shown in Scheme 2-1. The calculated MALDI-TOF *(m/z)* [M+H]+ for AII was 4863.29, and the observed signal was 4863.12. The MALDI-TOF peak corresponding to the auto-oxidized disulfide ssDNA appears at 7558.2.
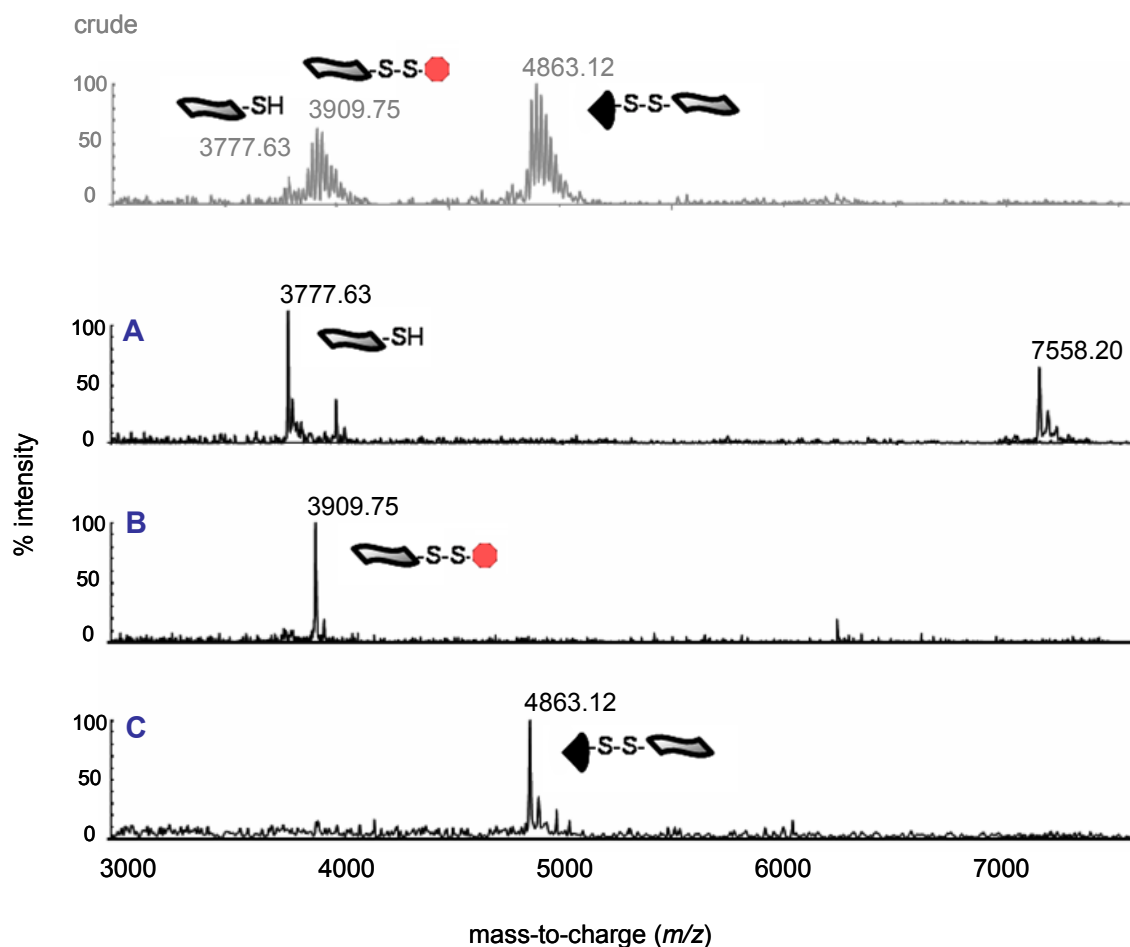
Figure 2-5. MALDI-TOF spectra corresponding to **AII** crude reaction material (top) and purified fractions A, B, and C from HPLC (chromatogram shown in Figure 2-4).

Evidence for AII from gel electrophoresis. Polyacrylamide gels (20%) allowed successful separation of the initial G2-dendrimer, the ssDNA, and the DNA-dendrimer products as shown in Figure 2-6. Gel (A) was stained with ethidium bromide, which stains DNA but not the dendrimers used in this study, and gel (B) was stained with

coommassie brilliant blue R-250, which stains the dendrimer but not the DNA. Starting from the lowest band in Figure 2-6 A, lane 3, the three bands correspond to unreacted DNA-thiol, DNA-dendrimer conjugate, and a disulfide-coupled DNA dimer. The two bands present in lane 2 of Figure 2-6 A correspond to DNA-thiol (lowest band) and the anticipated DNA dimer (top band), which is produced by oxidation of two DNA-thiol oligonucleotides to a DNA-S-S-DNA disulfide. Lane 1 in Figure 2-6 A contains a DNA ladder (10-100 base pair). The lowest band in lane 2 corresponds to double stranded 12-mer. Double-stranded DNA (dsDNA) is rigid and therefore is retarded on a 20% polyacrylamide gel while ssDNA migrates more efficiently through the dense matrix. Thus, the single stranded 24-mer (two disulfide linked 12-mers) shows up just below the double stranded 10-mer (which contains 20 bases). Removal of ethidium bromide, followed by staining with Coomassie Brilliant Blue R250 resulted in the gel shown in Figure 2-6 B. Only the middle band in lane 3, corresponding to the DNA-dendrimer, is visible. In contrast, all other bands corresponding solely to DNA are not stained. The absence of a band corresponding to the cationic dendrimer is attributed to the inability of these charged species to enter the polyacrylamide gel (they would migrate toward the cathode).
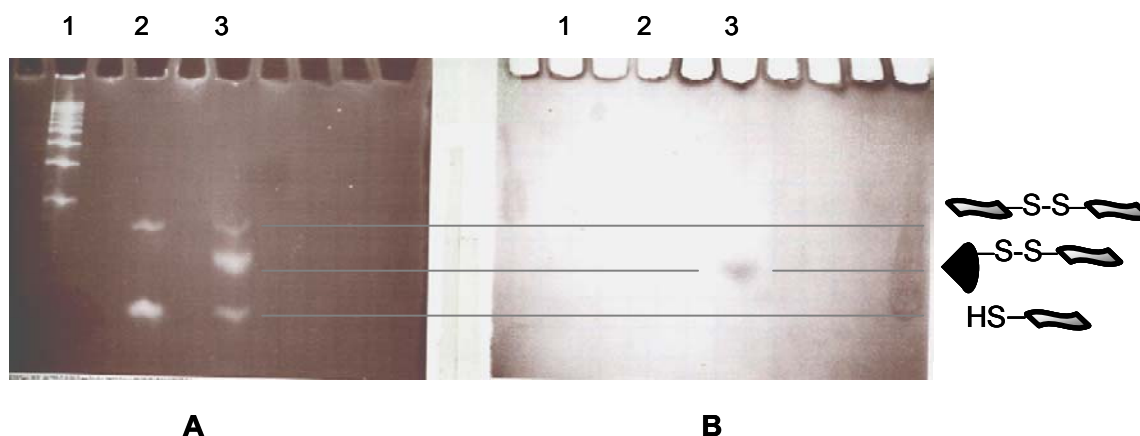
Figure 2-6. 20% polyacrylamide gel of **AII** visualized by differential staining with (A) ethidium bromide and (B) Coomassie Brilliant Blue R-250.

Evidence for AIII from MALDI-TOF. Disulfide exchange between the di-thio-pyridyl G2 dendrimer with two Oregon Green labeled 12-mers did not proceed efficiently. Both disulfide formation between two 12-mers and re-oxidation of the 12-mers with the C3 thiol modifier (protecting group) as supplied by Trilink were competing with formation of the desired product. Data from the crude reaction material is shown as proof that the construct can be prepared. Thiol-terminated DNA is present in the MALDI spectrum at m/z = 4474.1 (calculated m/z = 4474.0), and the corresponding doubly charged species appears at m/z = 2238.4 (calculated m/z = 2238.0). Reformation of the thiol-protected starting material through disulfide formation with the 3-mercaptopropanol-modifier resulted in a peak at m/z = 4566.7 (calculated m/z = 4564.2). A peak corresponding to one ssDNA addition to the G2 dendrimer was observed at m/z = 5807.4 (calculated m/z = 5800.8).
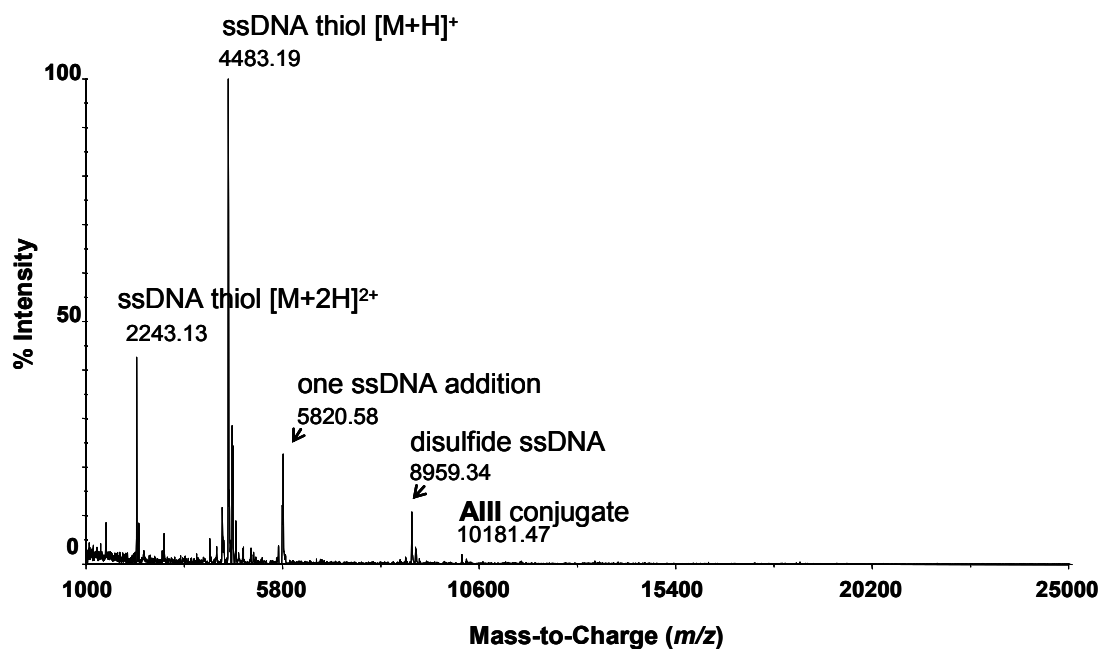
Figure 2-7. MALDI-TOF spectrum corresponding to crude **AIII**.

Evidence for AIII from gel electrophoresis. Crude reaction material from the conjugation of 2 equivalents of thiol-terminated 12 mer ssDNA with the dithiopyridyl dendrimer shown in Scheme 2-2, was run on a 20% polyacrylamide gel with 12-mer ssDNA post-reduction with TCEP. As shown in Figure 2-8, the thiol-terminated 12-mer and the auto-oxidized 12-mer disulfide were visible in lane 1 after ethidium bromide staining. In lane 2, a significant amount of starting material was present relative to the products corresponding to singly and doubly substituted dendrimer. As demonstrated for the **AII** conjugate, the conjugation reaction did not appear to go to completion owing most likely to the competing auto-oxidation reaction between thiol-terminated 12-mers.

The intensity of ethidium bromide staining for thiol- and disulfide- ssDNA relative to ssDNA-dendrimer is consistent with MALDI-TOF relative intensities. Poor yields precluded the ability to visualize the dendrimer by coomassie staining, which has a detection limit in the 0.5 µg range for large proteins vs. ethidium bromide which can detect as little as 1 ng plasmid DNA.[116]
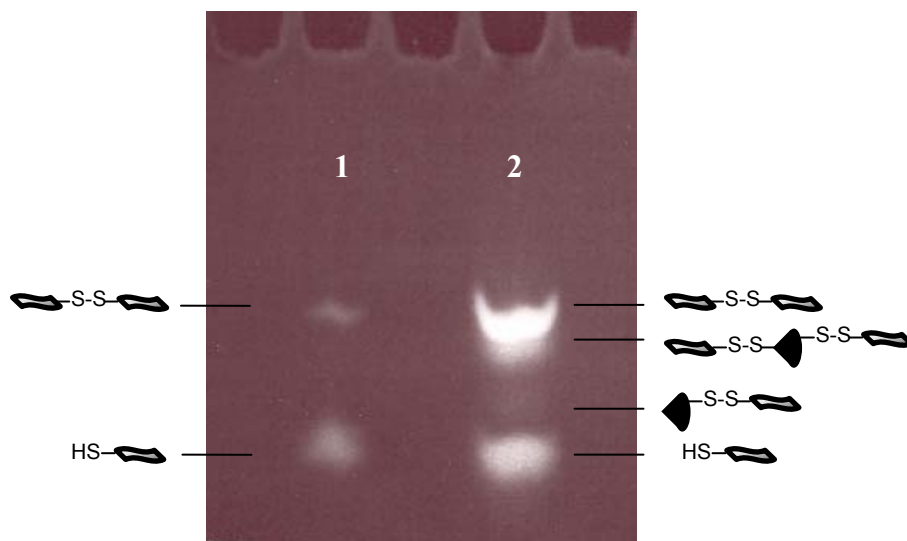
Figure 2-8. Ethidium bromide stained 20% Polyacrylamide gel of crude **AIII**.

Evidence for BI from MALDI-TOF. The 12-mer oligonucleotide sequence for **BI** formation was: (Oregon Green)5′-TAGGCGTTACGC-3′(C3-SH). A difference spectrum (Figure 2-9, C) was used to determine if low molecular weight signals were arising from the ssDNA, or if they were impurities from the conjugation reaction. A spectrum of purified oligonucleotide (Figure 2-9, B) was subtracted from the signals

arising from the conjugate reaction material (Figure 2-9, A). Only signal corresponding to the formed DNA-dendrimer conjugates remained. The peak at 5560 arose from the presence of the G2 monochloride intermediate shown in Scheme 2-4. The $[M + H]^+$ calculated for DNA-dendrimer **BI** was 7226.4, and signal was observed at 7227.3.
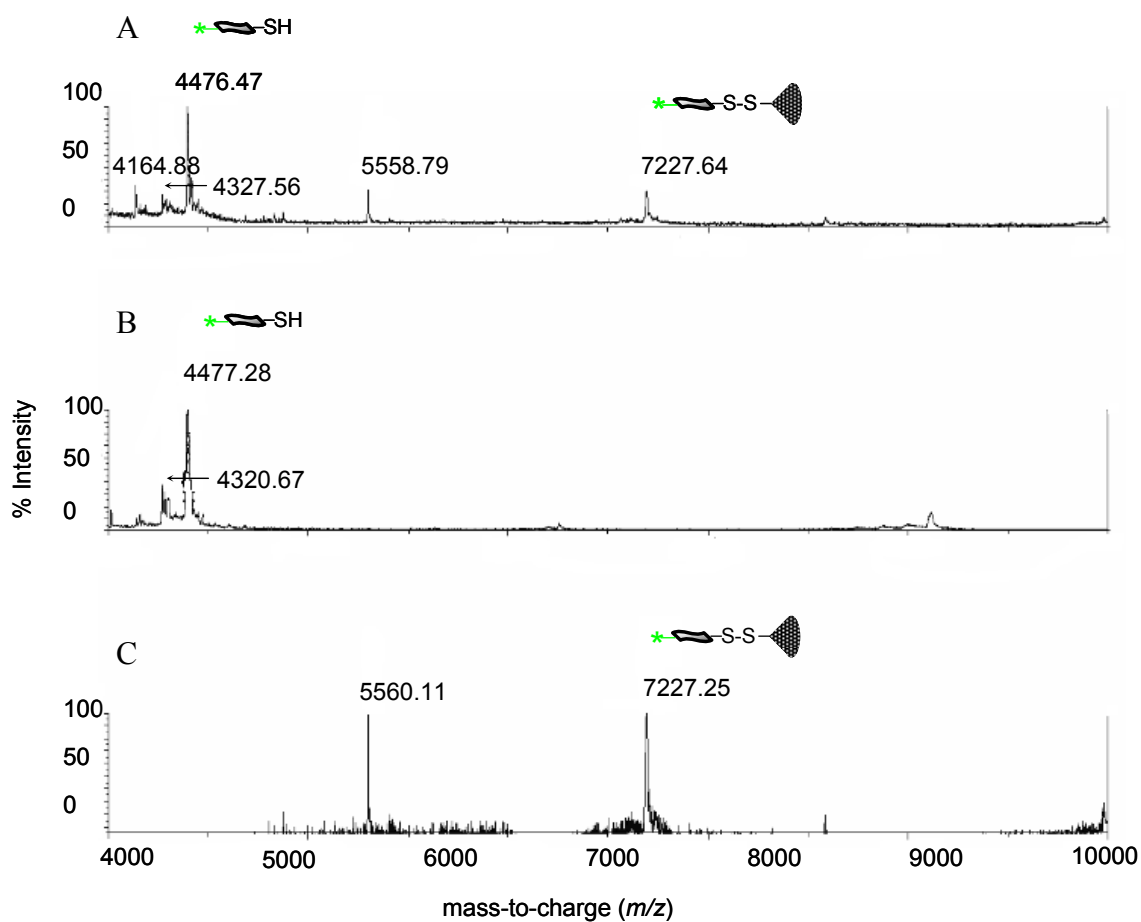
Figure 2-9. MALDI-TOF spectra corresponding to **BI**, G3 dendrimer − 12-mer ssDNA. A corresponds to crude product, B corresponds to HPLC-purified ssDNA starting material, and C is the difference spectrum obtained by subtracting B from A.

Evidence for BI from gel electrophoresis. Throughout the course of these studies, attempts to observe G3 dendrimer-ssDNA conjugates were never successful. Neither ethidium bromide nor coomassie staining ever revealed or suggested the presence of the conjugate, yet after extensive de-salting procedures, a G3-12-mer was in fact observed by MALDI-TOF (see *MALI-TOF evidence for BI*). It was suspected that either the dendrimer was too bulky to penetrate the polyacrylamide matrix, or the positively charged dendrimer would not travel toward the cathode, or both. To determine if the dendrimer-ssDNA conjugate was in fact trapped in the loading well, a gel was run according to the procedures outlined above, then left intact. That is, the glass plates sandwiching the gel were not removed, and the gel was visualized on a fluorescence macroscope, provided by Dr. Paul Cremer, Texas A&M University, Department of Chemistry. We conclude that Oregon-green labeled ssDNA 12-mer was trapped in the loading well. Unconjugated ssDNA, loaded in an adjacent well was not observed in the well. As shown in Figure 2-10, the outline of the well is evident as a result of the Oregon green fluorescence emission. Unconjugated ssDNA was observed as a band in the gel, consistent with MALDI data indicating incomplete conjugation.
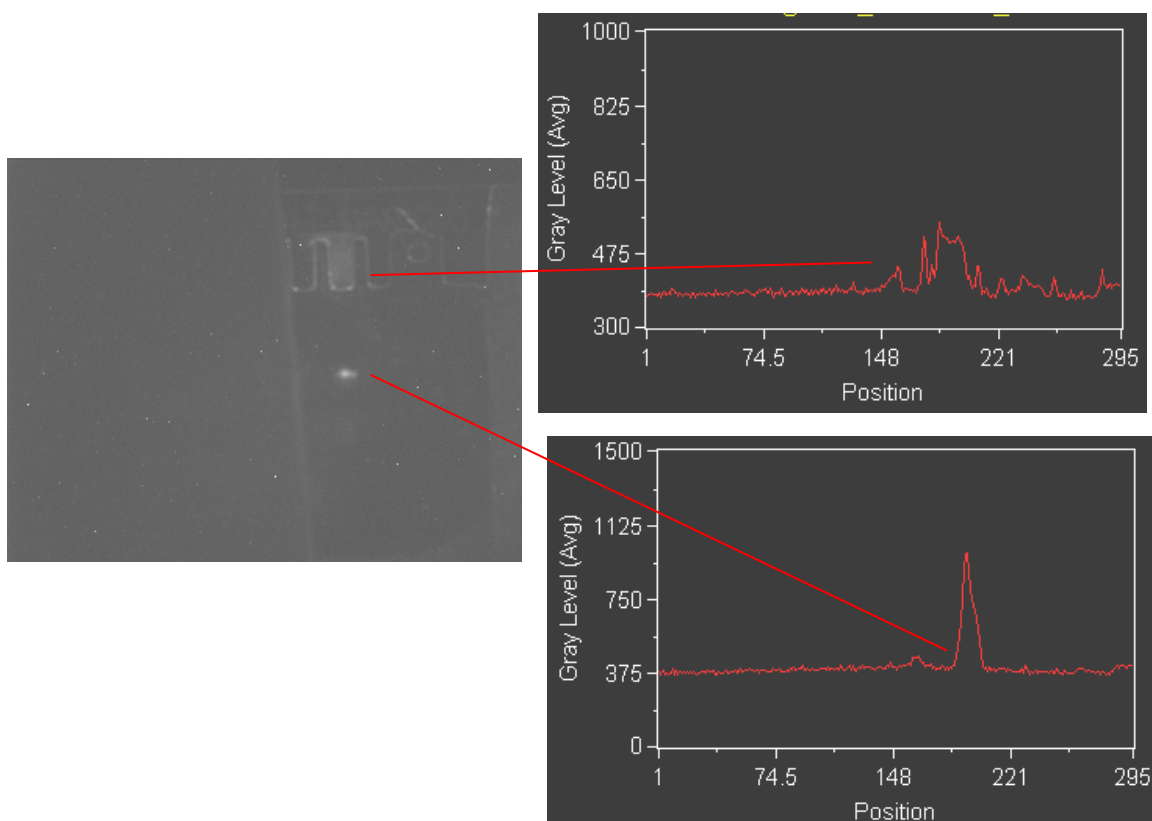
Figure 2-10. PAGE gel of **BI** prior to removal from glass plates showing that the fluorescently labeled DNA-dendrimer conjugate does not penetrate the gel. The band in the gel corresponds to unconjugated ssDNA.

Evidence for BII from MALDI-TOF. As indicated previously, there are two potential linking motifs for the DNA-dendrimers: electrostatic and covalent. The mass difference between these two adducts is only 2 Da. Nevertheless, it is possible to distinguish between the two theoretical products using accurate-mass MALDI-TOF

analysis. With bovine insulin as an internal calibrant (insulin mass to charge ratio *(m/z)* $[M + H]^+ = 5734.39$), the measured $[M + H]^+$ *m/z* of **BII** was 5561.97 (Figure 2-11 B). This compared with the expected $[M + H]^+$ of 5561.76, corresponding to an error of only 36 ppm. An electrostatic adduct ($[M + H]^+ = 5563.85$) would have resulted in a much larger mass error of 200 ppm. When insulin was used as an external calibrant, that is it was not mixed with the sample being analyzed, $[M + H]^+$ *m/z* of **BII** was observed at 5561.62 (Figure 2-11 A).

In addition to mass spectrometry, Ellman's test (for free thiol) was used to distinguish between covalent and electrostatic attachment of DNA to the dendrimers. Ellman's reagent oxidizes free thiols to mixed nitrobenzyl disulfides, which are easily identifiable by mass spectrometry. No Ellman's adduct was observed for **BII**. Addition of a reducing agent, TCEP, to **BII** led to the disappearance of MALDI-TOF signal corresponding to the ssDNA-dendrimer conjugate and disulfide modified ssDNA, as shown in Figure 2-12. The disappearance of both disulfides confirmed that the ssDNA was linked to the dendrimer *via* disulfide bond formation.
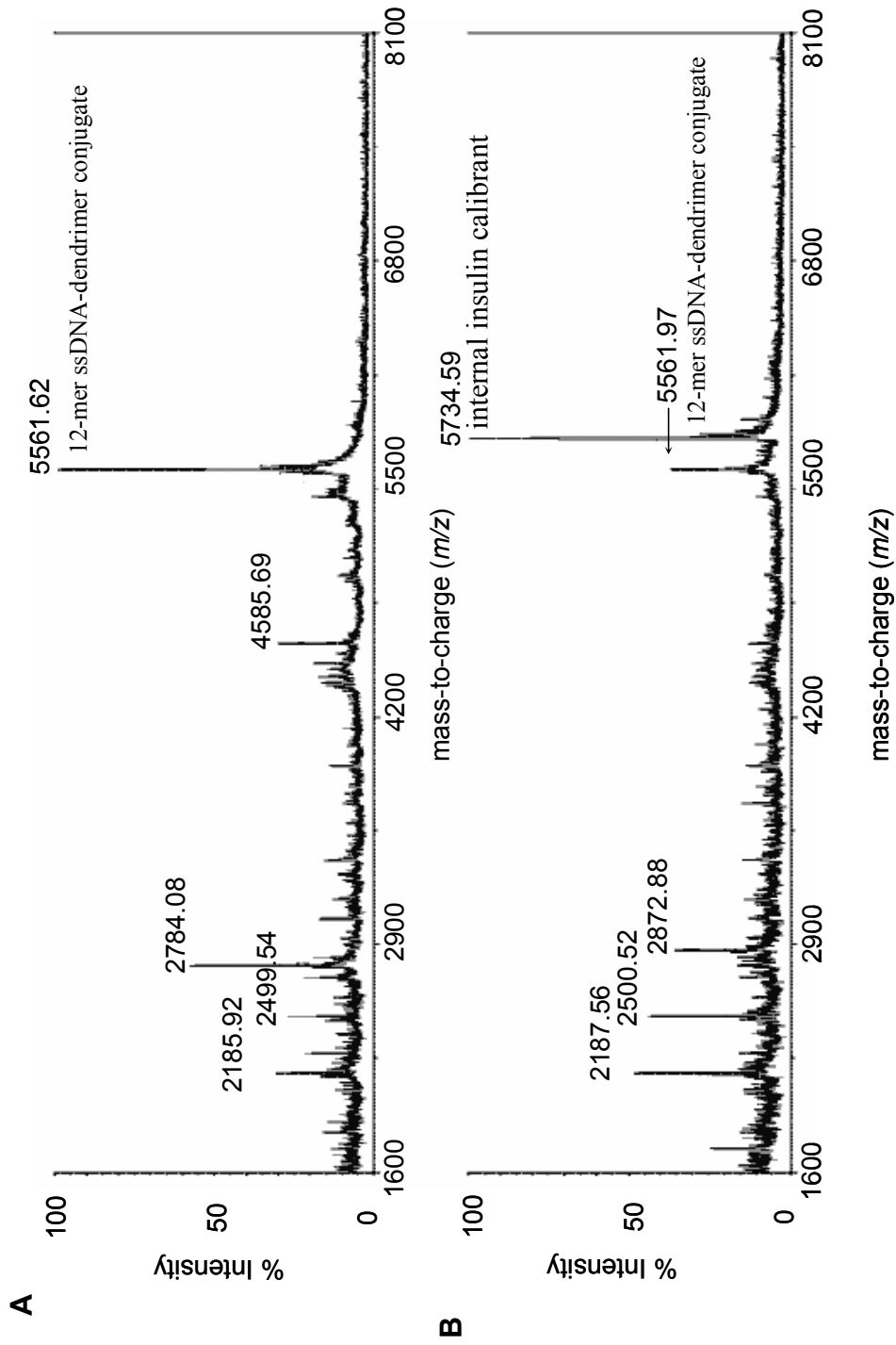
Figure 2-11. MALDI-TOF spectra corresponding to (A) externally calibrated **BII** and (B) internally calibrated **BII** using insulin (MW ~ 5735) as the calibrant.
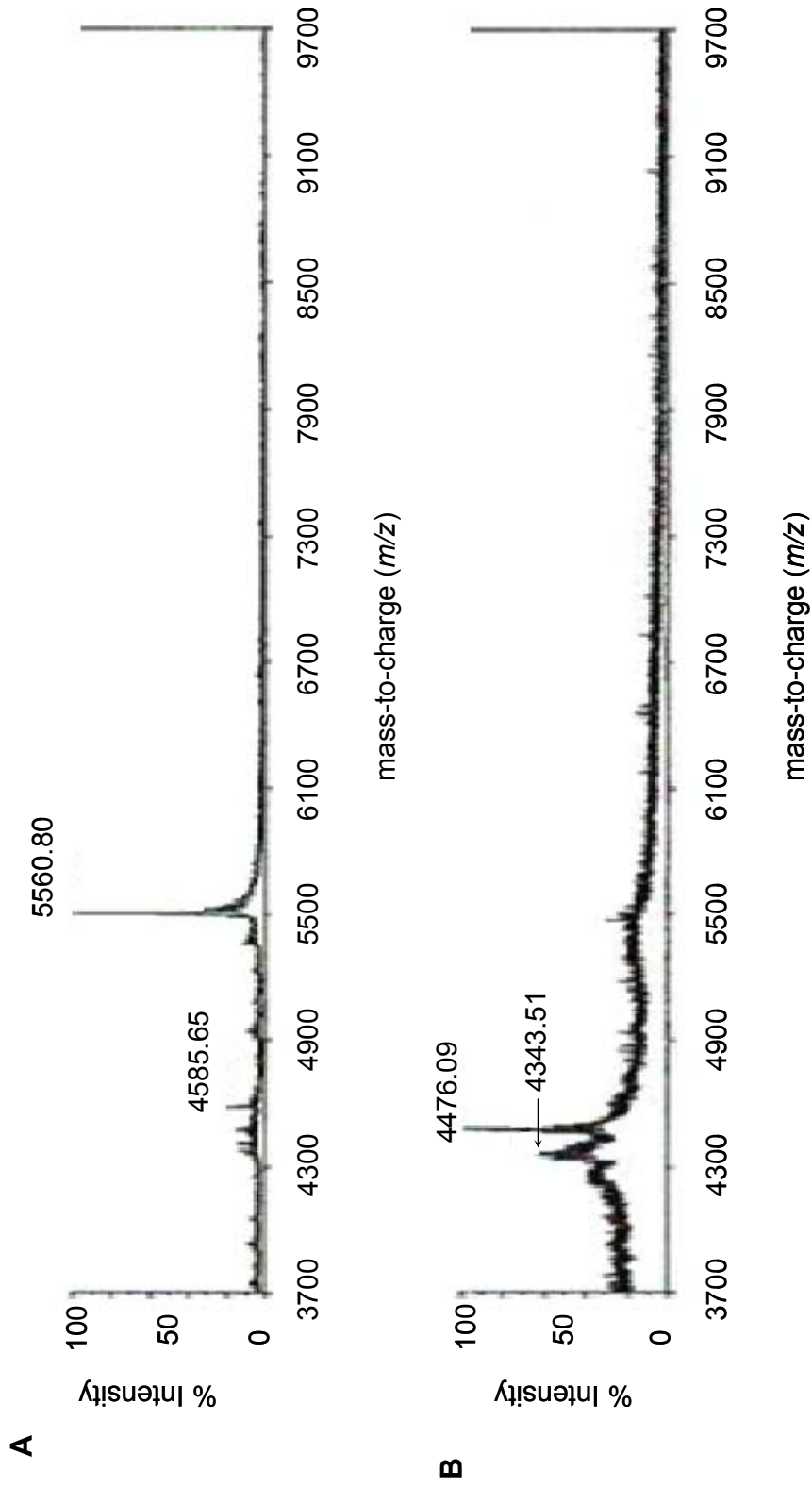
Figure 2-12. MALDI-TOF spectra corresponding to (A) intact **BII** conjugate mode and (B) subsequent

TCEP-reduced thiol-terminated ssDNA.

Scheme 2-10

$C_{151}H_{184}F_5N_{46}O_{83}P_{13}S_3$
Exact Mass: 4562.73
Mol. Wt.: 4565.19

Scheme 2-11

$C_{148}H_{178}F_5N_{46}O_{82}P_{13}S_2$
Exact Mass: 4472.71
Mol. Wt.: 4475.04
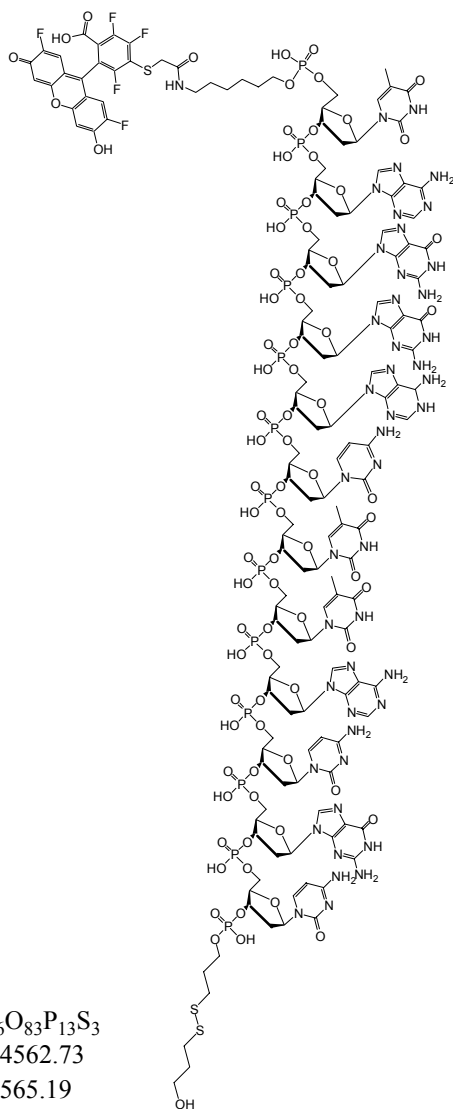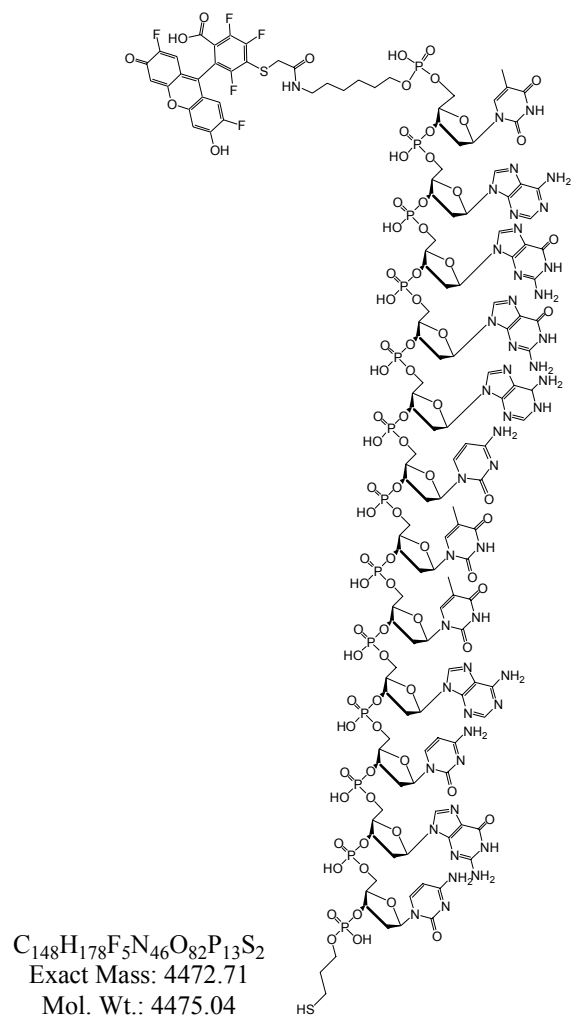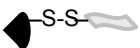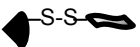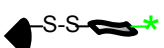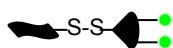
Evidence for BIII from MALDI-TOF. Mass spectrometry data clearly indicates that the majority of the ssDNA remained unbound to the dendrimer, as both peaks corresponding to the approximate molecular weight of dendrimer and ssDNA are present in the spectrum. The broadness of the peaks indicates the saltiness of the sample. Each phosphate on the ssDNA backbone can accommodate a sodium or potassium ion, giving rise to the observed mass distribution. A comparison of theoretical and experimental MALDI values for **AI** through **BIII** is shown in Table 2-2.
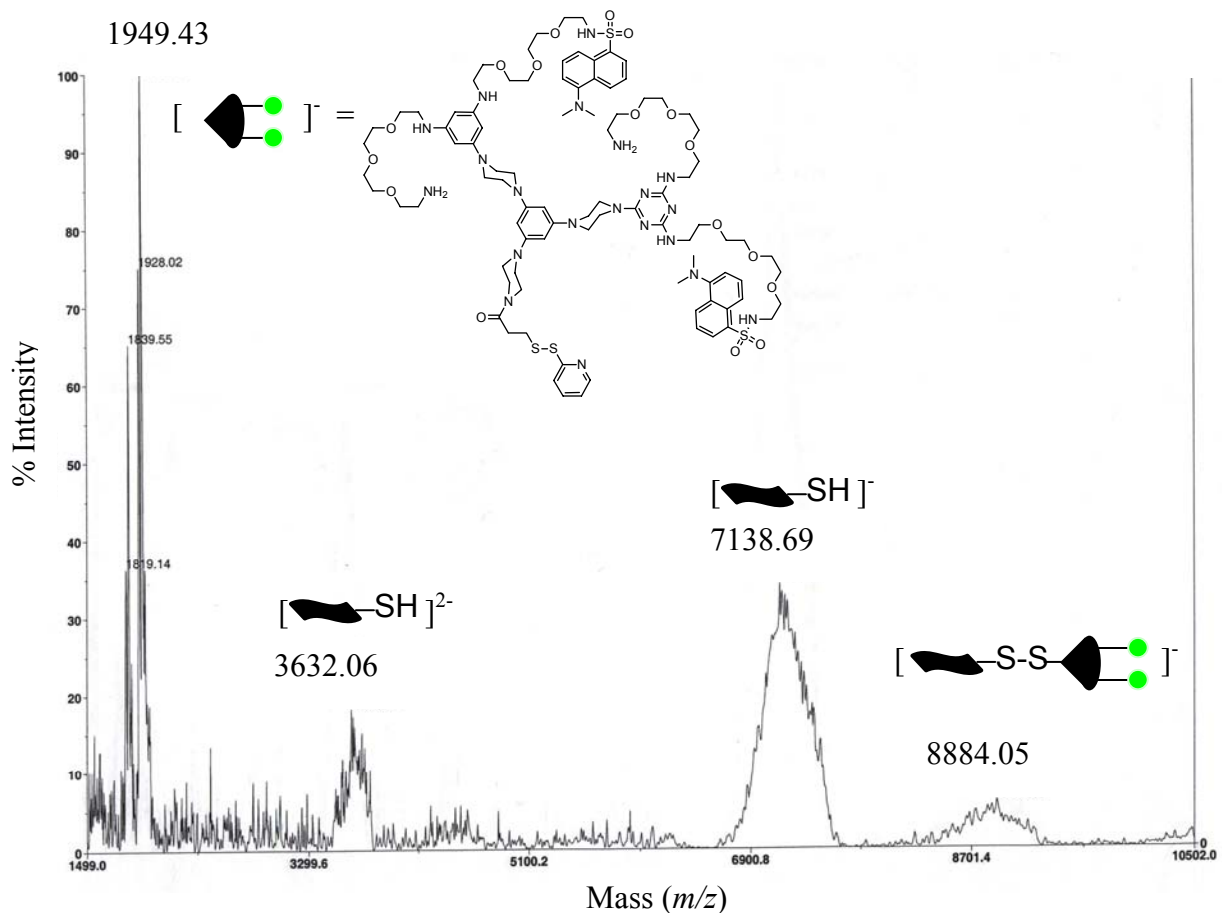
Figure 2-13. MALDI-TOF data indicating the presence of **BIII**, and demonstrating the effect of trace salt contamination on mass spectral data acquisition.

Table 2-2. Comparison of theoretical and experimental MALDI *(m/z)* values.

		Calculated *(m/z)*	Found *(m/z)*
AI		10,725.0	10,724.8
AII		4,863.3	4,863.1
AIII		10,161.2	10,171.1
BI		7,228.4	7,227.3
BII		[†]5,561.76	5,561.97
BIII		[††]8,641 - 9,147	8,884.1

[†] Used internal and external mass calibration for greater accuracy.
[††] Product not subjected to stringent de-salting procedures, so a broad signal corresponding to all possible sodium additions across the sugar-phosphate backbone resulted.

CONCLUSIONS

A synthetic route toward ssDNA-dendrimer constructs has been presented and the nature of their interaction has been unambiguously proven to be covalent rather than electrostatic. The motivation for using cationic dendrimers stems from both the high water solubility that these groups afford, and the opportunity for electrostatic binding with ssDNA, which may be useful for enhancing the rate of covalent bond formation between the two species.

Successful bulk-phase DNA computing requires the synthesis of soluble DNA-bearing macromolecules that display a certain number of ssDNA strands of designated sequences. The final construct must offer a means to easily manipulate the attached DNA sequences and allow for routine spectroscopic analysis. To this end we have synthesized dendrimers based on melamine to contain a specific number of fluorophores and a specific number of covalently bound DNA strands.

CHAPTER III

THE DETECTION OF DNA HYBRIDIZATION OF DNA-DENDRIMER

CONSTRUCTS ON SURFACES

BACKGROUND

DNA hybridization, or dsDNA formation, of DNA- dendrimer constructs was detected using three different surface analysis techniques: Fourier transform infrared external reflection spectroscopy (FTIR-ERS), fluorescence imaging, and surface plasmon resonance imaging (SPRi). FTIR/ERS data shows evidence for surface hybridization of disulfide-linked, dansyl-functionalized DNA-dendrimer constructs with surface-bound probe DNA. Fluorescence imaging of a patterned ssDNA surface, created using μ-contact printing, clearly shows that binding of these DNA-dendrimer conjugate occurs predominately in the regions containing covalently bound complementary probe ssDNA.

Covalently attached dendrimers without fluorophore labels were shown to inherently increase the sensitivity of SPRi, which simultaneously detects changes in refractive index across an entire microarray. SPRi has been shown to effectively measure bioaffinity interactions including DNA hybridization without the use of expensive labels or radiological tags.[117] Imaging experiments, unlike conventional SPR experiments however, are performed at a fixed angle of incidence resulting in decreased sensitivity. To compound matters, the concentration of biological targets such as DNA, proteins or antibodies often approaches the limits of detection using many surface analysis techniques including SPR.

Second generation dendrimers based on melamine are shown to enhance SPR signal by increasing the molecular mass of the covalently bound target DNA, resulting in a proportionate change in refractive index. Dendrimers based on melamine have several surface groups for oligonucleotide attachment so they possess the ability to further increase signal as a function of dendrimer size, or generation, and number of attached oligonucleotides.

SPR allows for the analysis of weak interactions between unlabeled biomolecules, thus circumvents the need to work with expensive fluorescent or potentially harmful radiological labels. To date, the most commonly used methods for increasing the sensitivity of SPR measurements rely on *secondary* signal enhancement, meaning that the signal enhancement event follows the measured recognition event, in this case hybridization. The proposed method is inherently more accurate, because the source of SPR signal amplification is the molecule participating in the recognition event, *ie*. the DNA-dendrimer conjugate.

Currently, the most popular form of secondary signal enhancement in SPR is based on the enzyme-linked immunosorbent assay (ELISA) system, or sandwich assay.[118] This method either measures or takes advantage of highly specific antigen-antibody interactions at the surface. Once an antibody, referred to as the primary antibody, is target-bound, it serves as the target for yet another antibody, termed the secondary antibody. In conventional ELISA, the secondary antibody is attached to an enzyme that converts a given substrate into a readily detectable chromagen. SPR eliminates the need to rely on chromagenic detection and the activity of highly pH and temperature sensitive enzymes, and instead measures the secondary antibody directly. Liposomes[119] and latex

particles[120] have been used in conjunction with the sandwich assay to further enhance SPR signal. With respect to surface bound oligonucleotides, the polymerase chain reaction (PCR)[121] and rolling circle amplification (RCA)[122] have gained the most attention as sources of signal enhancement, but PCR has its drawbacks in surface analysis. RCA became more popular for use in microarrays due to the ability to localize amplified DNA and thus prevent interactions among DNA strands that originated from different locations on the array. Again, by coupling DNA-dendrimer conjugates with SPR analysis, measurements can be made directly without the need to perform enzymatic reactions. Colloidal gold particles,[123] nanoparticles,[124] cationic latex[125] and biotin-streptavidin systems[126] have also been used to enhance SPR signal, but like all of the other examples, these methods rely on a secondary event for signal enhancement.

The ability to engineer a certain number of unique reactive sites on the periphery of the dendrimer offers a degree of control and flexibility that is unparalleled by other microarray-based, label-free detection strategies. [127] Branched oligonucleotides, or "DNA dendrimers" have been prepared with similar goals in mind, however, the labile nature of the proposed DNA-dendrimer disulfide linkages offer reversibility and the opportunity to attach bioaffinity targets other than DNA.[128]

EXPERIMENTAL PROCEDURES

Materials. Reagents for monolayer formation, 11-Amino-1-undecanethiol, hydrochloride ($HSC_{11}H_{22}NH_2$, 98%, Dojindo Molecular Technologies, Inc.) and 11-mercapto-1-undecanol ($HSC_{11}H_{22}OH$, 97%, Aldrich Chemical Co.) were used as

received. The lyophilized powders were dissolved in UV/UF purified (Barnstead) water [0.1 OD/μL]. Positive photoresist (AZP4620) and developer solution were obtained from the Clariant Co. (Somerville, NJ). Poly(dimethylsiloxane) (PDMS) elastomers were obtained from Dow Corning (Sylgard 184, Midland, MI). Gold-coated substrates were prepared by electron-beam evaporation of 10 nm of Ti followed by 200 nm of Au onto Si(100) wafers (Lance Goddard Associates, Foster City, CA). The wafers were subsequently diced into 2.6 cm x 1.3 cm pieces. Before each experiment all wafers were cleaned in low-energy ozone cleaner for 10 min (Boekel Industries, Inc., model 135500).

Synthesis of fluorescent ssDNA-dendrimer for FTIR and micropatterning. Synthesis of the dansylated second generation dendrimer (**5**) used in FTIR and fluorescence imaging experiments was discussed in Chapter II (Scheme 2-1). Subsequent characterization of the disulfide-linked ssDNA-dendrimer formed from disulfide exchange between a thiol-terminated 22-mer ssDNA and **5** was also presented in Chapter II (to yield conjugate **BIII**). The procedure outlined in Chapter II for reduction of disulfide modified ssDNA to form thiol-terminated ssDNA was improved upon for this work as detailed below for the synthesis of 31-mer conjugates. Figure 3-1 illustrates the effectiveness of the improved method by MALDI-TOF. Peaks are resolved indicating decreased salt content, and thiol-terminated ssDNA has been effectively separated from incompletely reduced ssDNA.
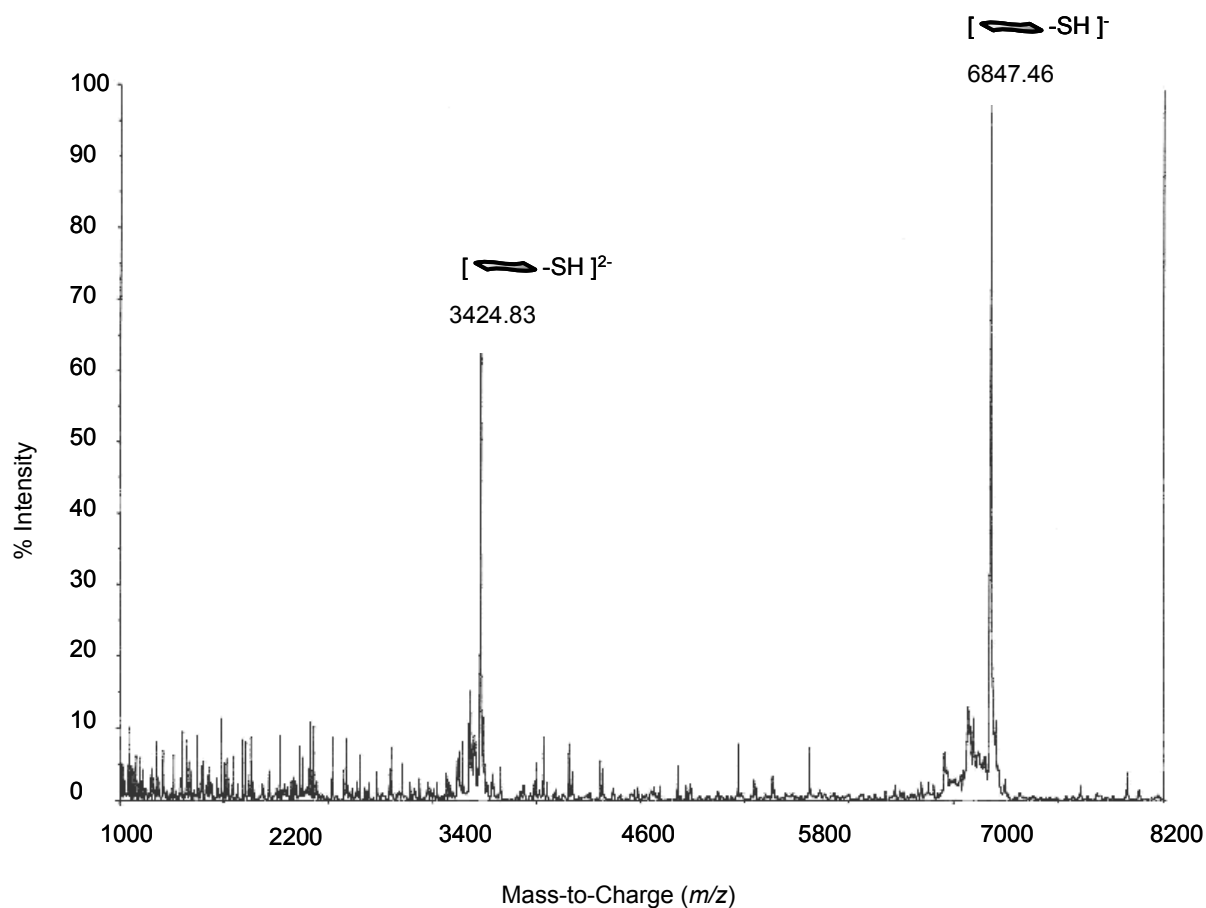
Figure 3-1. MALDI-TOF spectrum of 22-mer illustrating improved thiol deprotection and de-salting techniques.

To prepare the conjugate, thiol terminated DNA was reacted with 1 eq. thiopyridyl functionalized dendrimer in 0.1 M TEAA pH 7, at room temperature for 12 hours. Separation of the conjugate from the unreacted oligonucleotide and dendrimer was accomplished by centrifugation of the sample for 2 hours on Microcon 10,000 MWCO spin filters (Millipore) at 6,500 RPM. The sample was desalted by adding ultrapure water

to the sample retained in the spin filter, equal to the volume of filtrate, once every 30 minutes for 5 cycles.

Surface attachment of ssDNA. Surface attachment (and subsequent surface analysis) was performed by Dr. Sang-Keun Oh and instrumentation provided by Dr. Richard Crooks, Texas A&M University. Gold coated substrates were immersed in a mixed ethanolic solution of 1 mM amine- and hydroxy-terminated alkanethiols (9:1 $NH_2(CH_2)_{11}SH : HO(CH_2)_{11}SH$) for 24 hours. The substrates were removed and rinsed with ethanol and water, and dried with N_2. The heterobifunctional crosslinker, sulfosuccinimidyl 4-(N-maleimidomethyl) cyclohexane-1-carboxylate (SSMCC), was used to convert the amine terminated SAM to an SSMCC activated surface by immersing the substrates in a 1 mM SSMCC solution in 0.1 M TEA (pH 7.1) for 30 minutes. After rinsing the surface with DMF and water, 2 μL 1 mM thiol terminated ssDNA in 0.1 M TEA (pH 7.1) was spotted onto the SSMCC activated surface. The surface was covered with a cover glass in a humidity chamber for 6 hours. The DNA exposed surface was rinsed with water, soaked for 1 hour in 2X SSPE (20 mM NaH_2PO_4, 300 mM NaCl, 2 mM EDTA), 0.2% (7 mM) SDS buffer to remove non-specifically adsorbed DNA, and thoroughly rinsed with water. Hybridization was performed by immersing the DNA modified substrates in a 2 μM solution of complementary ssDNA-dendrimer conjugate in 2X SSPE buffer.

Scheme 3-1

Surface patterning of ssDNA. PDMS stamps were made by casting the prepolymer components of Sylgard 184 on a photopolymer master made by photolithography. Patterned SAMS were prepared by microcontact printing (μCP) of a 2 μM ethanolic solution of hexadecane thiol on a gold coated surface using polydimethylsiloxane (PDMS) stamps followed by immersion in a 1 mM mixed solution of 9:1 $NH_2(CH_2)_{11}SH$: $HO(CH_2)_{11}SH$ for 2 hours to fill the unprinted region. Printed

regions were prepared according to the method outlined above for ssDNA surface attachment.

Characterization of patterned DNA surfaces. FTIR-external reflection spectroscopy (FTIR) measurements were carried out using an FTS-6000 spectrometer (Bio-Rad, Cambridge, MA) equipped with a Harrick Scientific Seagull reflection accessory (Ossining, NY) and a liquid-N_2-cooled, narrow-band MCT detector. All spectra were obtained at 4 cm^{-1} resolution using *p*-polarized light at an 84° angle of incidence with respect to the Au substrate. Fluorescence images of the patterned DNA surfaces were acquired with a fluorescence microscope (Nikon Eclipse TE 300, Nicon Co., Tokyo, Japan) equipped with band-pass filters, a 100 W mercury lamp, and a charged-coupled device camera (Photometrics Ltd., Tucson, Arizona). The patterned DNA surfaces were placed face down in a droplet of 2×SSPE buffer on a glass coverslip placed on the microscope stage, and the fluorescence images were collected.

Synthesis of 31-mer ssDNA-dendrimer for SPRi. The 31-mer G2 ssDNA-dendrimer constructs used for SPRi work were synthesized according to the method reported in Chapter II to yield **AI (a)** and **AI (b)**. Oligonucleotide words **W1** and **W2** (W for *words*) were synthesized on an automated synthesizer in Robert Corn's Lab at University of Wisconsin, Madison. The 5′ thiol modified 31-mer oligonucleotides:

5′ DMT- C_6H_{12}-S-S-C_6H_{12}-TTT TTT TTT TTT TTT AGA CTC TGA CTC AGT G 3′

and

5′ DMT- C_6H_{12}-S-S- C_6H_{12}-TTT TTT TTT TTT TTT ATG CTT CGA TGC AAC G 3′

were synthesized by Trilink Biotechnologies on a 0.2 μmole scale. HPLC purified

oligonucleotides were shipped as lyophilized powders and reconstituted just prior to use

in ultrapure water at a concentration of 0.1 ODs/ μL. For products reported herein, the 5′

thiol modifier was removed by incubating 0.1 μmole oligonucleotide with immobilized

TCEP (Pierce). The procedure outlined in Chapter II for DNA–dendrimer conjugation

was improved upon for this work. Originally, this procedure yielded approximately 80

nmoles thiol terminated oligonucleotide which was then incubated at room temperature

with 1.25 eq. thiopyridyl functionalized dendrimer to yield the disulfide linked conjugate.

An alternate improved method for reduction of thiol modified oligonucleotides was to

dissolve the lyophilized oligonucleotides in 100 μL 0.1 M DTT, 0.1 M TEAA pH 7 for

30 minutes at room temperature to yield the 5′ oligonucleotide thiol and the

dimethoxytrityl (DMT) protected thiol modifier. The DMT protected thiol modifier was

the cause of greatly reduced yields in prior syntheses, so it was removed from the

oligonucleotide solution on a Poly Pak cartridge (Glen Research). The cartridge was

equilibrated with 2 mL HPLC-grade acetonitrile followed by 2 mL 2M TEAA pH 7. The

reduced oligonucleotide was diluted to 5 mL and loaded onto the cartridge. The cartridge

was flushed with 3 mL 0.1 M TEAA pH 7, followed by 10 mL 5% acetonitrile in TEAA

to remove the DTT. Oligonucleotides were eluted in 500 μL 50% acetonitrile in water,

while DMT protected thiol modifier remained bound to the cartridge. Mass spectrometry

was able to demonstrate the improved efficiency of the DTT mediated thiol deprotection

protocol relative to the previously employed deprotection on TCEP gel. There was no

evidence of incompletely reduced 25-mer, and the DTT removal on the Poly-Pak

cartridge also accomplished significant desalting, greatly improving the peak resolution by MALDI-TOF.

Surface Plasmon Resonance imaging (SPRi). Gold surfaces were patterned according to the methods used above for *Surface Patterning of ssDNA* and *Surface Attachment of ssDNA*. The instrumentation used for SPRi measurements is shown in Scheme 3-2, obtained with permission from authors, as published in *Annual Reviews of Physical Chemistry*, **2000**, *51*, 41-63 (Appendix B).

Scheme 3-2
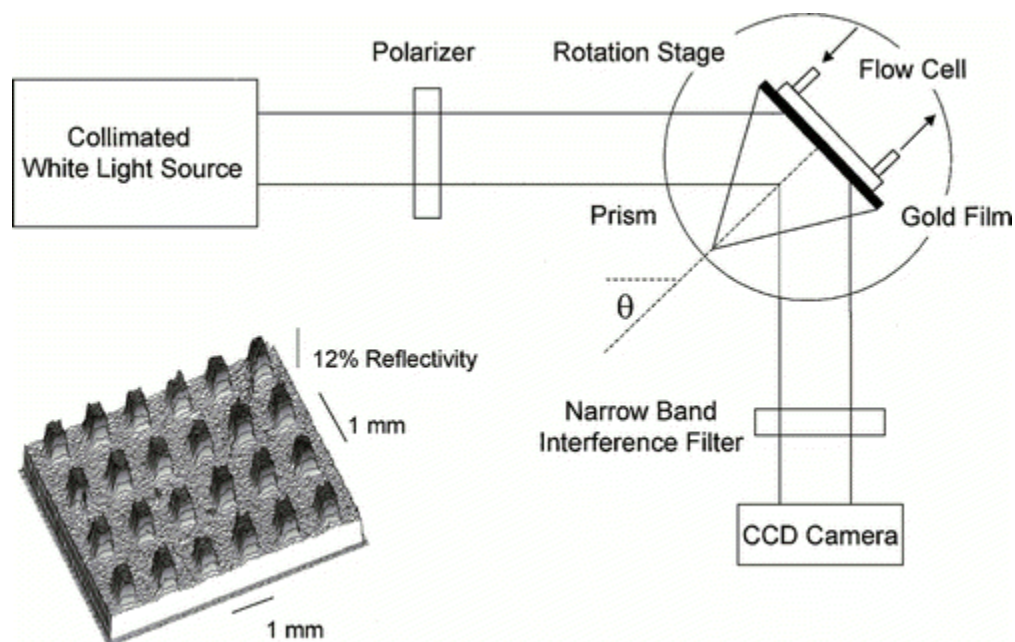
Briefly, light from a collimated polychromatic source was passed through a polarizer and onto a prism/Au sample assembly at a specific angle of incidence (θ). The reflected light

then passed through a narrow-band interference filter and was detected with a CCD camera. An image of an oligonucleotide array onto which ssDNA-dendrimer conjugates **C1** and **C2** were bound is shown on the lower left in Scheme 3-2.

RESULTS AND DISCUSSION

FTIR. Figure 3-2 shows the FTIR spectra corresponding to each modification step. Spectrum A corresponds to the product of SSMCC activation. The appearance of a peak at 1710 cm^{-1} arising from the in-phase stretch of the maleimide carbonyl groups confirms the presence of the thiol-reactive maleimide groups on the surface. Unfortunately, spectrum B does not differentiate the carbonyl groups in the previous step from the carbonyl groups on the nucleotide bases. Thus the success of the surface attachment of ssDNA was not determined at this time. However, addition of ssDNA-dendrimer conjugate **BIII** (Chapter II) to the surface bound probe ssDNA resulted in a loss of signal at 1710 cm^{-1}, indicating the absence of carbonyl functionality at the surface and an enhanced signal around 1100 cm^{-1} indicating the presence of carbon-oxygen single bonds corresponding to the peg groups along the periphery of the dendrimer.
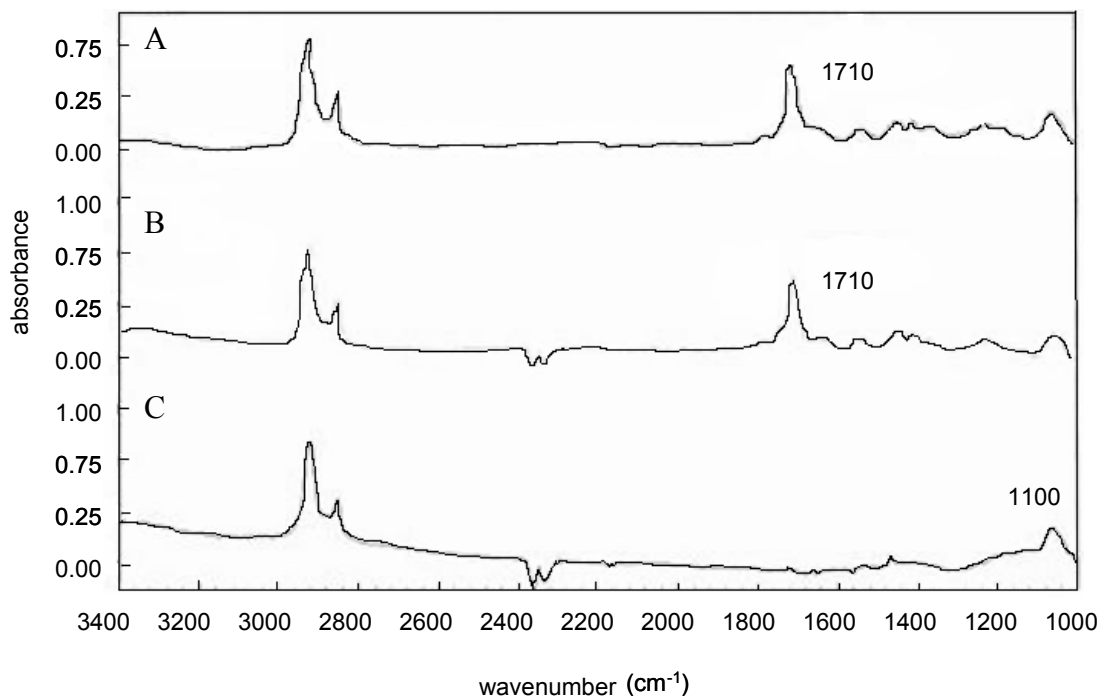
Figure 3-2. FTIR spectra showing: (A) the presence of maleimide carbonyl groups, (B) presumably the nucleotide carbonyl groups, which also give rise to a stretch ~1710 cm^{-1}, and (C) the carbon-oxygen single bonds (1100 cm^{-1}) arising from the PEG-functionalized dendrimer upon hybridization with ssDNA-dendrimer conjugate.

Surface patterning. Fluorescence imaging of the resulting DNA surface clearly shows that binding of the ssDNA-dendrimer conjugate occurs predominantly in the regions that contain covalently bound, complementary ssDNA. In Figure 3-3, the light (or bright green) areas correspond to those areas containing the surface-bound probe ssDNA. The resulting bright square regions arise from the fluorescence signal corresponding to the ssDNA-dansyl-modified-dendrimer conjugate that has successfully base paired with surface-bound ssDNA. The dark regions correspond to areas that do not contain surface-bound complementary ssDNA and thus do not retain fluorescent dendrimer. This

experiment indicates that the ssDNA surface attachment was successful and suggests that the ssDNA-dendrimer-modified surface might be useful for the development of functional DNA microarrays and templates for further fabrication of nanostructures. Subsequent wash-off experiments of these surfaces showed no reduction in the fluorescence intensity, further indicating that the nature of the interaction between the dendrimer and ssDNA is a covalent bond.
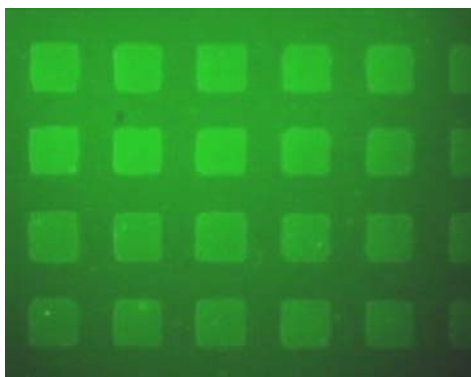
Figure 3-3. Micropatterned surface showing preferential hybridization of dansyl containing ssDNA-dendrimer conjugate (**BIII**) to areas on the surface containing complementary surface bound ssDNA.

Surface plasmon resonance. Since the thermodynamic stability of DNA is dependent upon the number of guanine-cytosine (G/C) base pairs, all oligonucleotides were designed to contain the same G/C content. Consequently, their masses are identical, and the masses of their complements and dendrimer-bound complements, referred to as **C1** and **C2** (C for *complements*) in this chapter (**AI (a)** and **AI (b)** in Chapter II), are

identical. Table 3-1 displays the oligonucleotide sequences for **W1**, **W2**, **C1**, and **C2**.

MALDI characterization for these conjugates was discussed in Chapter II.

Table 3-1. Sequence information for oligonucleotide words (W) and dendrimer-bound complements (C).

Name	Sequence Identity	Cartoon
W1	5′ C ACT GAG TCA GAG TCT 3′	
W2	5′ C GTT GCA TCG AAG CAT 3′	
C1	5′ ◆ TTT TTT TTT AGA CTC TGA CTC AGT G 3′	
C2	5′ ◆ TTT TTT TTT ATG CTT CGA TGC AAC G 3′	

A surface array was constructed with two DNA strands, or words (**W1** and **W2**) of the same molecular mass, but with different sequences. The pattern of immobilized DNA probes **W1** and **W2** is shown in Scheme 3-3 (A). A side view of the surface array is shown in (B). The side view after exposure to **C2** is shown in (C), and after exposure to **C1** is shown in (D).

Scheme 3-3.

A

B

C

D
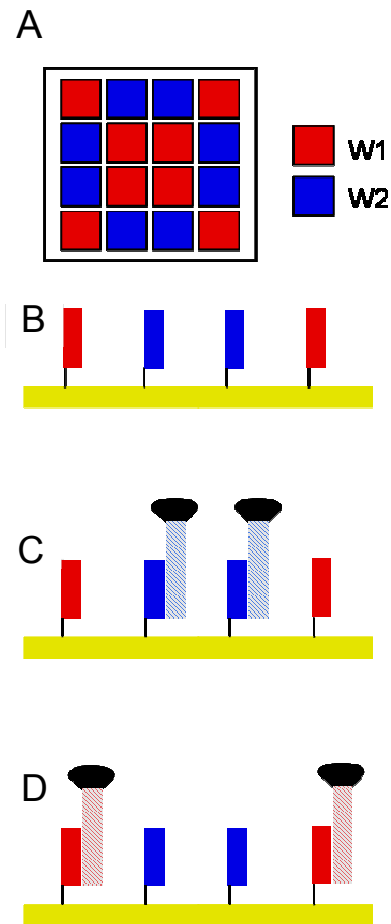
SPRi revealed the hybridization of compliment **C1** to the immobilized probe **W1**, but not to mismatch **W2** resulting in the SPR image and linescan shown in Figure 3-4 (A). Likewise, **C2** hybridized specifically with **W2** in the presence of **W1**, as shown in Figure 3-3 (B).
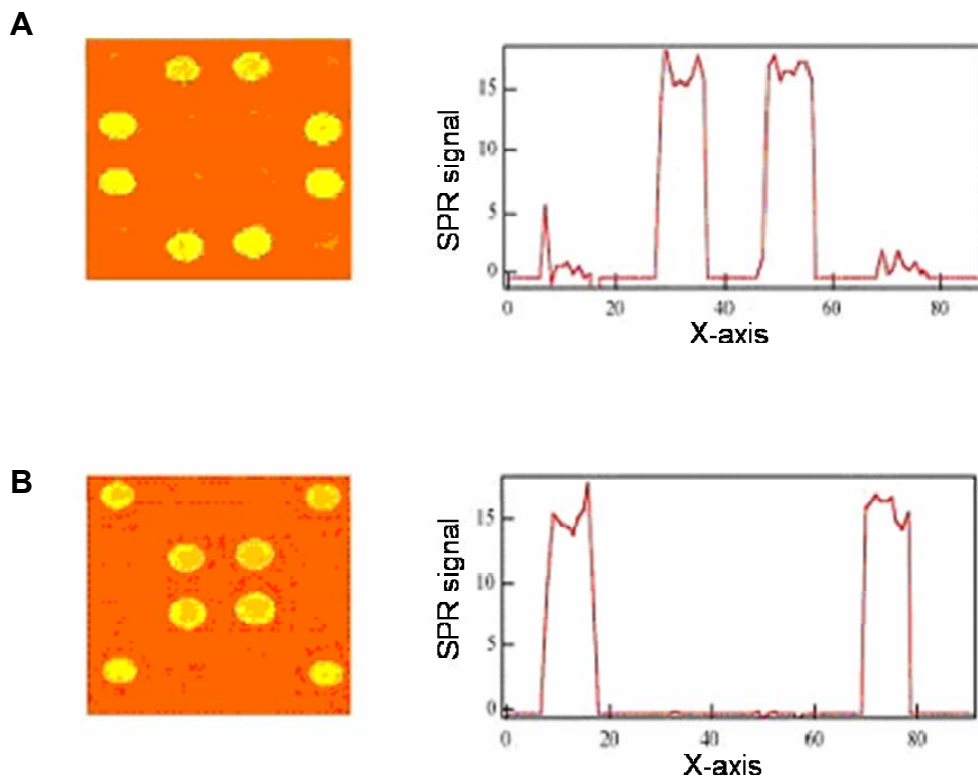
Figure 3-4. SPR image and linescan of (A) **C1** and (B) **C2** hybridized to surface-bound complement words, **W1** and **W2** respectively.

Hybridization of complementary ssDNA with no bound dendrimer revealed a similar SPR image, but required higher sample concentration to make up for decreased sensitivity. Thus, increasing the molecular mass of the target led to an enhanced SPR signal and significantly decreased the limit of detection. Although this work only reports SPR data for surface-bound DNA-DNA hybridization, the method could be used to detect DNA-RNA and DNA-protein interactions as well as many other biological interactions, as long as one molecule is amenable to dendrimer functionalization and the other to surface immobilization.

CONCLUSIONS

DNA-dendrimer constructs have been successfully hybridized with ssDNA attached to a gold surface, indicating that the covalently attached dendrimer does not preclude duplex DNA formation. Furthermore, disulfide linked DNA-dendrimer conjugates were shown to increase the sensitivity of surface oligonucleotide hybridization using surface plasmon resonance, demonstrating their potential as signal enhancement techniques. Moreover, due to the homogenous nature of these constructs they are also amenable to solution phase analytical techniques like gel electrophoresis, mass spectrometry, and a variety of automated spectral techniques for rapid analysis. Homogeneous detection capabilities allow for the opportunity to conduct real-time spectral analysis of several interactions between DNA and various other biomolecules.

The ability to successfully hybridize covalently linked DNA-dendrimer conjugates with surface-bound probe DNA is significant in two general aspects; it offers *i)* evidence that dendrimers based on melamine are suitable for applications that rely on DNA hybridization and could be greatly improved by the incorporation of a dendrimer and *ii)* a rapid, highly engineerable alternative to the many attempts that have been made to detect the interactions of surface bound biomolecules directly without using labels. Variations of the reported conjugates could be a versatile and cost effective addition to many nanofabrication techniques that rely on hybridization including the *i)* preparation of more effective biosensors, *ii)* self-assembly of more complicated nanostructures, *iii)* development of more powerful DNA-computation strategies, and even *iv)* construction of more robust gene therapy agents.

CHAPTER IV

PREPARATION, CHARACTERIZATION, AND ENZYMATIC MANIPULATION OF

NON-DISULFIDE LINKED DNA-DENDRIMER CONJUGATES

BACKGROUND

One of the many reasons for the predominant use of oligonucleotides in nanoconstruction is their ability to be easily manipulated by a host of different commercially available enzymes. Standard restriction endonuclease protocols typically require the addition of dithiothreitol (DTT), mercaptoethanol, or a similar reducing agent to the restriction cocktail. Since disulfide-mediated conjugation would be unstable under such experimental conditions, interest turned to non-disulfide-mediated conjugation chemistry.

Two standard nucleases were used for this work: BAM HI (from Bacillus amyloliquefaciens H) restriction endonuclease and EXO III, a unidirectional exonuclease. Endonuclease digestion is sequence-specific, and targets only double-stranded DNA (dsDNA) leaving any ssDNA intact. Scheme 4-1 illustrates the BAM-HI endonuclease recognition sequence indicating the DNA sequence that must be present in order for cleavage to occur, and the specific bases in which cleavage takes place. The resulting two strands contain overhanging ends that are complementary to one another ("sticky ends") so that in non-denaturing or "native" conditions (buffer, ~pH 7-8), the strands may remain base paired but contain "nicks" or breaks in the phosphodiester backbone where

the enzyme has cleaved. Denaturing gels containing urea and formamide must be used to verify endonuclease cleavage since nicked and intact oligonucleotides are indistinguishable on a native gel.

Scheme 4-1

5'..G↓GATCC..3'   5'..G │GATCC..3'
3'..CCTAG↑G..5' $\xrightarrow{\text{BAM HI}}$ 3'..CCTAG │G..5'

Exonuclease III, on the other hand catalyzes the stepwise unidirectional cleavage of mononucleotides from the 3′ terminus (3′ overhangs of ≥ 4 bases are protected) of dsDNA yielding nucleoside 5′ phosphates (dA, dG, dT, and dC) and the remaining ssDNA (Scheme 4-2). Since the enzyme is specific for dsDNA, the complementary strand remains intact.

Scheme 4-2

5'..GGATCC..3'   5'..GGATCC..3'
3'..CCTAGG..5' $\xrightarrow{\text{EXO III}}$ dC, dC, dT, dA,✂ GG..5'
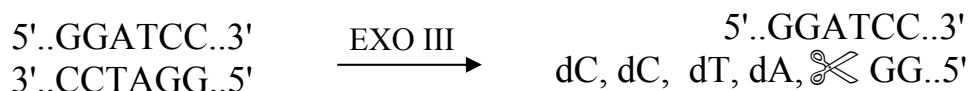
Initially, a G3 dendrimer with a thiol-reactive maleimide functional group (Scheme 4-3 A) at the core was attached to both 5′ thiol terminated 25-mers (a) and (b). Purification

and characterization by MALDI-TOF was successful, but consistent with previous attempts, the G3 dendrimer was too large to travel through polyacrylamide gels. Even gradient gels starting at 4% polyacrylamide, the loosest polyacrylamide matrix available, did not permit dendrimer migration. A smaller G1 maleimide (Scheme 4-3 B) was linked to 25-mer (a) in order to demonstrate that maleimide-crosslinked ssDNA-dendrimer conjugates do travel through polyacrylamide gels. The G1 construct was not large enough for ideal resolution on a polyacrylamide gel, and was decidedly too small for most DNA-dendrimer applications which require a G2 dendrimer or larger. Therefore, further evaluation of hybridization and enzymatic manipulation relied on spectral studies of the G3 conjugates.

Scheme 4-3

A

$C_{163}H_{284}N_{52}O_{43}$
Exact Mass: 3658.16
Mol. Wt.: 3660.32

B

$C_{56}H_{90}N_{12}O_{11}$
Exact Mass: 1106.69
Mol. Wt.: 1107.39
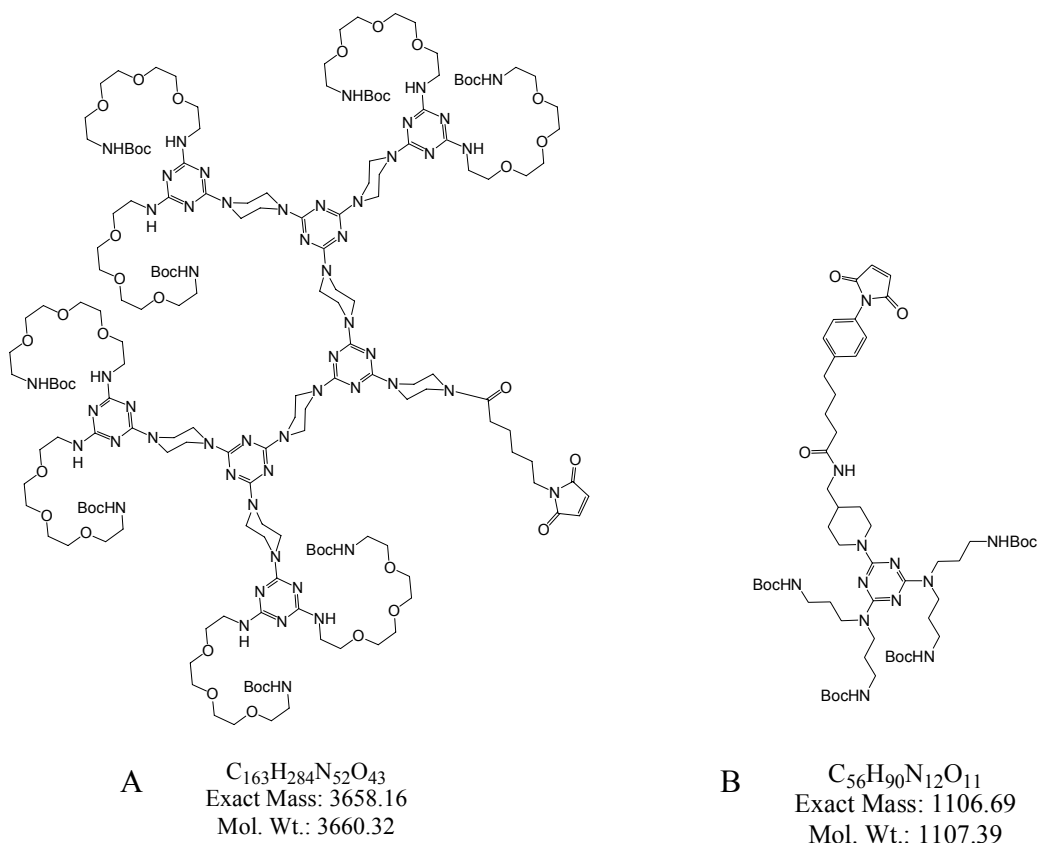
EXPERIMENTAL PROCEDURES

Dendrimer synthesis. The monochloride G3 dendrimer (MW 3417) used to prepare the conjugates for this work was provided by Dr. Alona Umali. The purified monochloride (30 mg, 8.8 μmol) was reacted with 10 equivalents of piperazine (10 mg) in 1 mL THF at 50ºC overnight which afforded the crude piperazine-activated product. Excess piperazine was precipitated in 0.6 mL of 5:1 methanol: water and the soluble portion was filtered on a 0.22 μm spin filter (Millipore) and dried *in vacuo*. The resulting yellow oil was dissolved in 0.5 mL dichloromethane and extracted twice in water to yield the semi-purified piperazine activated G3 dendrimer in 69% yield (~20.8 mg). Just prior to DNA conjugation, the heterobifunctional crosslinker, *N*-(6-maleimidocaproxy)succinimide (EMCS, 6.7 mg, 22 μmoles) was added (in 0.25 mL THF) dropwise from a syringe needle to the piperazine-activated G3 dendrimer (19.2 mg, 5.5 μmoles) in a final volume of 0.5 mL THF. The reaction proceeded at room temperature for 1 hour and the sample was dried *in vacuo*. Excess linker was removed by solid-phase sequesteration of the excess NHS ester on piperazinomethyl polystyrene (slurry, 0.1 g in 0.4 mL acetonitrile) in a final volume of 0.8 mL. Linker sequesteration proceeded at room temperature for 20 minutes and the semi-purified dendrimer was removed in a 0.22 μm spin filter. Dendrimer was recovered from the beads in 65% yield (~13 mg).

Thiol-terminated ssDNA preparation. Base-pair complementary thiol terminated 25-mer oligonucleotide sequences (25-mers (a) and (b) shown below) containing 5′ C6 thiol modifiers were purchased from Trilink Biotechnologies, Inc.

25-mer (a) - (HS-C6)5′-GGTTGGATATCTTTTTGGATCCTTC-3′

and

25-mer (b) - (HS-C6)5′-GAAGGATCCAAAAAGATATCCAACC-3′

Polyacrylamide gel analysis and HPLC purification were also provided by Trilink. Approximately 40 OD's 25-mer (~0.15 μmoles) ssDNA was dissolved in 100 μL 0.1 M dithiothreitol (DTT) in 0.1 M triethylamine acetate (TEAA) pH 8.32, vortexed for 10 seconds and allowed to sit at room temperature for 30 minutes. An *O*-dimethoxy trityl (DMT)-on Poly-Pak cartridge (Glen Research) was prepared by flushing the cartridge with 2 mL acetonitrile followed by 2 mL triethylamine acetate (TEAA) pH 7.4. The sample was loaded at a rate of 1-2 drops per second then pushed through the cartridge a second time. The loaded cartridge was washed with 3 mL 1:20 ammonium hydroxide followed by 2 mL ultrapure water. The ssDNA was detritylated by washing the cartridge with 2 mL 2% trifloroacetic acid (TFA) then flushed with 2 mL ultrapure water. Oligonucleotide was eluted in 20% acetonitrile. The first 4 drops were collected in a microcentrifuge tube, and 6 drops per tube were collected for the next 3 fractions. Usually the detritylated thiol terminated DNA was eluted in the 2nd and 3rd fractions as determined by UV-vis measurements at 260 nm (Chart 4-1).

Chart 4-1

Poly-Pak Elution Profile
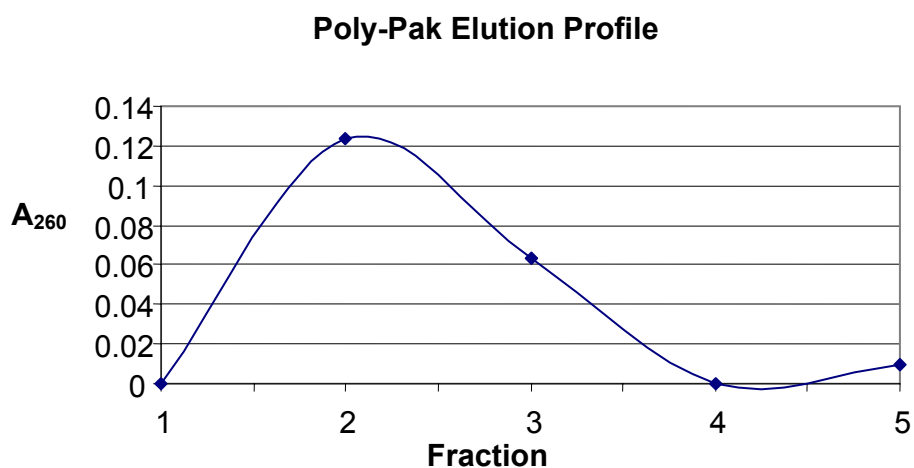
Linker-mediated conjugation. Thiol terminated ssDNA eluted from the Poly-Pak was dried *in vacuo,* reconstituted in 50 μL water, and added dropwise from a syringe to a solution of EMCS-activated G3 dendrimer (0.2 μmoles) in 1 mL acetonitrile containing 10% diisopropylethylamine (DIPEA). The reaction proceeded at room temperature over 1 hour and was dried to a pellet *in vacuo*. Excess ssDNA starting material was removed on (mercaptomethyl)polystyrene (Sigma product number 63767) in 100 μL acetonitrile for 2 hours. Beads were removed from the soluble conjugate on a 0.22 μm spin filter.

It was necessary to deprotect the boc-protected amine periphery in order to afford water solubility for enzymatic reactions. Since partial boc-deprotection was observed after detritylation in 2% TFA on the Poly-Pak column, a dilute solution of TFA in acetonitrile (~5%) was used to remove the boc groups without degrading the ssDNA. After 1 hour at room temperature the TFA mixture was added to a 10,000 MWCO spin

filter and spun at 14,000 X g for 45 minutes. Filtrate was removed and 50 μL ultrapure water was added to the retentate. The sample was spun for 30 minutes at a time, 5 times, with the addition of 50 μL water between spin intervals to accomplish both desalting and separation from any remaining low molecular weight impurities.

It was not possible to visualize the G3 crosslinked conjugates by gel electrophoresis. Therefore smaller constructs were prepared with the goal to demonstrate enzymatic manipulation of covalently-linked conjugates by gel electrophoresis. A G1 dendrimer with a maleimide functionalized arm, provided by Dr. Hui-Ting Chen, was used as proof of concept that a covalently crosslinked ssDNA-dendrimer conjugate could be observed by gel electrophoresis. The GMBS linker used for this work differed from the EMCS linker from the previous construct by one less methylene in the hydrocarbon chain. The same protocol for formation of a covalent linkage between a thiol-terminated ssDNA and a maleimide activated dendrimer was used.

Quantification. It is difficult to accurately quantify ≤ 2 mg product, but there are two different spectophotometric methods that are often employed to approximate ssDNA yield from oligonucleotide syntheses. For this work, matters are complicated by the significant overlap between the UV-vis absorption spectrum of ssDNA ($\lambda_{max} = 260$) and that of the triazine-based dendrimers ($\lambda_{max} = 254$) used for conjugation. Thus the yield calculated using the first approximation (EQN 4), which does not take into account the presence of the dendrimer, could be an under-approximation since some unknown amount of absorption was actually due to the dendrimer. Indeed a background reference containing only dendrimer could be used to solve this problem if the concentration of dendrimer in the sample was known. The second method for approximating ssDNA yield

takes into account the number of bases in the ssDNA and can therefore be tailored to contain more "bases" than are actually present. This method was employed for comparison.

A 10 μL aliquot of ssDNA-dendrimer conjugate was diluted by a factor of 90 to yield 1 mL final volume for absorbance readings. The absorbance at 260, for a 90X dilution of ssDNA-dendrimer product was 1.11 (OD = 1.11, where OD = optical density). The conversion factor (cf) for calculations was 50, because $1/50^{th}$ of the sample was used to measure absorbance at 260 nm (A_{260}).

The first approximation states that 1 OD ($A_{260} = 1$) equals 32 μg ssDNA (EQN 4-1a). Taking the cf into consideration, as shown in EQN 4-1b, this approximation results a value of 1.78 mg for product yield (EQN 4-1c).

1 OD = 32 μg DNA   (EQN 4-1a)

(measured A_{260}) X (cf) X (0.032 mg) = yield (mg)   (EQN 4-1b)

(1.11) X (50) X (0.032 mg) = 1.78 mg   (EQN 4-1c)

A second rule for quantifying ssDNA yield states that 1 μmol ssDNA is equal to 10 OD multiplied by the number of oligonucleotide bases (EQN 4-2a). The absorption properties of G2 dendrimers based on melamine are similar enough to that of nucleotide bases that the ε_{260} values are on the same order of magnitude. With that in mind, it was possible to count the dendrimer as an additional base in the 25-mer to make the total number of bases

to equal 26 (EQN 4-2b). Applying the second approximation resulted in a value of 2.28 mg for product yield (EQN 4-2c). The values obtained from the two approximations are comparable enough with one another to estimate that approximately 2 mg EMCS-linked ssDNA-dendrimer was obtained using the synthetic procedures outlined above.

$$1 \text{ μmole ssDNA} = (10 \text{ OD}) \text{ X (\# bases)} = 260 \text{ OD} \qquad \text{(EQN 4-2a)}$$

$$(55.5 \text{ OD X 1 μmole)} \div 260 \text{ OD} = 0.213 \text{ μmole} \qquad \text{(EQN 4-2b)}$$

$$(10{,}700 \text{ mg/ mmol)} \text{ X } (0.213 \text{ X } 10^{-3} \text{ mmole)} = 2.28 \text{ mg} \qquad \text{(EQN 4-2c)}$$

Hybridization. All buffer salts were purchased from EM sciences. Hybridization buffer (0.16 M KCl, 0.02 M Na_2HPO_4, 1 mM EDTA pH 7.5) was prepared with Barnstead ultrapure water and filtered through a 0.2 um spin filter just prior to use. Double stranded (ds) oligonucleotides were prepared by mixing a 1:1 ratio (16 μg, 2 nmoles) of complementary ssDNA 25-mer (a) and 25-mer (b) at a final concentration of 0.4 mM (5 μL) in hybridization buffer. Samples were kept at 37 ºC overnight then stored at 4 °C. To prepare dendrimer-bound dsDNA, a 10-fold molar excess of 25-mer (a) or (b) ssDNA-dendrimer conjugate (16.7 nmol) was added to the corresponding complementary ssDNA (1.7 nmol) in 50 μL hybridization buffer. Samples were kept at 37 ºC overnight then stored at 4°C.

UV-vis spectral comparisons. Nucleotide base stacking between complementary strands in dsDNA results in a decrease in UV absorption compared to ssDNA. This phenomenon is referred to as the hyperchromic effect. Due to this effect, the molar absorptivity for bases in dsDNA compared to that of ssDNA increases to 6.6 X 10^3. For all spectral measurements, the total concentration of DNA was diluted to ~30 ng/ μL in 2X hybridization buffer.

Melting point determination. The hyperchromic effect is used in a simple way to study the melting of duplex DNA. Increasing the temperature of the sample denatures the strands resulting in an absorption increase as the strands begin to exhibit ssDNA behavior. The melting temperature (T_m) can be determined experimentally by heating the duplex DNA while recording A_{260} measurements and plotting temperature vs. absorbance. The T_m is determined by calculating the temperature at which half of the maximal absorption has occurred, or in other words, the temperature at which 50% of a given oligonucleotide is hybridized to its complementary strand. In the absence of destabilizing agents, like formamide or urea, T_m will depend on 3 major parameters:

1. The sequence: a GC-rich sequence has a higher melting temperature.[129]

2. The strand concentration: high oligonucleotide concentrations favor hybrid formation, which results in a higher melting temperature.[130]

3. The salt concentration: high ionic strength results in a higher T_m as cations stabilize the DNA duplexes.[131]

For oligonucleotides greater than 15 bases long, there is a simple calculation to approximate the melting temperature:

$$T_m \, (^\circ C) = 81.5 + 16.6 \log M + 41(XG + XC) - 500/ L - 0.62F \qquad \text{(EQN 4-3)}$$

Where:

M = molar concentration of monovalent cations

XG and XC = mole fractions of G and C in the oligonucleotide

L = length of the shortest strand in the duplex

F = molar concentration of formamide

Solving for M = 0.4 (hybridization buffer contributed ~0.4 M [Na^+] and [K^+] after drying the sample and re-dissolving it in fresh buffer), XG + XC = 0.4, L = 25, and F = 0:

T_m = 81.5 + 16.6 (log 0.4) + 41 (0.4) - 500/ 25 - 0.62 (0) = **71.3 °C**

Enzymatic manipulation. Restriction digests were prepared according to the standard procedure supplied by Promega for Bam HI and Exo III enzymes. Three enzyme concentrations were tested for optimal digestion conditions. All digest mixtures were incubated at 37°C for 4 hours unless otherwise noted. Scheme 4-4 depicts the BAM HI digestion of thiol-terminated dsDNA.

Scheme 4-4

(HS-C$_6$H$_{12}$)5′-GGTTGGATATCTTTTTGGATCCTTC
        CCAACCTATAGAAAAACCTAGGAAG-5′(C$_6$H$_{12}$-SH)

BAM HI

(HS- C$_6$H$_{12}$)5′-GGTTGGATATCTTTTTGGAT   CCTTC
        CCAACCTATAGAAAAAC   TAGGAAG-5′(C$_6$H$_{12}$-SH)
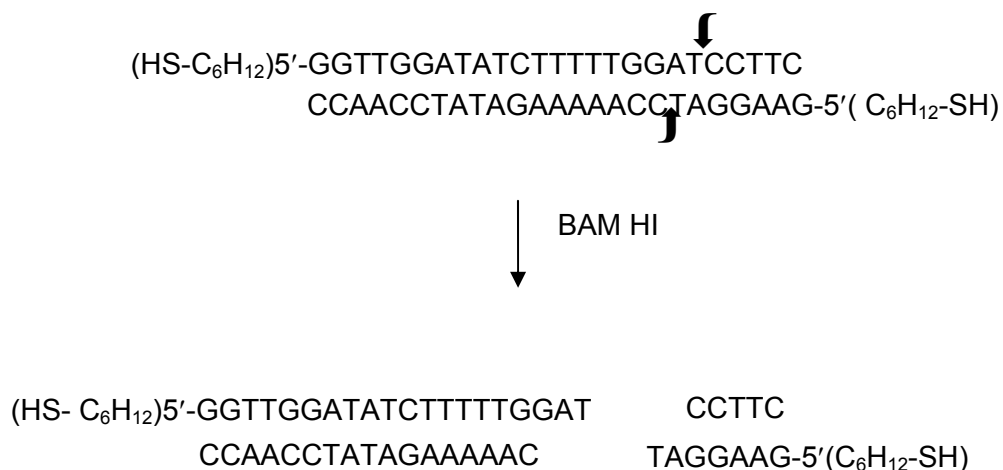
MALDI-TOF. For MALDI-TOF, aqueous sample solutions (1μM) were mixed with the 2,4,6-trihydroxyacetophenone (THAP) matrix (15 mg/ml in acetonitrile) and aqueous ammonium citrate (15 mg/ml) at a ratio of 1:1:1 prior to the application of 1 μL aliquots on a bed of THAP matrix.[132] The analyte-doped matrix crystals were washed 10 times with 5 μL of cold water to remove sodium and potassium ions. An Applied Biosystems (Framingham, MA) Voyager-DE STR mass spectrometer operating in positive- and negative-ion mode was used to obtain the mass spectra. The system is equipped with a N$_2$ laser providing 337 nm, 3 ns wide pulses with the accelerating voltage maintained at 25 kV for this study. Delayed extraction (~ 600 ns) mode was applied in linear time-of-flight detection.

Denaturing gel electrophoresis. All gels were run on a Mini-Protean 3 Cell gel running apparatus from Bio-Rad. 5X Tris-borate EDTA (TBE) buffer pH 8.3 and DNA loading buffer were purchased from eppendorf. For denaturing conditions, 19%

polyacrylamide gels were prepared by adding 3.15 g urea to 3.75 mL 40% bis-acrylamide stock (BioRad) and 1.5 mL 5X TBE. Mild heating (60°C) and agitation was required to dissolve the urea. Just prior to pouring, 45 μL 10% ammonium persulfate (APS) and 3.5 μL TEMED were added. All gels were run in 1X TBE, 80 V, 120 minutes. Samples were prepared by adding 1 μL DNA loading buffer (Eppendorf) and 1 μL formamide per 10 μL sample in 1X TBE. The gel was run for 30 minutes at 80 V prior to loading as a means to remove any excess acrylamide or polymerizing agents from the loading wells, and just prior to loading, wells were cleared out with a 20 μL pipet. These steps proved very helpful in preventing the streaking of bands in the gel.

Non-denaturing (native) gel electrophoresis. All 20% polyacrylamide gels were prepared by mixing 6.7 mL 40% bis-acrylamide stock (BioRad), 1.3 mL ultrapure water, and 2.0 mL 5X TBE. Just prior to pouring, 45 μL 10% ammonium persulfate (APS) and 3.5 μL TEMED were added. Gels were run in 1X TBE, 80 V, 120 minutes. Samples were prepared by adding 1 μL DNA loading buffer (Eppendorf) per 10 μL sample in 1X TBE. As before, all wells were cleared of excess acrylamide and the gel was pre-run for 30 minutes at 80 V.

RESULTS AND DISCUSSION

Purification. The ssDNA-dendrimer conjugated products were larger than 10,000 Da, therefore their purification by spin filtration was greatly simplified. Experience has shown that while most low molecular weight impurities are retained on 3,000 molecular

weight cutoff (MWCO) spin filters (Millipore), 10,000 MWCO spin filters are more effective at separating larger dendrimers from low molecular weight impurities.

MALDI-TOF. Mass spectrometry indicates the significant improvement in product isolation using the 10,000 MWCO spin filters. As shown in Figures 4-1 and 4-2, all unbound ssDNA was removed. Only signal corresponding to EMCS-linked ssDNA-dendrimer conjugates remained. Figure 4-1 shows the MALDI-TOF spectrum corresponding to EMCS crosslinked construct containing 25-mer (a) and the structure and formula corresponding to this construct is shown in Scheme 4-5. Likewise, Figure 4-2 shows the MALDI-TOF spectrum corresponding to EMCS crosslinked construct containing 25-mer (b) and the structure and formula corresponding to this construct is shown in Scheme 4-6.

.
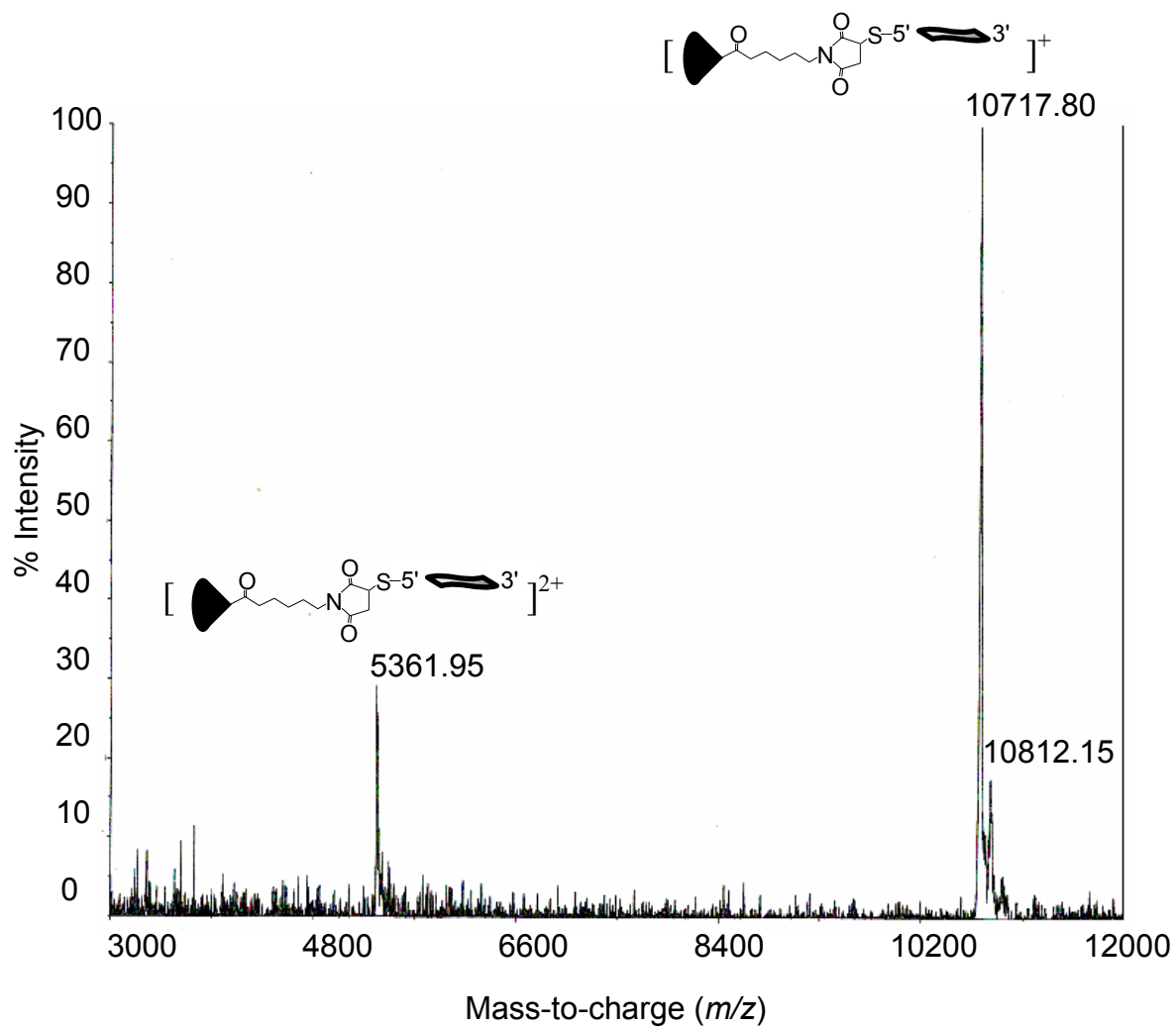
Figure 4-1. MALDI-TOF spectrum corresponding to EMCS crosslinked construct containing 25-mer (a).

Scheme 4-5

C₃₇₅H₅₄₆N₁₃₃O₁₈₇P₂₅S
Exact Mass: 10710.05
Mol. Wt.: 10715.54
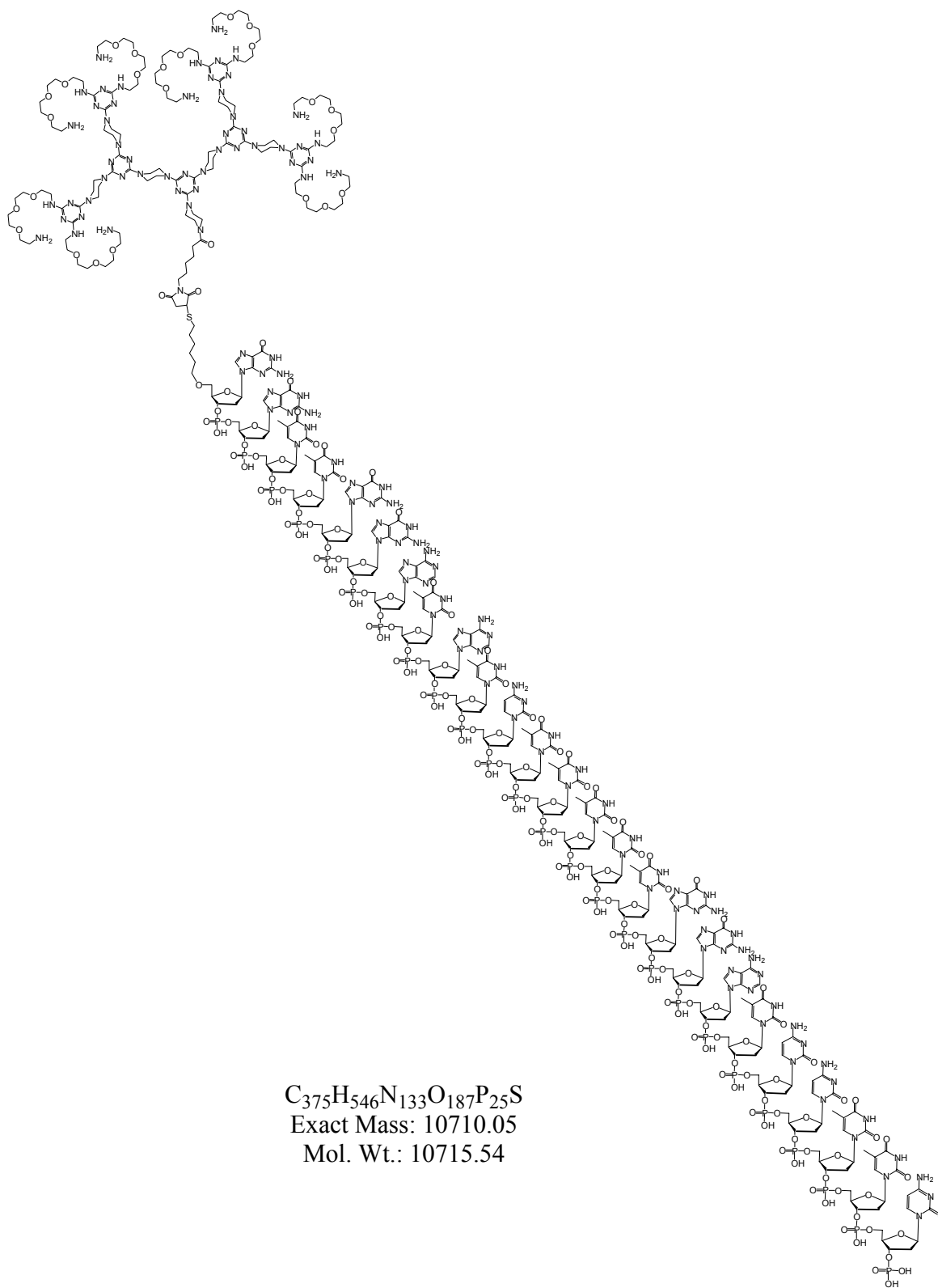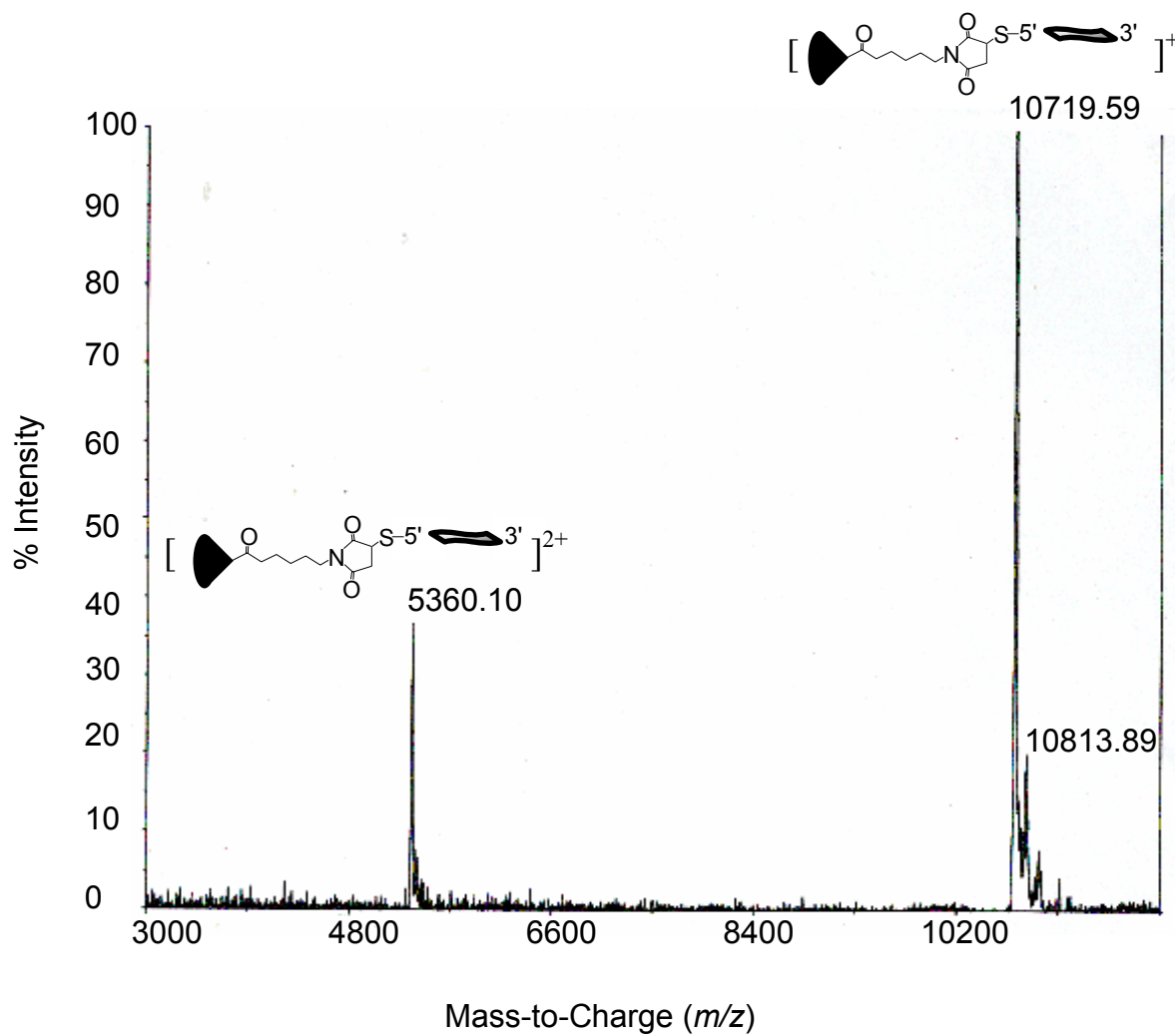
Figure 4-2. MALDI-TOF spectrum corresponding to EMCS crosslinked construct containing 25-mer (b).

Scheme 4-6

$C_{373}H_{537}N_{156}O_{169}P_{25}S$
Exact Mass: 10711.14
Mol. Wt.: 10716.61
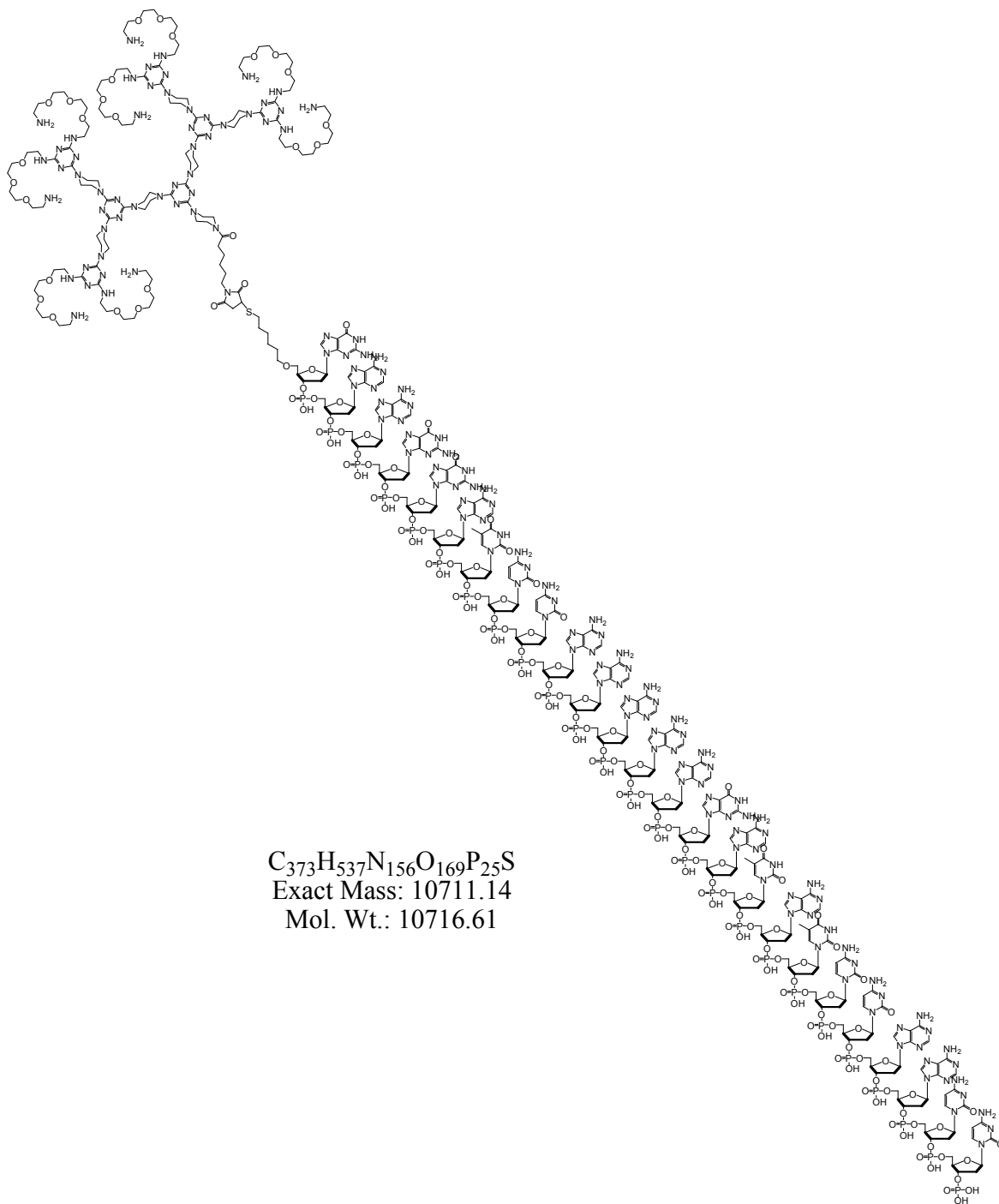
Gel electrophoresis (evidence of GMBS-linked conjugate). A characteristic band pattern for thiol terminated DNA and DNA-dendrimer conjugate was observed upon staining with ethidium bromide. The G1 dendrimer, however, was smaller than the previously observed G2 dendrimer, so it traveled lower on the gel, closer to the thiol terminated ssDNA. An image from the charge coupled device (CCD) camera (Figure 4-3) shows poor separation between the three bands in lanes 2 and 3. Lane 1 contains ~0.5 μg thiol terminated ssDNA, with the top band corresponding to the disulfide, and the lower band to the free thiol. Lanes 2 and 3 contain 2 different concentrations (1μg/ μL in lane 2, and 2μg/ μL in lane 2) of the same GMBS conjugated DNA-dendrimer sample. Both overloading (lane 3) and smearing (lanes 2 and 3) made these gels very difficult to analyze. Attempts to coomassie stain the dendrimer proved unsuccessful also likely due to the small size of the dendrimer resulting in an inability to retain the dye.
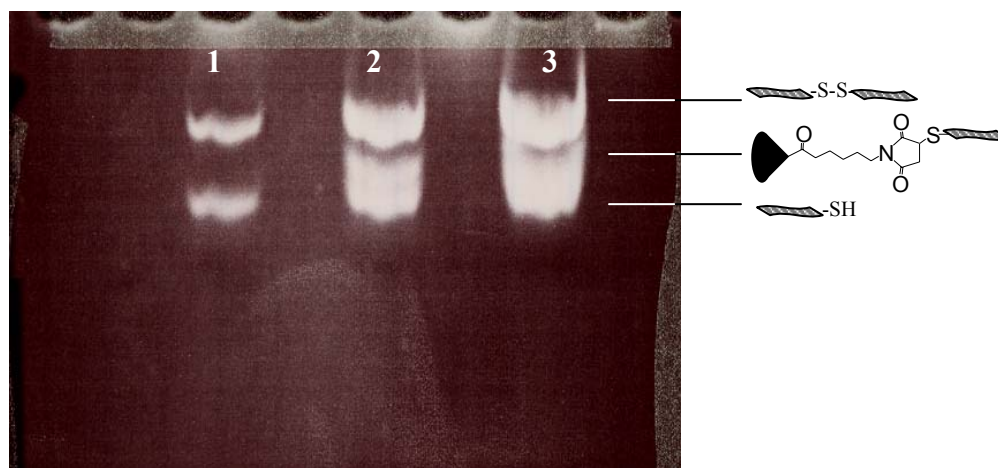
Figure 4-3. Ethidium bromide stained 20% polyacrylamide TBE gel of a G1 dendrimer crosslinked to thiol-terminated ssDNA with GMBS.

UV-vis spectral comparisons. The hyperchromic effect is readily observed when comparing the UV-vis spectrum of ssDNA to that of dsDNA, a distinct decrease in absorbance at 260 nm is observed upon addition of 1 equivalent of complementary ssDNA. Much flatter spectra are observed for both dendrimer-conjugated ssDNA and dsDNA, indicating the presence of base stacking of ssDNA-dendrimer conjugates relative to that of ssDNA. When complement ssDNA is added to the conjugate, absorbance at 260 nm slightly decreases indicating a small increase in the ordering or base stacking of the DNA. Based on these results alone, it is not possible to conclude that hybridization is or is not occurring between the complementary DNA strands, but is suggestive of an interaction between the ssDNA and dendrimer that results in a more ordered arrangement of bases on the DNA strand. Such an interaction could account for the inability of ssDNA-dendrimers to migrate through polyacrylamide gels partly due to the formation of a densely packed, globular structure, and partly due to charge neutralization affected by the terminal amine groups of the G3 dendrimer.

Chart 4-2

Comparison of Spectra
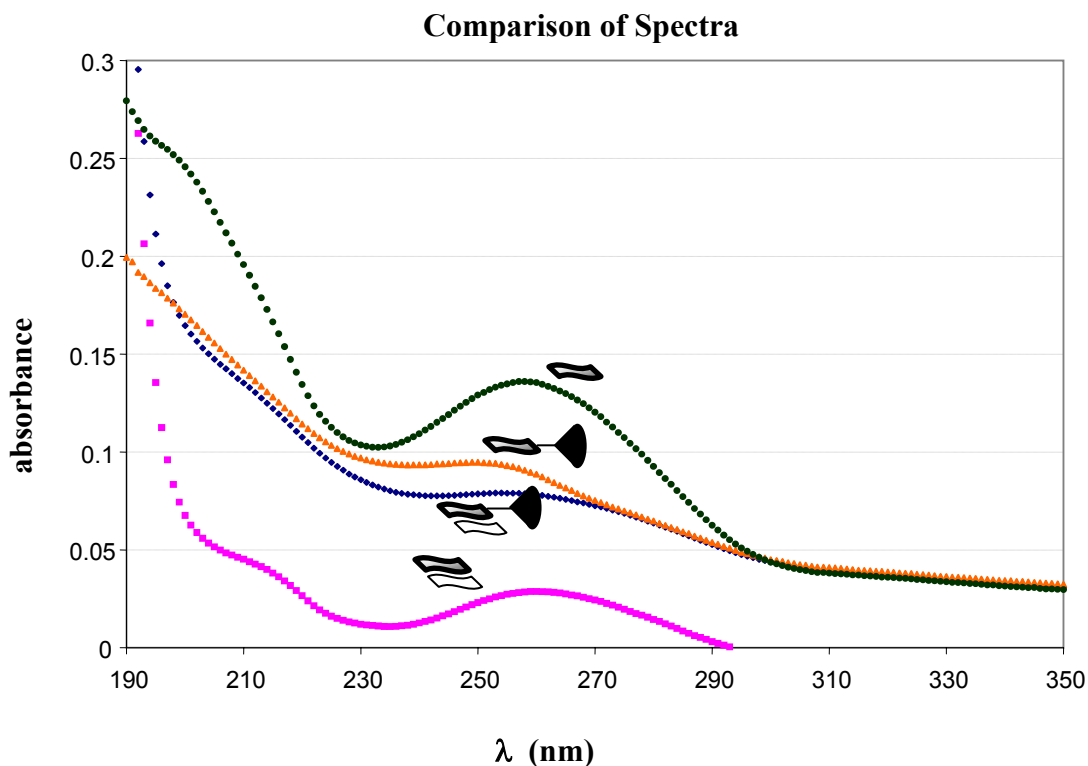
Melting temperature comparison. The experimentally determined melting temperature (T_m) was very close to the calculated value (71.3 °C) discussed in EQN 4-3. The dendrimer has an obvious impact on the hyperchromic effect, but interestingly does not seem to prevent hybridization from taking place as determined by surface hybridization studies discussed in Chapter III. Melting curves show that disrupting any hybridization that could be occurring between the DNA strands does not give rise to a characteristic hyperchromic effect. Some ordered arrangement of DNA bases still exists at high temperatures giving rise to a much lower absorbance than would be expected for ssDNA. Nonetheless, addition of one equivalent of ssDNA to form the dsDNA-

dendrimer conjugate results in a *decrease* in absorbance rather than an *increase*, as shown in Chart 4-2, indicating that a hyperchromic effect is observed in DNA-dendrimer systems. Indeed it appears that the curve corresponding to DNA-dendrimer conjugate in Chart 4-3 would continue to increase in A_{260} if heated above 85 °C, but temperatures exceeding 90 °C were beyond experimental capabilities. Experiments with dendrimer alone showed no increase in A_{260} upon sample heating. Since interactions between DNA and dendrimer versus DNA with DNA cannot be distinguished from one another using the hyperchromic effect, this method was not as helpful in discerning the extent of DNA hybridization as were the solid-phase hybridization studies in Chapter III.

Chart 4-3
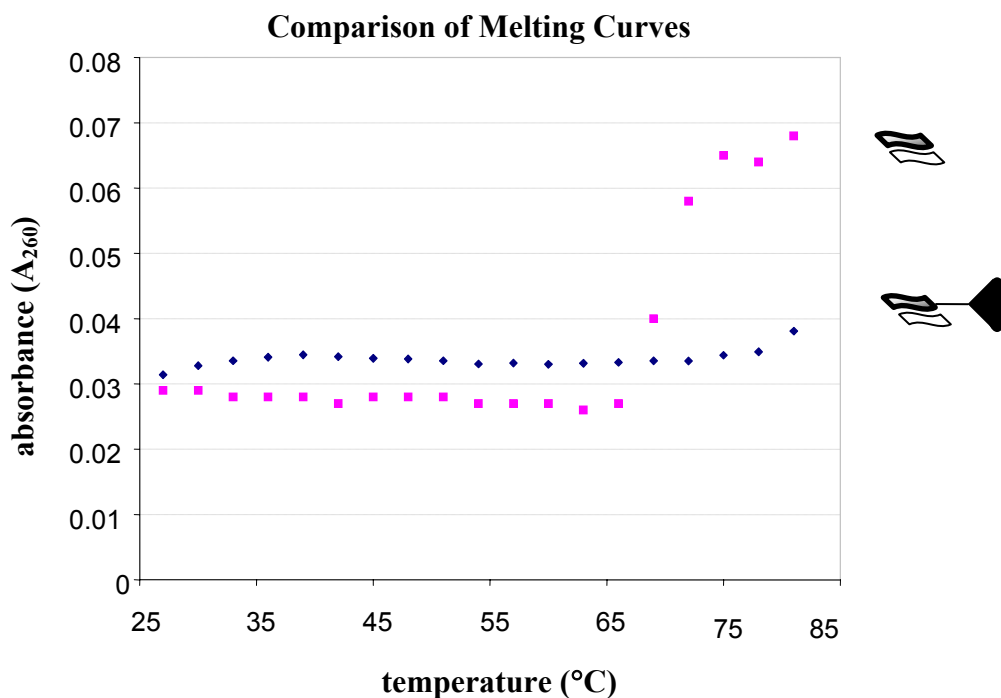
Enzymatic digestions. BAM HI endonuclease digestions were performed according to Scheme 4-7 A, and Exo III digestions according to Scheme 4-7 B. Each species has been assigned a number that corresponds with the numeric labels on the polyacrylamide gel studies that follow. The first column in Scheme 4-8 A corresponds to the hybridization of ssDNA strands 25-mer (a) and 25-mer (b) to form **2** with subsequent endonuclease digestion by BAM HI to yield **3**. This first column was used as a control to compare the hybridization and enzymatic cleavage of the dsDNA-dendrimer conjugates. The second column shows the hybridization of ss25-mer (b), to the dendrimer-bound 25-mer (a) conjugate **4**, to form **5** with subsequent digestion by BAM HI to form **6**. The third column shows the hybridization of ss25-mer (a) to the dendrimer-bound 25-mer (b) conjugate **7** and subsequent enzymatic cleavage by BAM HI to yield **8**. The difference between the second and third columns arises from which of the two 25-mers (a or b) was covalently attached to the dendrimer. Scheme 4-7 B shows the Exo III digestion of ds25-mer **2** and dsDNA-dendrimers **5** and **8** from Scheme 4-7 A, to form **10**, **11**, and **12**, respectively.

Scheme 4-7

A

B
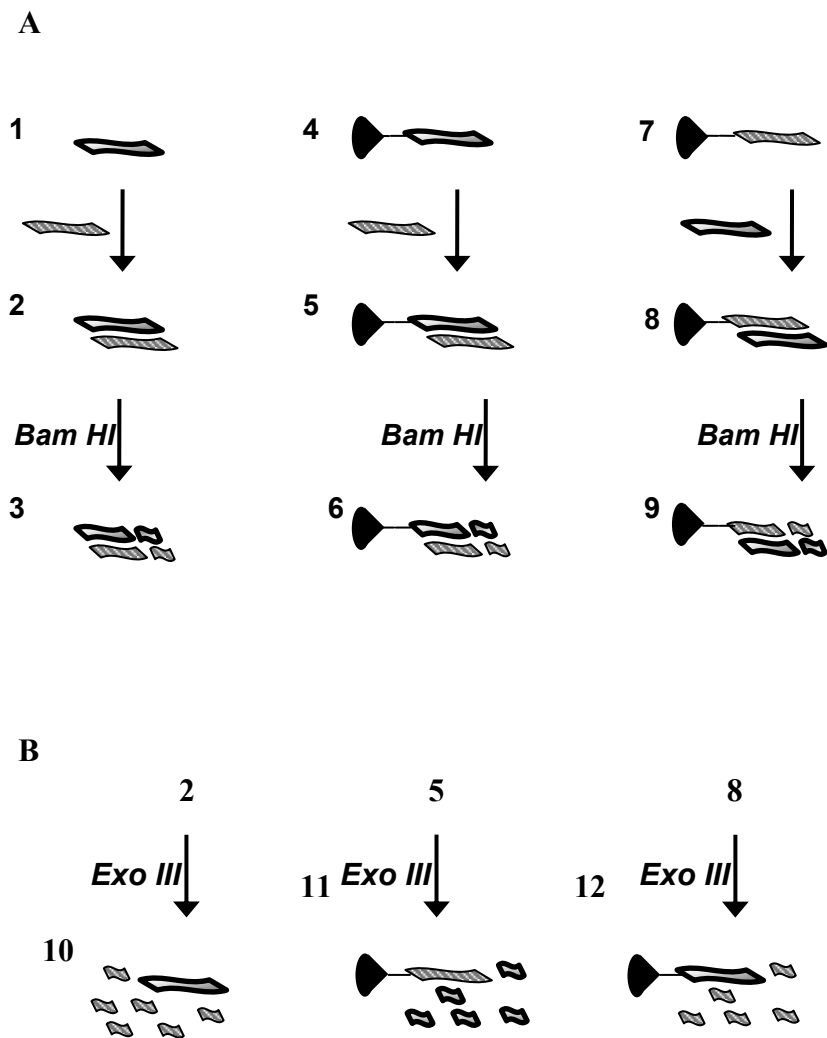
Denaturing gel electrophoresis (evidence for BAM HI digestion). The ethidium-bromide stained 19% denaturing polyacrylamide gel is shown in Figure 4-4. The first two lanes contain single-stranded DNA (1) and dsDNA (2) resulting from the hybridization of 25-mer (a) with 25-mer (b). No band corresponding to hybridized DNA, which would lie higher on the gel, was observed in lane 2, revealing that the denaturing

conditions successfully separated dsDNA. BAM HI successfully cleaves the dsDNA (3) presumably yielding two large strands and two small strands that show up on the gel as two distinct bands. Conjugates (conjugate **4** from Scheme 4-7 A is shown) do not penetrate the gel. Hybridization with complement ssDNA to yield **6** results in a band corresponding to ssDNA, as expected under denaturing conditions. BAM HI cleavage occurs with **5** revealing the same pattern shown for digested dsDNA (3). The BAM HI digest of conjugate **4** reveals the same band pattern. BAM HI is specific for dsDNA. So although a denaturing gel cannot indicate successful hybridization, the DNA-dendrimer and ssDNA must have hybridized (or annealed) in order for enzymatic digestion to have taken place. Thus, at least partial hybridization occurs in the presence of dendrimer. A coomassie stain confirms that no dendrimer is present in the gel, consistent with ethidium bromide results indicating that G3 dendrimer-bound ssDNA does not penetrate the polyacrylamide matrix. The fact that no free ssDNA is observed in lane 4, corresponding to the covalent ssDNA-dendrimer conjugate allows us to confirm that the DNA present in lanes 5, 6, and 9 are not artifacts of excess unconjugated ssDNA. All experiments were performed using the same ssDNA-dendrimer stock solution, which according to gel electrophoresis is free of any unconjugated ssDNA.
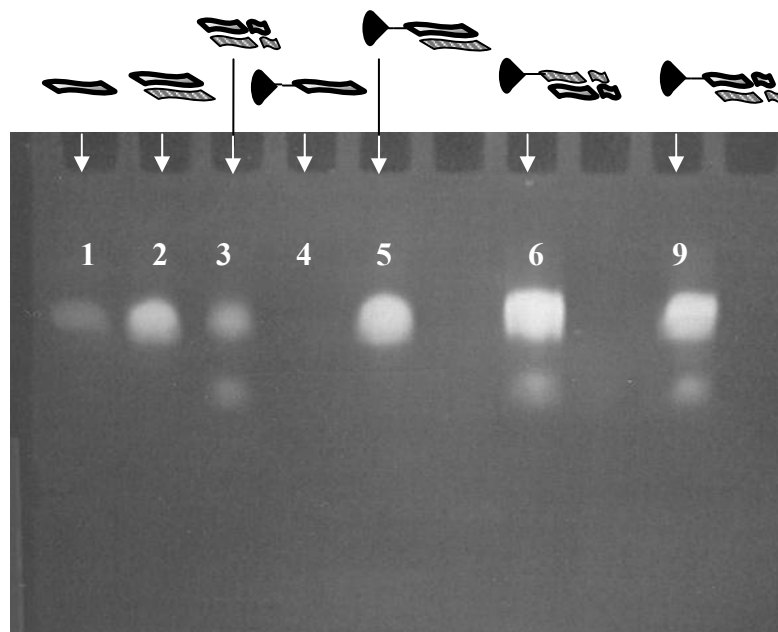
Figure 4-4. Ethidium bromide stained 19% denaturing polyacrylamide gel of ssDNA **1**, dsDNA **2**, BAM HI digested dsDNA **3**, ssDNA-dendrimer **4**, dsDNA-dendrimer **5**, and BAM HI digestions of two different dsDNA-dendrimers (**4** and **7**) to yield **6** and **9.**

Denaturing gel electrophoresis (evidence for Exo III digestion). Another ethidium-bromide stained 19% denaturing polyacrylamide gel, this one illustrating the success of EXO III cleavage, is shown in Figure 4-5. The same band patterns for **2**, **4**, **5**, and **8** were observed in this denaturing gel. EXO III digestion of dsDNA yields no bands, as presumably the free nucleotides run off the bottom of the gel during electrophoresis. The same is observed for dsDNA-dendrimer. Two exonuclease cleavage times are shown for **11**. The first lane corresponds to a 1 hour digestion, and the 2nd to a 12 hour digestion

indicating that the cleavage of dendrimer bound dsDNA requires more time than cleavage of dsDNA (for **10**, reaction time = 1 hour).
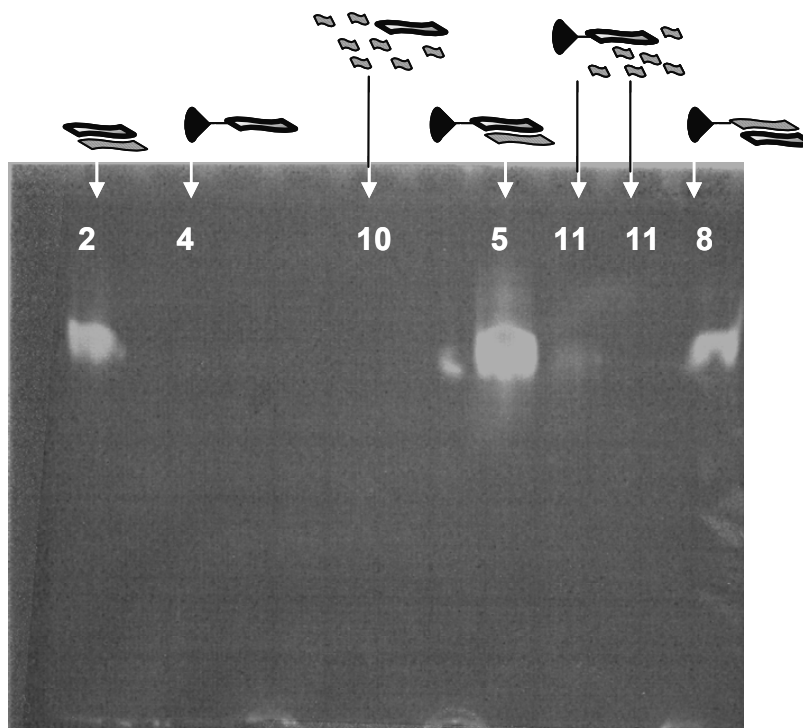
Figure 4-5. Ethidium-bromide stained 19% denaturing polyacrylamide gel of dsDNA **2**, ssDNA-dendrimer **4**, Exo III digestion of ds DNA **10**, dsDNA-dendrimer **5**, Exo III digested dsDNA-dendrimer **11** at reaction times = 1 hour and 12 hours shown fron left to right, and dsDNA-dendrimer conjugate **8.**

Non-denaturing gel electrophoresis The results from 19% non-denaturing polyacrylamide gel electrophoresis are shown in Figure 4-6. This gel provides evidence of base-pairing for BAM HI endonuclease digested dsDNA **6** that could not be detected

in denaturing conditions. Exo III digestion does not allow base pairing of the cleavage products, so base pairing is not observed for the ssDNA-dendrimer Exo III digestion in lane 11. Incomplete digestion is however observed, as it was on the denaturing gels if the digestion was not allowed to proceed over ~12 hours. Again, ssDNA-dendrimer **4** did not enter the gel, but addition of complement allowed for visualization of mostly ssDNA. Comparing ethidium bromide intensities between dsDNA **2** and dsDNA-dendrimer conjugate **5**, it appears that a small amount of **5** is base paired.
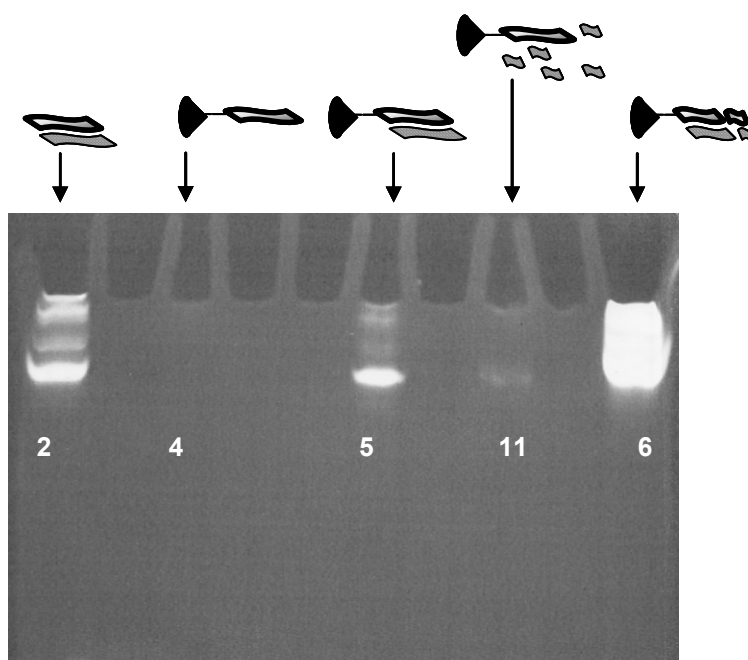
Figure 4-6. 19% non-denaturing polyacrylamide gel of dsDNA **2**, ssDNA-dendrimer **4**, dsDNA-dendrimer **5**, Exo III cleaved dsDNA-dendrimer **11**, and BAM HI cleaved dsDNA-dendrimer **6**.

CONCLUSIONS

DNA cleavage is particularly useful for creating dynamic nanostructures and many surface-based techniques such as DNA-based computation, rely on the ability to strategically synthesis ("program") DNA to contain specific cleavage sites for the removal of target DNA or the excision of DNA strands of predetermined length.

New ways to exhibit control over DNA-dendrimer nanostructures through the use of dozens of commercially available, sequence-selective enzymes are just beginning to be explored. The ability of enzymes to function in the presence of covalently-linked dendrimers based on melamine, as demonstrated here, is hopeful as it suggests that the analysis of enzyme-substrate interactions and assays for sequence specificity using these constructs as scaffolds will be possible.

CHAPTER V

SYNTHESIS OF MEGAMERS: MULTIVALENT STREPTAVIDIN-BASED

PEPTIDE-DENDRIMER BIOCONJUGATES FOR TARGETED DRUG DELIVERY

BACKGROUND

An efficient synthetic strategy is proposed herein for the synthesis and characterization of macromolecules that exceed the threshold for EPR while displaying multiple end groups for manipulation using protein-ligand interactions. This work demonstrates that biotinylated TAT peptide-dendrimer conjugates can assemble in the presence of streptavidin, a 60 kDa tetramer that binds 4 biotin molecules with a remarkably high association constant of 10^{14} M^{-1}.[133] Scheme 5-1 illustrates the assembly of 4 peptide-dendrimers around a streptavidin core to form a multi-dendrimer unit, or megamer. The chemical synthesis of the building blocks is straightforward,[134] and noncovalent assembly occurs spontaneously. Streptavidin has been used extensively to carry biotinylated molecules *in vivo*, most notably to increase the delivery of radioactivity to tumor tissue.[135] The biotin-streptavidin interaction is stable in a wide range of temperatures, pH, organic solvents, and in the presence of sodium dodecyl sulfate (SDS) and urea.

TAT is an arginine-rich protein transduction domain from HIV-1 that facilitates cell surface recognition, aids in transport across the membrane, and protects the transferred material from lysosomal degradation.[136] TAT has been used to transfer

antibodies, polymers with and without drug bound, and a wide range of proteins.[137-139] The TAT sequence was synthesized on-bead, and a G2 monochloride dendrimer was attached as the terminal "residue" using the conjugation protocol discussed below.

Scheme 5-1
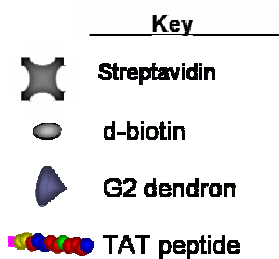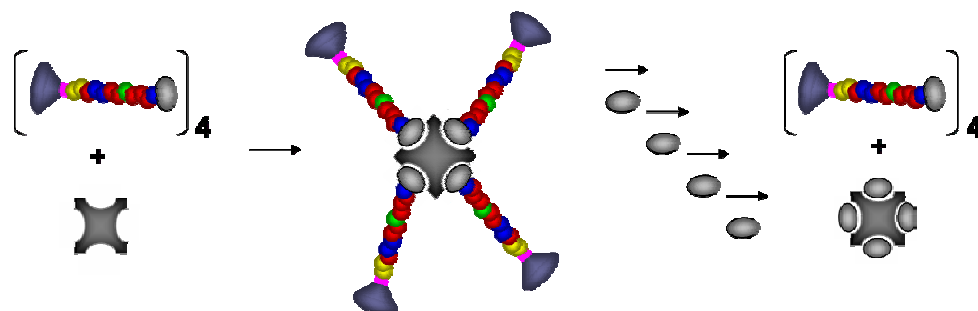
The characterization of megamers relied on sodium dodecyl sulfate polyacrylamide gel electrophoresis (SDS-PAGE), matrix-assisted laser desorption ionization (MALDI) mass spectrometry, and spectral titrations using the HABA method.[133]

EXPERIMENTAL PROCEDURES

Solid phase peptide synthesis (SPPS) materials. Coupling agents: Benzotriazol-1-yl-oxytripyrrolidinophosphonium hexafluorophosphate (PyBop) and *N*-hydroxybenzotriazole (HOBT) were purchased from NovaBiochem along with fluorenyl methoxy carbonyl (Fmoc) protected amino acids: Glycine (Fmoc-Gly-OH), tert-butoxy carbonyl (boc)-protected L-lysine (Fmoc-Lys(boc)OH), 2,2,4,6,7-pentamethyldihydrobenzofuran-5-sulfonyl (pbf)- protected L-arginine (Fmoc-Arg(pbf)-OH), and trityl-protected L-glutamine (Fmoc-Gln(trt)-OH). Fmoc-protected 4-carboxypiperidine (isonipecotic acid, Inp) and Fmoc-Lys(biotin)-wang resin were purchased from Advanced Chemtech. HPLC grade *N,N*-dimethylformamide (DMF) was used for all deprotection and coupling reactions.

SPPS. Peptide were synthesized on a 0.25 mmol scale by manual Fmoc solid phase peptide synthesis on Fmoc-Lys(biotin)-wang resin. Fmoc deprotection of the resin and all subsequent Fmoc deprotections were carried out in 4:1 DMF: piperidine in 10 mL final volume for 3 minutes and repeated 2 times. Beads were washed several times with dichloromethane then 2 times with DMF after each step. Amino acid coupling to the Fmoc deprotected resin required 4 equivalents (eq) amino acid in ~10 mL DMF, 4 eq PyBop, 8 eq HOBT, and a catalytic amount of *N*-methyl morpholine (~200 μL). Reaction vessels were placed on a shaker at room temperature for 1 to 4 hours. The Kaiser test (1 drop each of 3 solutions: i) 5 g ninhydrin in 100 mL ethanol, ii) 80g of phenol in 20 mL of ethanol, and iii) 2 mL of a 1 mM aq. solution of potassium cyanide in 98 mL pyridine) was performed after each coupling and deprotection step to monitor the reaction progress.

If free amine was present, the beads turned blue upon heating for ~1 minute. After each coupling step, 1:1 pyridine:acetic anhydride was used to cap any unreacted amines. After on-bead conjugation with the G2 dendrimer, the beads were washed 5 times with DMF, 5 times with methanol, and 15 times with dichloromethane (~5 mL per wash). The resin was dried in a dessicator overnight and washed with dicloromethane again prior to cleavage. Cleavage in 95% TFA, 2.5% water, 2.5% TIS for 3 hours followed by ether precipitation yielded 41 mg orange powder. All amino acid protecting groups were removed in the TFA cleavage cocktail.

Peptide-dendrimer conjugation. A silica gel purified G2 monochloride dendrimer containing an Oregon Green tag (Scheme 5-2) was provided by Dr. Mackay Steffensen.

Scheme 5-2

$C_{68}H_{95}ClF_2N_{22}O_{11}$
Exact Mass: 1468.72
Mol. Wt.: 1470.07
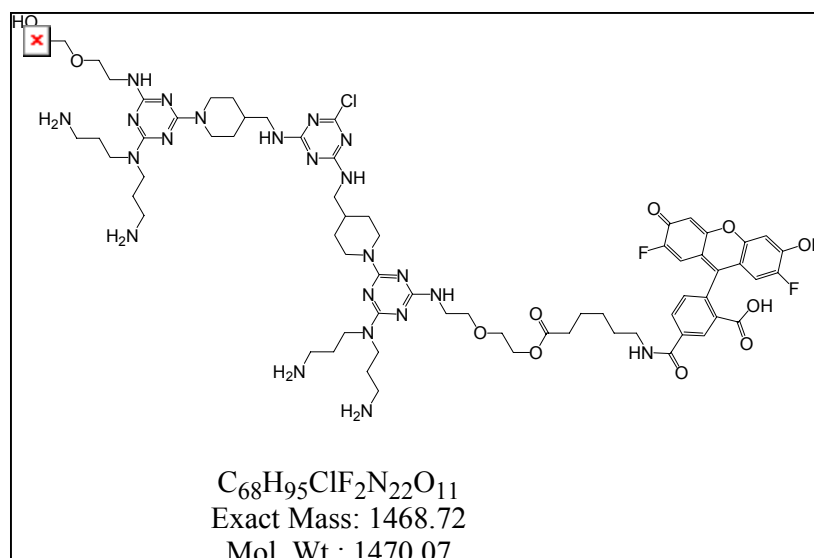
Substitution of the monochloride core with a secondary amine from the N-terminal isonipeocotic acid residue of the TAT peptide was achieved in 3 mL DMF with a drop of

N,N-diisopropyl ethylamine (DIPEA). The 3368 molecular weight product was filtered on a 3000 molecular weight cut-off (MWCO) spin filter (Millipore) according to the manufacturer's protocol, to remove small impurities.

HPLC of peptides. After 3000 MWCO spin filtration, the peptide was dissolved in 4.1 mL (~10 mg/ mL) 5% acetonitrile, 0.1% TFA and filtered through a 0.22 μm syringe filter. Sample separation was achieved using a Vydac C_{18} column with a 5 to 95% acetonitrile gradient in aqueous 0.1 % TFA, at a flow rate of 2.5 mL/ min over 30 minutes. Absorbance was monitored at 254 nm. Further analysis was performed on a Beckman 126 analytical HPLC system equipped with a Waters C_{18} X-Terra column (4.6 mm X 250 mm) using the same gradient at 1 mL/ min.

Gel electrophoresis. All gels were poured according to the standard procedure for the preparation of sodium dodecyl sulfate (SDS) polyacrylamide gels [116] and run on a BioRad Mini Protean 3 vertical mini-gel apparatus. Resolution gels containing 15% polyacrylamide prepared with stacking gels containing 5% polyacrylamide were run in 1X SDS buffer prepared from a 5X stock and were run for 120 minutes at 120 V. Samples Coomassie Brilliant Blue R-250 (Fisher Biotech) was used to visualize both streptavidin and dendrimer-peptide conjugate. Gels were soaked in the coomassie dye for 1 hour. To visualize the bands, the gel was immersed in 50 mL destaining solution: 40% methanol, 10% acetic acid in water, shaking gently until bands appeared. The destaining solution was removed and fresh added occasionally until any background staining was removed. A CCD camera was used for recording images.

MALDI-TOF. Sample solutions (1 μM) were mixed with one of several different matrix additives including: α-Cyano-4-hydroxycinnamic acid, 2,4,6-

trihydroxyacetophenone (THAP, 15 mg/ml in acetonitrile), ferulic acid, aqueous ammonium citrate (15 mg/ml), and/ or sinapic acid. The analyte-doped matrix crystals were washed 10 times with 5 μL of cold water to remove sodium and potassium ions. An Applied Biosystems (Framingham, MA) Voyager-DE STR mass spectrometer operating in positive- and negative-ion mode was used to obtain the mass spectra. The system is equipped with a N_2 laser providing 337 nm, 3 ns wide pulses with the accelerating voltage maintained at 25 kV for this study. Delayed extraction (~ 600 ns) mode was applied in linear time-of-flight detection.

Streptavidin addition. Conjugation with streptavidin (Sigma) was carried out in 5 mM phosphate buffered saline (PBS) at ~6 units streptavidin per 90 nmoles biotinylated peptide-dendrimer conjugate, a 3-fold molar excess of the recommended 1 μg biotin per unit streptavidin. The conjugation reaction was incubated at 27°C for 1.5 hours.

Biotin/streptavidin titrations. The concentration of streptavidin was determined using the BCA protein assay kit (Pierce). In a 1 mL UV-vis cuvette, 0.5 mg/ mL streptavidin was added. The streptavidin was complexed with 2-(4′-hydroxyazobenzene) benzoic acid (HABA) dye by adding 2 μg at a time from a 2μg/ μL (10 mM) stock while collecting UV-vis spectra after each addition. Sample was mixed thoroughly with a 10 μL pipet tip prior to each spectral reading. After adding ~7 μg of HABA (binding capacity for 244.3 g/mol HABA = 30 nmoles, 7 μg), the sample was spun on a 10,000 MWCO spin filter to remove any unbound dye. The resulting spectrum was used as the starting point for the titration experiment with D-biotin or biotinylated TAT-dendrimer conjugate. A 0.1 mg/ mL solution of D-biotin was prepared in water, and added to the

streptavidin solution 2 μL (0.2 μg) at a time. Again, samples were mixed thoroughly with a 10 μL pipet tip prior to each spectral reading. The procedure was repeated for TAT-dendrimer conjugate in place of D-biotin.

Both HABA-streptavidin and D-biotin-streptavidin absorb at 330 nm, but the release of HABA from streptavidin produces a decrease in absorbance at 500 nm corresponding to the rate of biotin-streptavidin bond formation. A plot of μg biotin added vs. absorbance at 500 nm yielded a binding curve. Binding curves for conjugate-streptavidin were compared to that of biotin-streptavidin.

RESULTS AND DISCUSSION

Synthesis. The possibility that unconjugated (dendrimer-free) peptide impurities (capable of competing with conjugate for streptavidin-binding sites) were present in the sample was a concern. The presence of biotinylated peptide failure sequences (capped intermediates from incomplete coupling reactions), if present, would greatly diminish the value of the gel electrophoresis results presented herein as they would contain biotin for streptavidin ligation but no dendrimer.

MALDI-TOF. As shown in Figure 5-1, the MALDI-TOF spectrum of crude reaction material, post ether precipitation indicated the presence of at least three impurities at m/z = 1468, 1535, and 2017. The target MW appears at m/z = 3369, and the expected $[M+H]^+$ m/z = 3369 as shown in Scheme 5-3 (calculated MW = 3368).
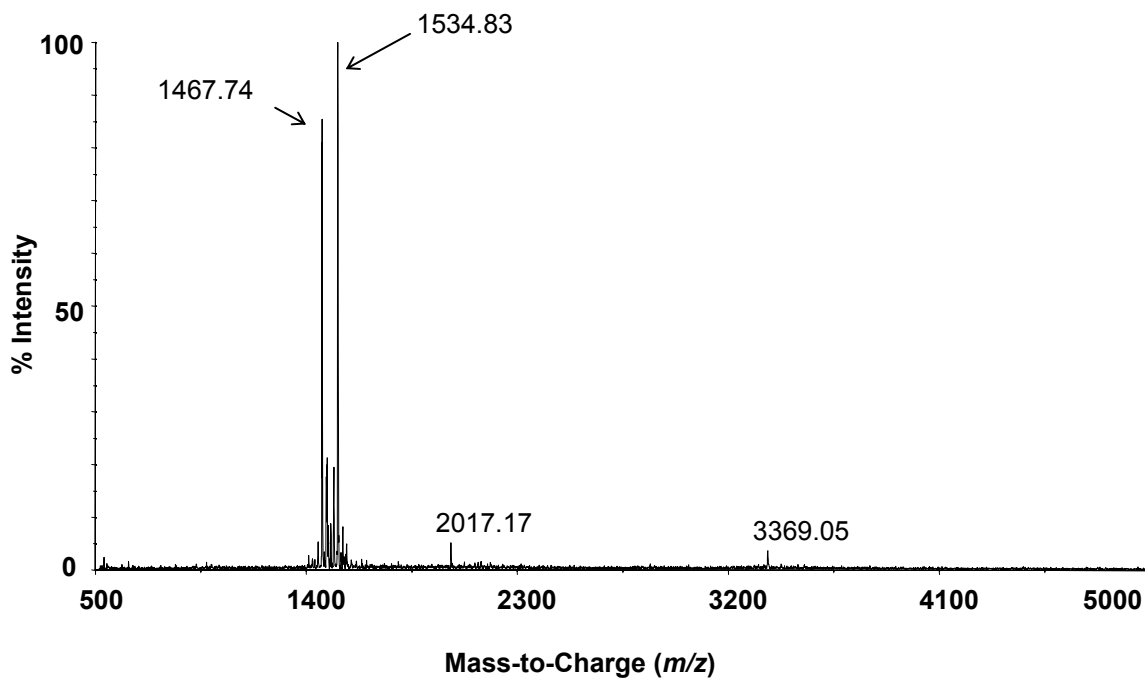
Figure 5-1. MALDI-TOF corresponding to solid-phase synthesized crude peptide-dendrimer conjugate post ether precipitation.

Scheme 5-3

$C_{147}H_{242}F_2N_{60}O_{28}S$
Exact Mass: 3365.90
Mol. Wt.: 3367.94
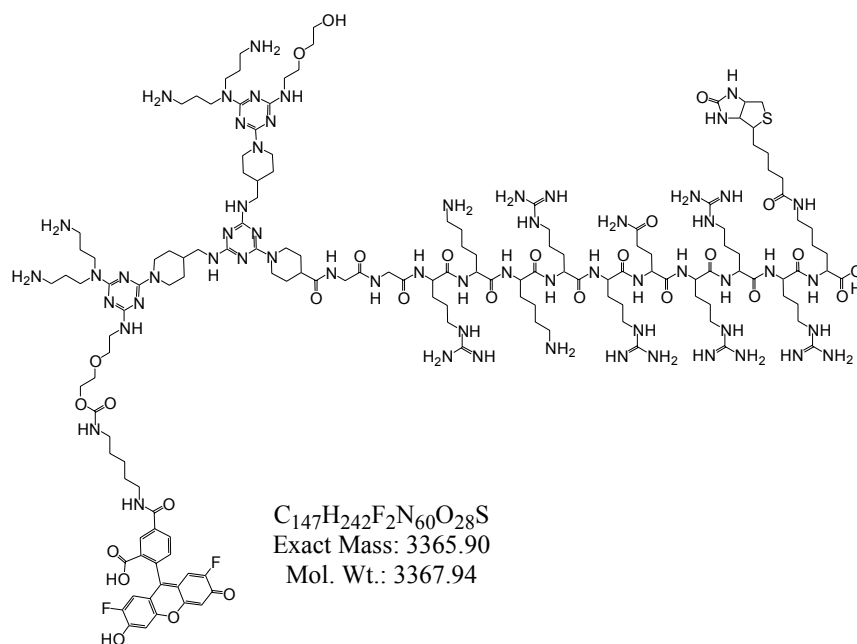
In an effort to separate the low molecular weight impurities from the desired product at m/z = 3369 in Figure 5-1, the product was filtered on a Millipore 3000 molecular weight cutoff (MWCO) centrifugal filter device. Spin filtration on a 3000 MWCO spin filter successfully separated the 1468 molecular weight (MW) impurity. The filtrate from the spin column was analyzed by MALDI-TOF, and the resulting spectrum is shown in Figure 5-2. A small amount of 1535 MW product was also observed in the filtrate.
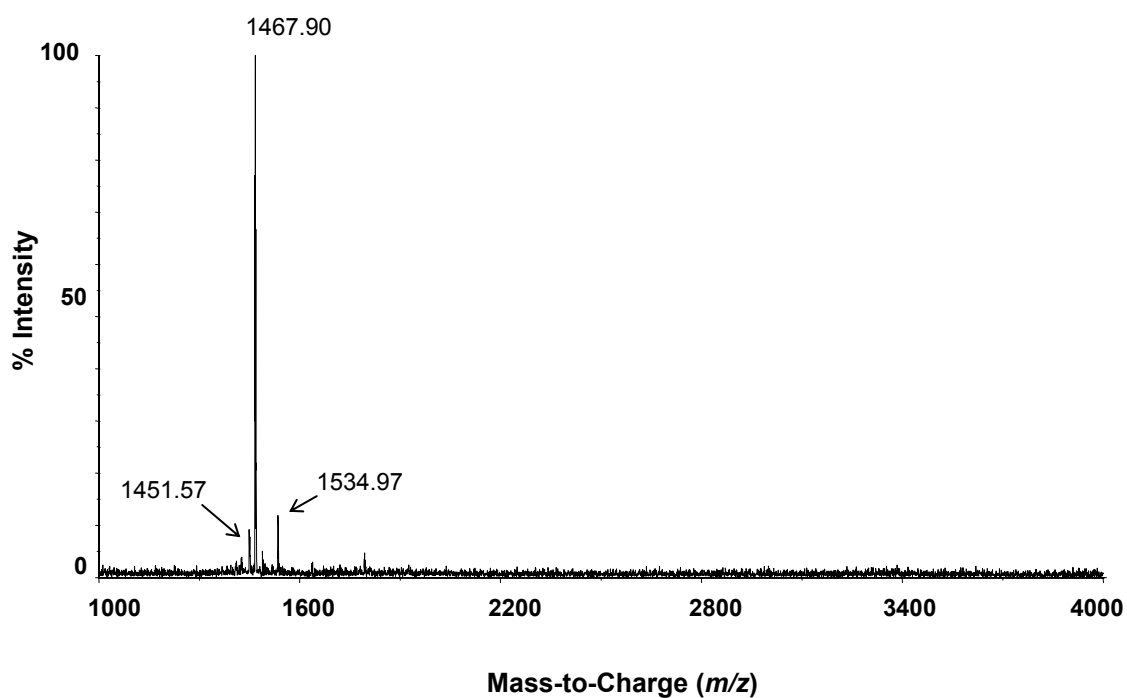
Figure 5-2. MALDI-TOF corresponding to crude peptide-dendrimer conjugate filtrate from a 3000 MWCO centrifugal spin filter

"Mini-PEG" linker coupling. One major impurity present after peptide cleavage was the result of an attempted peptide coupling step with a 8-amino-3,6-dioxaoctanoic acid ("mini-PEG") chain purchased in purified form from Peptides International. The "mini-PEG" was to serve as a biocompatible linker between the peptide and dendrimer. A positive Kaiser test indicated that the "mini-PEG" coupling failed.

Test cleavage to monitor "mini-PEG" coupling progress. Scheme 5-4 shows the structure and formula corresponding to the peptide product formed from this test cleavage. MALDI-TOF data from this small sample of cleaved intermediate supported Kaiser test results indicating that the "mini-PEG" coupling was unsuccessful. Figure 5-3 shows the MALDI-TOF results corresponding to the crude product formed from the test cleavage (MALDI-TOF: $[M+H]^+$ *m/z* expected for successful PEG coupling = 1840.2, not found; *m/z* $[M+H]^+$ expected for no mini-PEG coupling = 1695.1, observed = 1695.3). All other peaks present at this intermediate stage in the synthesis, were not found in the final product, and were attributed to imputities present only in the test cleavage reaction mixture.

Scheme 5-4
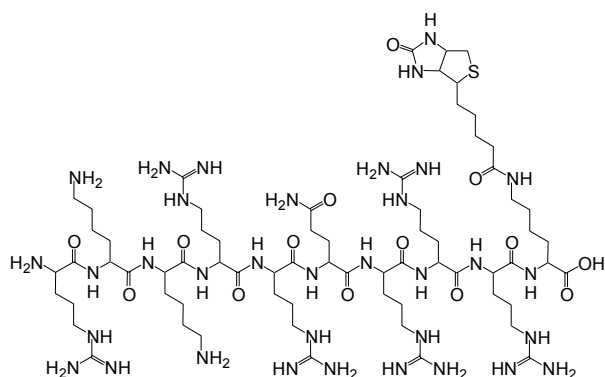
$C_{69}H_{132}N_{34}O_{14}S$
Exact Mass: 1693.04
Mol. Wt.: 1694.07

It should be noted that the two major impurities found after peptide-dendrimer cleavage with *m/z* [M+H]$^+$ of 1467.7 and 1534.8, shown in Figure 5-2, were not present at the test cleavage stage as they likely would be if they had originated from failure sequences (short peptide impurities that have been capped during peptide synthesis as a result of incomplete coupling reactions).
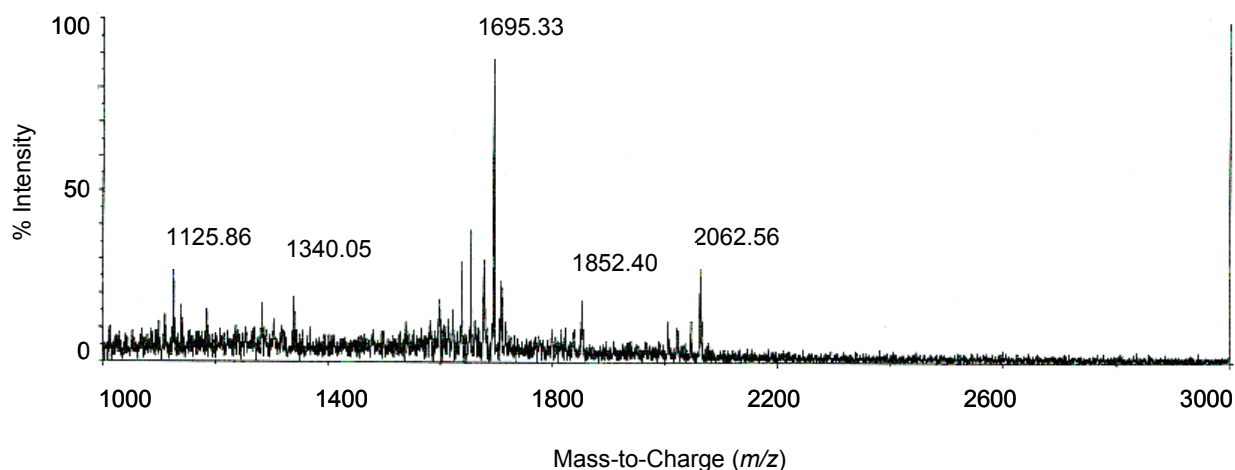
Figure 5-3. MALDI-TOF corresponding to peptide intermediate shown in Scheme 5-4 (calculated *m/z* [M+H]$^+$ = 1695.1) from the test cleavage.

Substituting glycine residues for "mini-PEG" linker. Since there was no evidence of PEG coupling at this stage, the remaining material was used to continue with the synthesis of a peptide-dendrimer conjugate. Two glycine residues, which readily coupled, were added in place of the "mini-PEG" to act as a short spacer. Evidence of "mini-PEG" coupling was eventually observed in the final product (Figure 5-4), giving rise to two different peptide-dendrimer conjugates, but since the dendrimer was attached

to both species the impurity contributed no impediment to our main synthetic goal which was to accomplish and demonstrate megamer formation. Scheme 5-3 (mentioned above) shows the structure and formula corresponding to desired peptide-dendrimer conjugate, and Scheme 5-5 shows the structure and formula corresponding to the "mini-PEG" containing peptide-dendrimer conjugate byproduct.
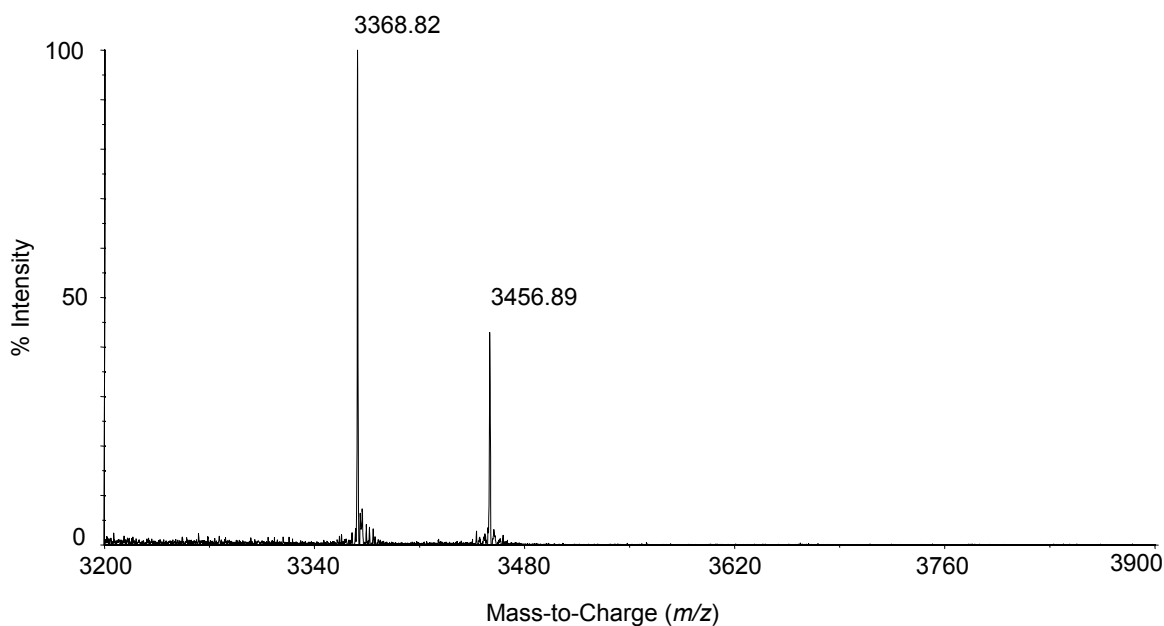
Figure 5-4. MALDI-TOF corresponding to target peptide-dendrimer (calculated m/z $[M+H]^+$ = 3368.9) and "mini-PEG" containing product (calculated m/z $[M+H]^+$ = 3457.1).

Scheme 5-5

$C_{151}H_{250}F_2N_{60}O_{30}S$
Exact Mass: 3453.96
Mol. Wt.: 3456.05
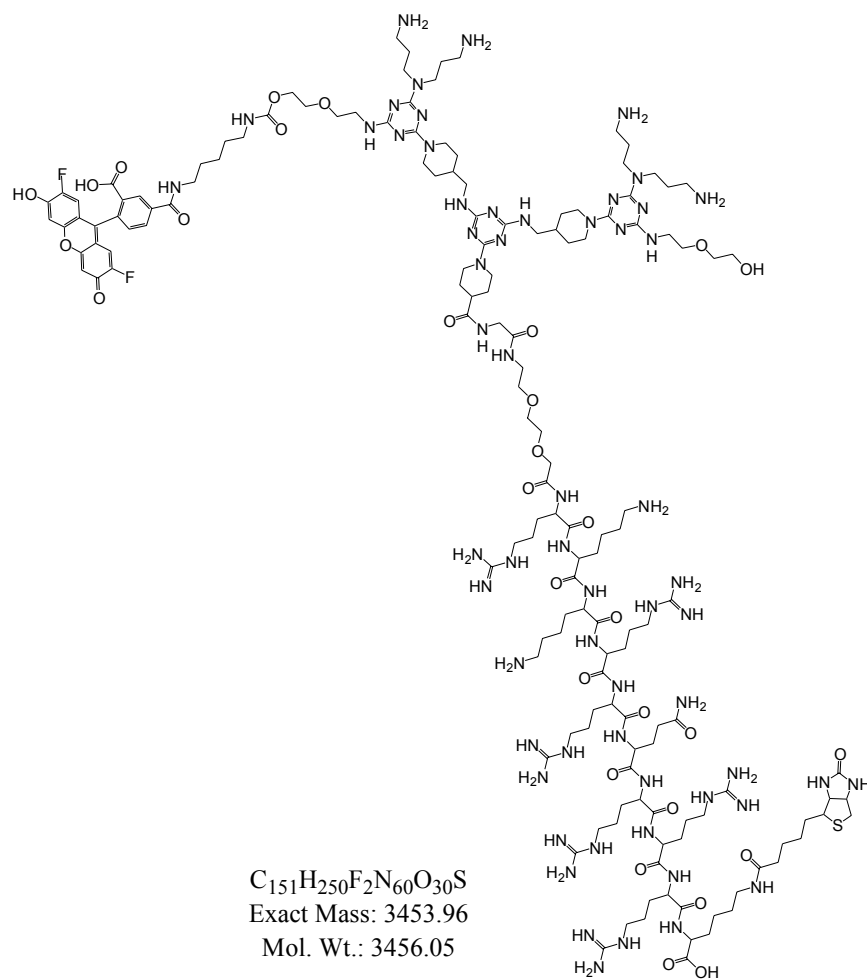
HPLC purification of TAT peptide. Two of the four HPLC fractions that were collected over the 30 minute gradient were yellow in color, one with a retention time of 5.7 minutes, and the other with a retention time of 8.2 minutes (Figure 5-5). The collected fractions from several injections were pooled, and the two resulting samples were dried *in vacuo* for MALDI-TOF analysis. The sample corresponding to elution at 8.2 minutes contained predominately two species, one corresponding to the desired target (MW = 3368 g/ mol), and the other corresponding to a "mini-PEG" containing byproduct (MW = 3456 g/ mol).

Detector 1 Results

Retention Time	Area	Area %	Height	Height %
2.810	2855	11.81	220	27.50
5.740	16781	69.39	339	42.38
8.187	3777	15.62	191	23.88
9.918	771	3.19	50	6.25
Totals	24184	100.00	800	100.00
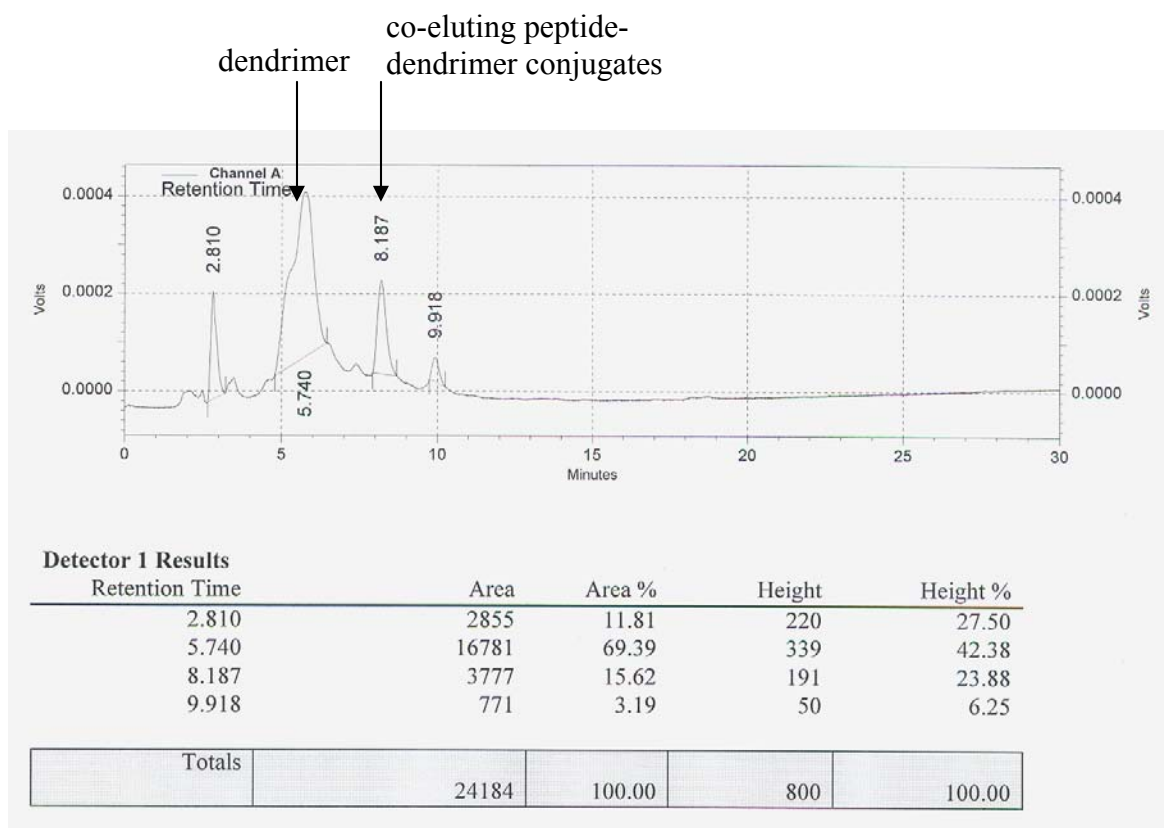
Figure 5-5. Preparatory HPLC trace of crude TAT-dendrimer conjugate.

Following peak identification by MALDI-TOF, the desired product (co-eluting with the "mini-PEG" containing side product) was run by analytical HPLC, resulting in one predominant peak around 14 minutes (Figure 5-6).
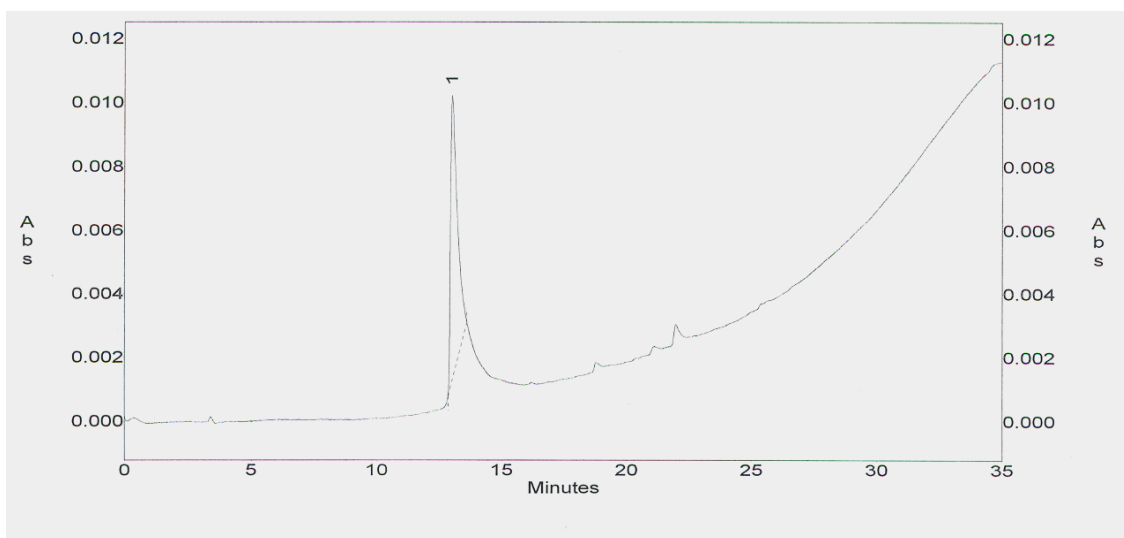
Figure 5-6. Analytical HPLC trace of semi-purified TAT-dendrimer conjugate.

Solution phase peptide-dendrimer conjugation. In an effort to increase yields, the TAT sequence was re-synthesized and cleaved from the resin after the isonipecotic acid coupling. Boc-protected Ipn was provided by Dr. Emily Hollink. Boc was released upon TFA cleavage affording the secondary amine in 75% yield. The attempted nucleophilic aromatic substitution reaction between the terminal secondary amine and the G2 monochloride dendrimer proceeded over many days, and never reached completion according to reverse-phase thin layer chromatography and MALDI-TOF. Several solvent systems and reaction conditions such as the addition of heat along with the addition of

denaturants like Tween-20 were employed to speed the reaction progress with no observed effect. Sterics may play a large role in the poor yields obtained in many of the biopolymer-dendrimer couplings discussed throughout this work. Figure 5-7 shows the MALDI-TOF result indicating formation of the desired product at m/z = 3369, as expected. The resulting product afforded one conjugate rather than two as above, but in much lower yield.
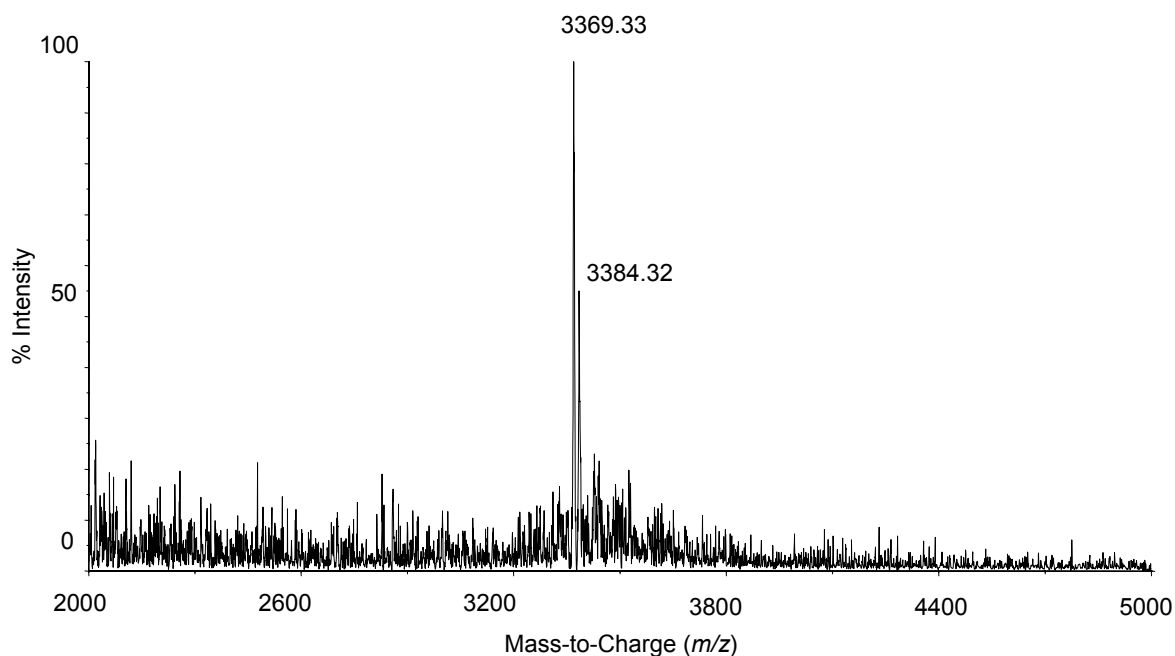
Figure 5-7. MALDI-TOF corresponding to product formed from the solution-phase synthesis of the TAT peptide dendrimer conjugate.

Possible role of steric hindrance. Coupling a more reactive triazine dichloride with the same secondary amine-terminated TAT peptide was unsuccessful, indicating that issues unrelated to the reactivity of the dendrimer are involved in the observed poor

yields. The preparation of a dichloride core from the reaction of an HPLC-purified piperazine-activated dendrimer with cyanuric chloride and subsequent conjugation.attempts are discussed below. This dendrimer would have yielded a construct amenable to further modifications through a maleimide functionality also present on the dendrimer, however, the attempted site of peptide conjugation was at the dichloride core of a dendrimer resulting from the reaction of the purified G2 dendrimer in Scheme 5-3 with cyanuric chloride, on ice, in THF containing a small amount of DIPEA. The poor conjugation yields observed with dichloride triazine-based dendrimers suggest steric hindrance could be the primary cause of low yields. A longer glycine chain separating the peptide from the dendrimer might have been beneficial for eliminating some of the steric hinderance thought to be causing poor reactivity.

Scheme 5-6

$C_{72}H_{92}N_{22}O_{15}$
Exact Mass: 1504.71
Mol. Wt.: 1505.64
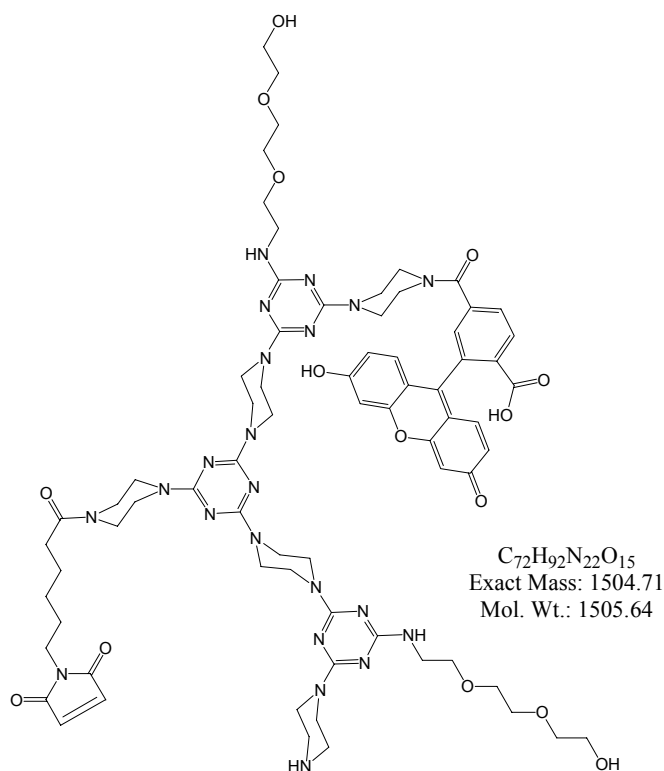
Gel electrophoresis. The gel shown in Figure 5-8 shows that a high molecular weight complex is formed (lane 3) upon the addition of conjugate to the streptavidin, which otherwise traveled through the SDS gel as a monomer at ~13 kDa. The two preceeding lanes contained 0.1 µg (lane 2) and 0.5 µg (lane 1) streptavidin. Comparison with the molecular weight marker reveals that the higher molecular weight band corresponds to a molecular weight $\cong$ 66 kDa (albumin standard) by gel electrophoresis indicating the presence of tetrameric streptavidin. Noted previously, biotin or biotinylated molecules stabilize the tetrameric form of streptavidin. In order to determine that the tetrameric streptavidin was bound to conjugate, the sample was titrated with free biotin, which has a higher affinity for streptavidin, and a much smaller dissociation constant (10^{-15} M).
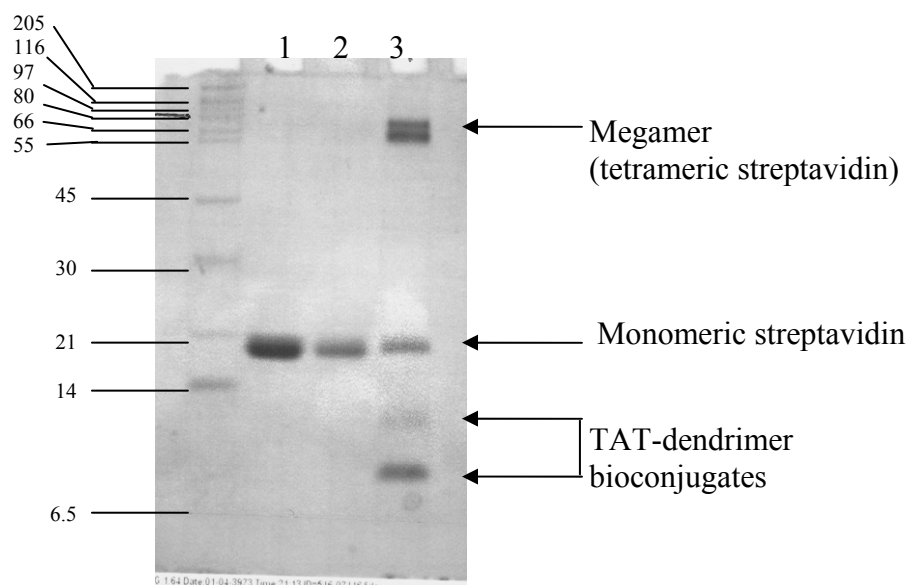
Figure 5-8. Coomassie stain of a 15% SDS polyacrylamide gel of streptavidin and megamer.

The gel shown in Figure 5-9 revealed a downward band shift indicating a decreased molecular weight of the tetrameric streptavidin as D-biotin replaced TAT-dendrimer conjugate. Lane 1 was loaded with the megamer prior to addition of D-biotin. Lanes 2 through 6 illustrated the removal of higher molecular weight conjugate and replacement with lower molecular weight D-biotin indicated by a downward band shift in the 66 kDa region. Importantly, the lower region of the gel showed an increase in fluorescent signal arising from an increase in the release of TAT-dendrimer bioconjugate from the streptavidin. Two bands were seen corresponding to the bioconjugate released, presumably because 2 major products (with and without mini-PEG) were formed. Lane 7 was loaded with D-biotin, and no bands were observed, as expected. Lane 8 contained TAT peptide-dendrimer conjugate. Lane 9 was loaded with streptavidin, and because there was no D-biotin present to stabilize the teramer, it is observed in the monomeric form ~13 kDa. Lane 10 contained molecular weight marker (Amersham wide range). The increase in coomassie uptake as biotin replaces the bioconjugate on streptavidin is thought to be due to the increased accessibility of the hydrophobic dye to streptavidin.

Spectral titrations. Figure 5-8 shows 2 different titrations. The top spectrum is a titration of streptavidin with HABA, which absorbs maximally ~350 nm. The streptavidin-HABA and streptavidin-biotin complexes also absorb ~350 nm, but the streptavidin-HABA complex is unique in that it absorbs at 500 nm. Unbound HABA does not absorb at 500 nm, allowing for spectral detection of HABA release as biotin (which has a much higher association constant with streptavidin than HABA) or biotinylated species bind to streptavidin.
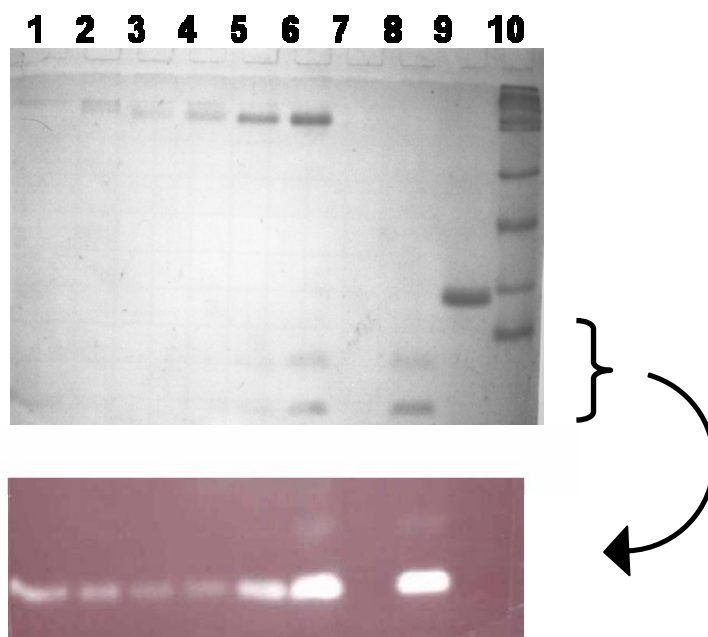
Figure 5-9. Coomassie stain of a 15% SDS polyacrylamide gel of megamer titrated from right to left with D-biotin. Fluorescence observed across the lower portion of the gel increases as the bioconjugate is released from the streptavidin.

Shown in Figure 5-10, when 2 μg HABA has been added to the streptavidin, an increase in A_{350} is observed. Likewise, an increase is observed when another 2 μg has been added, shown as 4 μg HABA in Figure 5-10. After the addition of another 2μg HABA (6 μg total), the sample was filtered to remove excess HABA. This sample was used as the starting material for the next titration. By titrating in biotin, shown in the bottom series of spectra, release of HABA is observed at A_{500}.
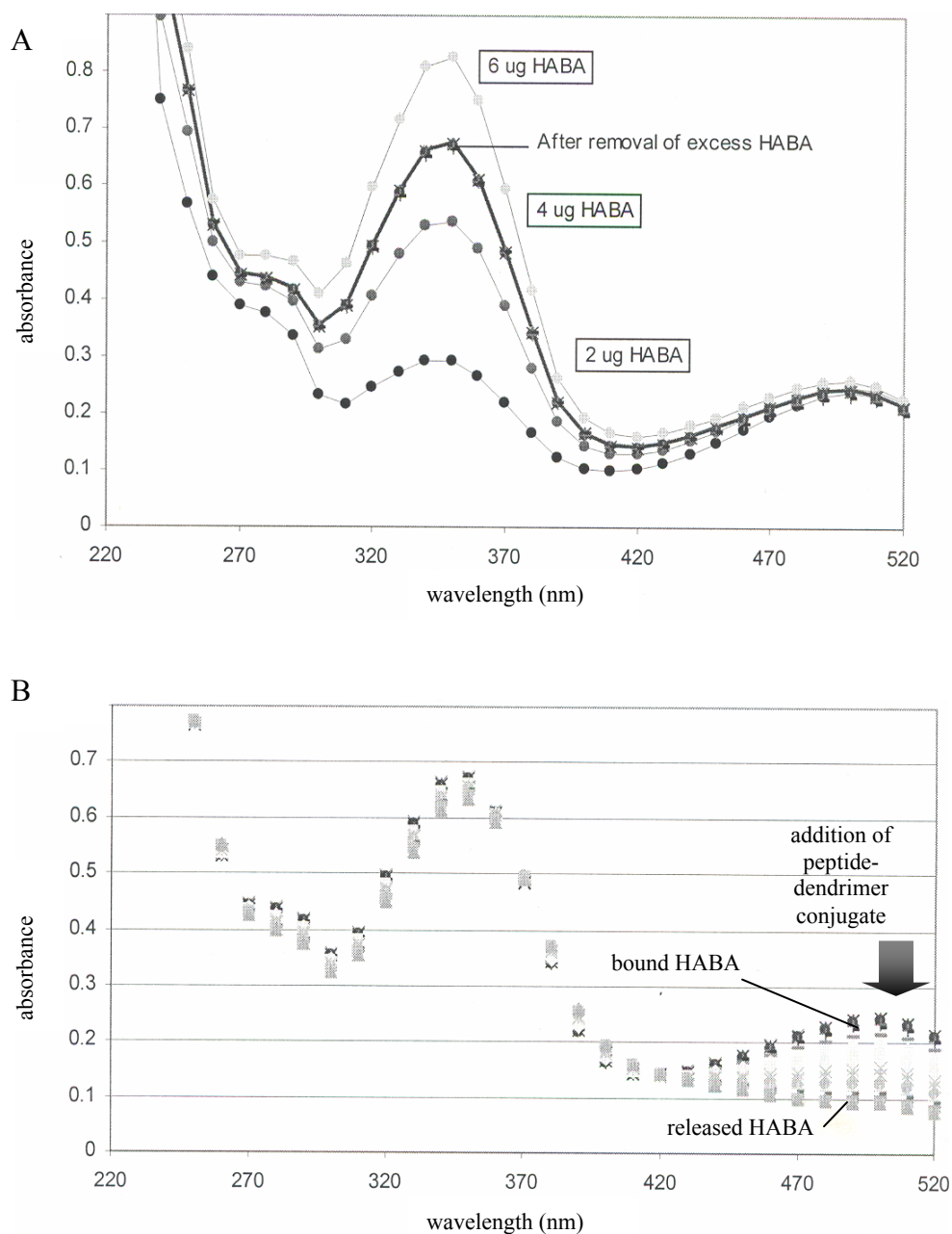
Figure 5-10. Spectral results from the titration of streptavidin (A) with HABA and (B) with TAT-dendrimer conjugate resulting in HABA release and a corresponding decrease in A_{500}.

Figure 5-11 compares the rates of HABA release upon the addition of D-biotin with that of biotinylated TAT-dendrimer conjugate. As shown, there is a rapid rate of HABA release when titrating with D-biotin that levels off at approximately 10 μg D-biotin added. Conjugate on the other hand binds to streptavidin at a much slower rate. D-biotin maximally bound to the streptavidin ~ 10 μg or 41 nmoles, very close to the theoretical 45 nmole binding capacity. The binding capacity was determined according to the following calculation:

$$(0.75 \text{ mg}/ 66,000 \text{ mg/mmol}) \times (1 \text{ mmol}/ 1,000,000 \text{ nmol}) = 11.36 \text{ nmoles tetramer}$$

$$1 \text{ tetramer binds 4 eq. biotin, therefore, } 11.36 \times 4 = 45.44 \text{ nmoles}$$

Maximal binding of streptavidin, on the other hand, took place at ~ 60 μg or 18 nmoles TAT-dendrimer conjugate indicating incomplete megamer formation possibly due to sterics.

MALDI-TOF. Protein subunits typically break apart using MALDI-TOF, so that only very stable subunit interactions are detected. In most cases, as is the case for streptavidin, the typical MALDI process will yield signal for the monomer only. Figure 5-12 shows the MALDI result for streptavidin alone, showing up at the monomer molecular weight ~13,000.
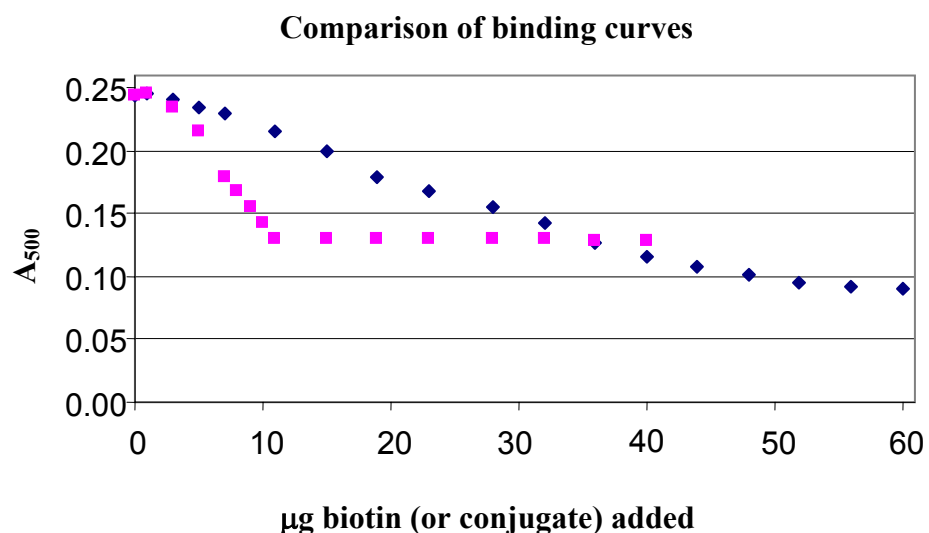
Figure 5-11. HABA-release curves of μg D-biotin (■) or biotinylated TAT-dendrimer conjugate (◆) vs. A_{500}.

As observed with the gels, however, the addition of biotinylated conjugate resulted in stabilization of the tetrameric form, and the protein was able to remain intact after being subjected to the MALDI process. Evidence of this is shown in Figure 5-13, where the the dimer ~26 kDa is evident as well as a trimer, presumably formed during the MALDI process ~39 kDa. Also evident by MALDI-TOF is the addition of new trimeric and tetrameric forms of the protein indicating megamer formation. In Figure 5-14, trimeric streptavidin is observed at 39 kDa. The addition of 3368 Da arising from a biotin-mediated interaction with the TAT bioconjugate is shown ~ 42 kDa, and the mini-PEG containing side product (MW 3456) appears ~ 100 Da higher. The same trend is observed for the tetrameric form seen at ~53 kDa.
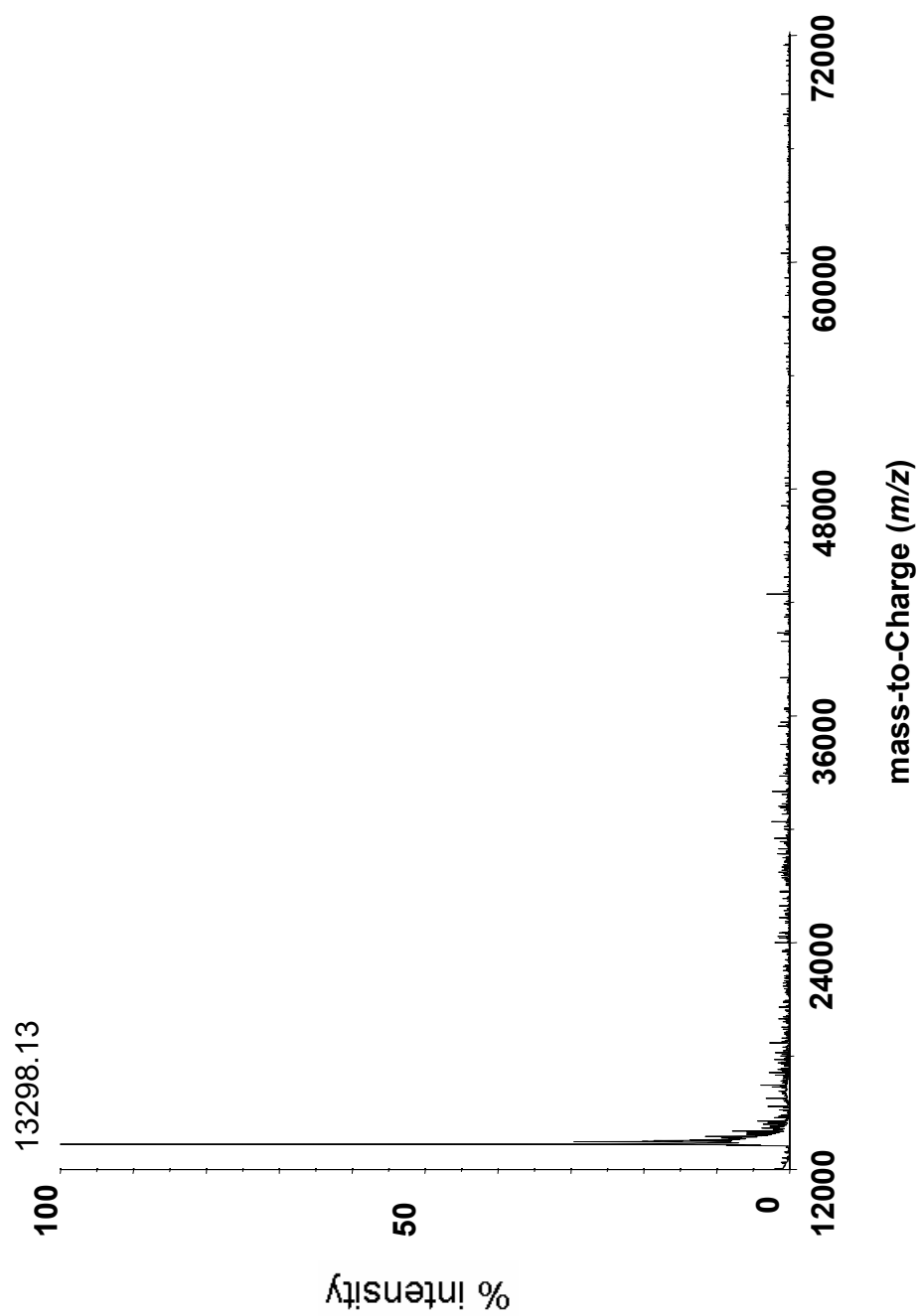
Figure 5-12. MALDI-TOF results for streptavidin, where streptavidin monomer appears ~13 kDa.
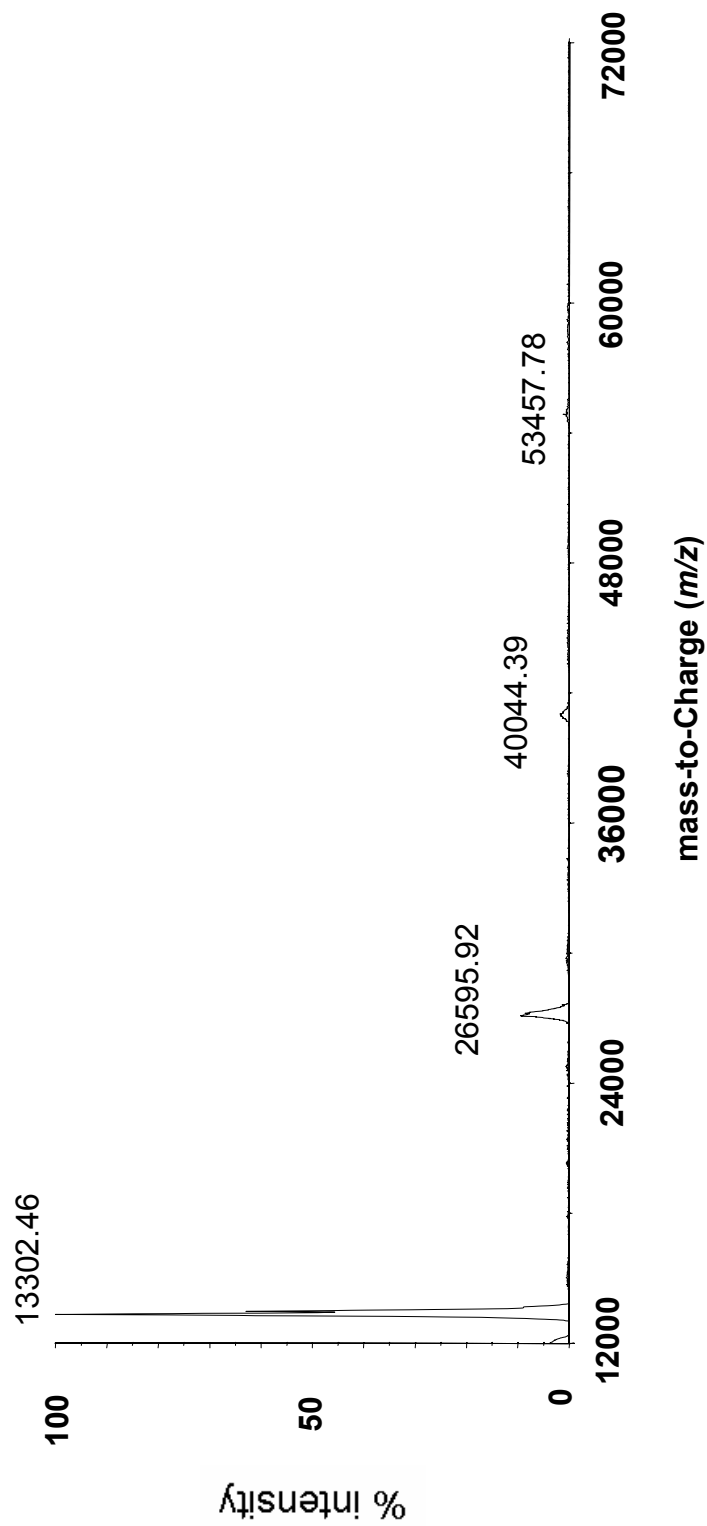
Figure 5-13. MALDI-TOF results for streptavidin plus TAT conjugate, where streptavidin is observed ~13.3 kDa. dimmer at ~26.6 kDa. trimer ~39.9 kDa. and tetramer ~53.2 kDa.
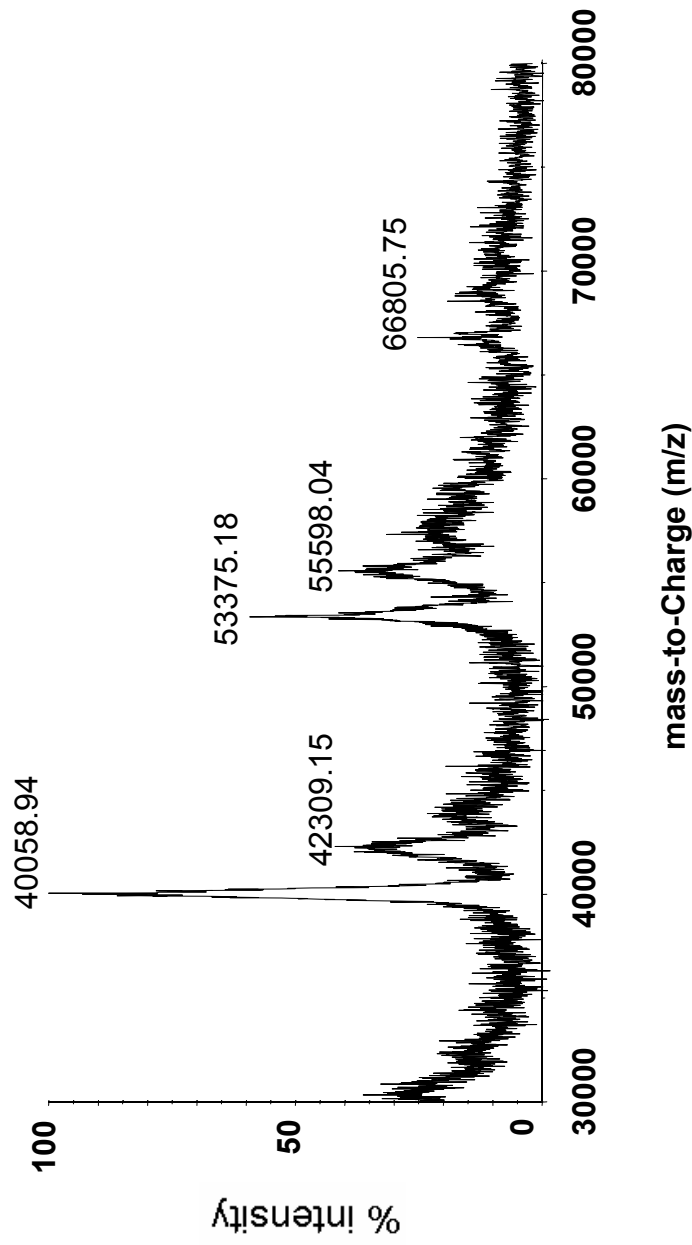
Figure 5-14. MALDI-TOF results for streptavidin plus TAT conjugate, where streptavidin trimer appears ~ 40 kDa and tetramer ~53 kDa. Peaks corresponding to the addition of TAT appear ~ 42 kDa and 56 kDa. The peak at 67 kDa corresponds to the tertamer bound by four 3368 MW TAT conjugates to form the desired megamer.

CONCLUSIONS

We show that dendrimers derivatized with biotin can assemble in the presence of streptavidin, a 60 kDa tetramer that binds 4 biotin molecules. While the non-covalent assembly is difficult to probe using MALDI-TOF, gel electrophoresis and titration experiments suggest that the assembly occurs spontaneously. The resulting macromolecule is naturally monodisperse, and facilitates the tetravalent display of dendrimers. Gel data suggests that at least some of the streptavidin was completely bound in the presence of an excess of TAT conjugate because four distinct band shifts were observed indicating the presence of four distinct streptavidin tetramers.

Dendrimer constructs with similar topologies are referred to as megamers, but none to date have relied on the interaction of a protein-*ligand* interaction. The megamer strategy looks promising for drug delivery because it is allows for chemically interchangeable surface groups or targeting and transport moeities that are located on the dendrimer's periphery to be "plugged into" a biocompatible macromolecular carrier. The size of the final construct exceeds the necessary molecular weight for the exploitation of EPR in tumors.

CHAPTER VI

SUMMARY AND CONCLUSIONS

This work illustrates the challenges involved in forming bioconjugates between dendrimers and ssDNA or peptides. Methods for purification of ssDNA-dendrimer constructs have been presented and techniques for the elucidation of solution-phase and solid-supported behavior of these conjugates have been discussed. Skepticism regarding the nature of the interaction between the cationic dendrimers and anionic ssDNA has been addressed. Although electrostatic binding with DNA may still exist in these systems, it may serve to enhance the rate of covalent bond formation.

The proposed covalent linkage could offer increased protection to the attached oligonucleotides, for use in gene therapy, since it is less likely to dissociate. Variations of the reported conjugates could be a versatile and cost effective addition to many nanofabrication techniques that rely on hybridization including the preparation of more effective biosensors, self-assembly of more geometrically or topologically complex nanostructures, and development of more powerful DNA-computation strategies.

Hybridization or duplex DNA formation *via* Watson-Crick base-pairing between ssDNA and ssDNA-dendrimer conjugates is essential for all of the applications mentioned herein. Thus it is of great interest that these ssDNA-dendrimer constructs have been successfully hybridized with ssDNA attached to a gold surface. This result indicates that hybridization is not adversely affected by the presence of a covalently attached dendrimer and further demonstrates their potential as signal enhancement techniques for measuring the extent of hybridization.

Chapter III discussed how disulfide-linked conjugates were shown to increase the sensitivity of surface hybridization studies using surface plasmon resonance. Due to the homogenous nature of these constructs they are also amenable to solution phase analytical techniques like gel electrophoresis, mass spectrometry, and a variety of automated spectral techniques for rapid analysis. Homogeneous detection capabilities allow for the opportunity to conduct real-time spectral analysis of several interactions between DNA and various other biomolecules.

Chapter IV discussed solution phase hybridization studies and the melting temperature of a 25-mer was compared to that of the dendrimer-bound analog. Results revealed that the dendrimer does not necessarily *preclude* duplex DNA formation as some hyperchomicity is detected upon the addition of complement. However, the solution-phase experiments do suggest that the DNA and dendrimer are interacting in some way resulting in an increased A_{260} relative to ssDNA prior to the addition of complement. The ability of enzymes to function in the presence of dendrimers based on melamine, as demonstrated in Chapter IV, is hopeful as it suggests that the analysis of enzyme-substrate interactions and assays for sequence specificity using these constructs as scaffolds will be possible.

Chapter V describes the self-assembly of peptide dendrimer conjugates around a streptavidin tetramer. Binding curve results indicate that the larger conjugate does not bind as quickly as D-biotin, and does not achieve maximal binding efficiency. Gel results, however, show that 4 distinct streptavidin tetramers were formed, suggesting that megamer formation was successful. Due to their size, scalability, and ease of preparation, megamers serve as an attractive target for drug delivery studies.

REFERENCES

(1)   Buhleier, E., Wehner, W., Vögtle, F. *Synthesis* **1978**, *2*, 155-158.

(2)   Chahan, A. S., Sridevi, S., Chalasani, K. B., Jain A. K., Jain, S. K., Jain, N. K., Diwan, P. V. *J. Controlled Release* **2003**, *90*, 335-343.

(3)   Duncan, R. *Polym. Mater. Sci. Eng.* **2001**, *84*, 214.

(4)   Esfand, R., Tomalia, D. A. *Drug Discovery Today* **2001**, *6*, 427-436.

(5)   Goller, R., Vors, J.-P., Caminade, A.-M., Majoral, J.-P. *Tetrahedron Lett.* **2001**, *42*, 3587-3590.

(6)   Ihre, H. R., Padilla De Jesus, O. I., Szoka, F. C., Fréchet, J. M. J. *Bioconjugate Chem.* **2002**, *13*, 443-452.

(7)   Padilla De Jesus, O. L., Ihre, H. R., Gagne, L., Fréchet, J. M. J., Szoka, F. C. *Bioconjugate Chem.* **2002**, *13*, 453-461.

(8)   Hecht, S., Fréchet, J. M. *Angew. Chem. Int. Ed.* **2001**, *40*, 74-91.

(9)   Enomoto, M., Aida, T. *J. Am. Chem. Soc.* **2002**, *124*, 6099-6108.

(10)   Maksimenko, A., Mendrouguine, V., Gottick, M., Bertrand, J.-R., Majoral, J.-P., Malvy, C. *The Journal of Gene Medicine* **2003**, *5*, 61-71.

(11)   Roessler, B. J., Bielinska, A. U., Janczak, K., Lee, I. Baker, J. R. *Biochem. Biophys. Res. Commun.* **2001**, *283*, 124-129.

(12)   Cheng, H., Zhou, R., Liu, L., Du, B., Zhou, R. *Genetica* **2000**, *108*, 53-56.

(13)   Wang, Y., Boros, P., Liu, J., Qin, L., Bai, Y., Bielinska, A. U., Kukowska-Latallo, J. F., Baker, J. R, Bromberg, J. S. *Molecular Therapy* **2000**, *2*, 602-608.

(14)   Prusiner, S. B., Supattapone, S., Scott, M. R.: U.S. Pat. **2001**, US 6,322,802 B1.

(15)   Marra, K. G., Choi, D., Boduch, K. *Polym. Mater. Sci. Eng.* **2001**, *85*, 47.

(16)   Bosman, A. W., Jansen, R. A. J. J., Meijer, E. W. *Chem. Rev.* **1999**, *99*, 1665 - 1688.

(17)   Crooks, R. M., Zhao, M., Sun, L., Chechik, V., Yeung, L. K. *Acc. Chem. Res.* **2001**, *34*, 181.

(18)   Fréchet, J. M. J. *Proc. Natl. Acad. Sci.* **2002**, *99*, 4782.

(19)   Zeng, F., Zimmerman, S. C. *Chem. Rev.* **1997**, *97*, 1681-1712.

(20)   Zimmerman, S. C., Lawless, L. J. *Top. Curr. Chem.* **2001**, *217*, 95.

(21)   Yoon, H. C., Hong, M-Y., Kim, H. S. *Langmuir* **2001**, 1234-1239.

(22)   Chang, A.-C., Gillespie, J. B., Tabacco, M. B. *Anal. Chem.* **2001**, *73*, 467-470.

(23)   Koo, B. W., Song, C. K., Kim, C. *Sens. Actuators* **2001**, *77*, 432-436.

(24)   Balzani, V., Ceroni, P., Gestermann, S., Gorka, M., Kauffmann, C., Vogtle, F. *Tetrahedron* **2002**, *58*, 629-637.

(25)   Kim, C., Park, E., Song, C. K., Koo, B. W. *Synth. Met.* **2001**, *123*, 493-496.

(26)   Crooks, R. M. *Chem. Phys. Chem.* **2001**, *2*, 644-654.

(27)   Li, H., Kang, D-J., Blamire, M. G., Huck W. T. S. *Nano Lett.* **2002**, *2*, 347-349.

(28)   Wu, X. C., Bittner, A. M., Kern K. *Langmuir* **2002**, *18*, 4984-4988.

(29)   McKendry, I. R., Wilhelm, T. S. H., Weeks, B., Fiorini, M., Abell, C., Rayment, T. *Nano Lett.* **2002**, *2*, 713-716.

(30)   Tsukruk, V. V. *Adv. Mater.* **1998**, *10*, 253-257.

(31)   Sideratou, Z., Foundis, J., Tsiourvas, D., Nezis, I. P., Papadimas, G., Paleos, C. M. *Langmuir* **2002**, *18*, 5036-5039.

(32)   Kobayashi, H., Kawamoto, S., Star, R., Waldmann, T., Tagaya, Y., Brechbiel, M. *Cancer Research* **2003**, *63*, 271-276.

(33)   Kobayashi, H., Saga, T., Kawamoto, S., Sato, N., Hiraga, A., Ishimori, T., Konishi, J., Togashi, K., Brechbiel, M. *Cancer Research* **2001**, *61*, 4966-4970.

(34)   Strable, E., Bulte, J. W. M., Moskowitz, B., Vivekanandan, K., Allen, M., Douglas, T. *Chem. Mater.* **2001**, *13*, 2201-2209.

(35)   Wang, J., Jia, X., Zhong, H., Luo, Y., Zhao, X, Cao, W., Li, M. *Chem. Mater.* **2002**, *14*, 2854-2858.

(36)   He, J.-A., Valluzzi, K. Y., Dolukhanyan, T., Sung, C., Kumar, J., Tripathy, S. *Chem. Mater.* **1999**, *11*, 3268-3274.

(37)   Street, S. C., Rar, A., Zhou, J. N., Liu, W. J., Barnard, J. A. *Chem. Mater.* **2001**, *13*, 3669-3677.

(38)   Amirpour, M. L., Ghosh, P., Lackowski, W. M., Crooks, R. M., Pishko, M. V. *Anal. Chem.* **2001**, *73*, 1560-1566.

(39)   Lupton, J. M., Samuel, I. D. W., Frampton, M., Beavington, R., Burn, P. L. *Adv. Funct. Mater.* **2001**, *11*, 287-294.

(40)   Lupton, J. M., Samuel, I. D. W., Burn, P. L., Mukamel, S. *J. Chem. Phys.* **2002**, *116*, 455-459.

(41)   Huang, J., Sooklal, K., Murphy, C. *Chem. Mater.* **1999**, *11*, 3595-3601.

(42)   Frankamp, B. L., Boal, A. K., Rotello, V. M. *J. Am. Chem. Soc.* **2001**, *124*, 15146-15147.

(43)   De Groot, D., Reek, J. N. H., Kamer, P. C. J., Van Leeuwen, P. W. N. M. *Eur. J. Org. Chem.* **2002**, *6*, 1085-1095.

(44)   Crooks, R. M., Lemon, B. I. III., Sun L. Yeung, L. K., Zhao, M. *Topics in Current Chemistry* **2001**, *212*, 81-135.

(45)   Van Heerbeek, R., Kamer, P. C. J., Van Leeuwen, P. W. N. M., Reek, J. N. H. *Chem. Rev.* **2002**, *102*, 3717-3756.

(46)   Sun, L., Crooks, R. M. *Langmuir* **2002**, *18*, 8231-8236.

(47)   Groot, D., Waal, B. F. M., Reek, J. N. H., Schenning, A. P. H. J., Kamer, P. C. J., Meijer, E. W., Leeuwen, P. W. N. M. *J. Am. Chem. Soc.* **2001**, *123*, 8453-8458.

(48)   Castagnola, M., Zuppi, C., Rossetti, D. V., Vincenzoni, F., Lupi, A., Vitali, A., Meucci, E., Messana, I. *Electrophoresis* **2002**, *23*, 1769-1778.

(49)   Haag, R., Sunder, A., Hebel, A., Roller, S. *J. Comb. Chem.* **2002**, *4*, 112-119.

(50)   Newkome, G. R., Yoo, K. S., Kabir, A., Malik, A. *Tetrahedron Lett.* **2001**, *42*, 7537-7541.

(51)   Caminati, G., Turro, N. J., Tomalia, D. A. *J. Am. Chem. Soc.* **1990**, *112*, 8515-8522.

(52)   Tomalia, D. A., Baker, H., Dewald, J., Hall, M., Kallos, G., Martin, S., Roek, J., Ryder, J., Smith, P. *Polym. J.* **1985**, *17*, 117-132.

(53)   Fréchet, J. M. J. *Science* **1994**, *263*, 1710-1715.

(54)   Zhang, W., Simanek, E. E. *Org. Lett.* **2000**, *2*, 843-845.

(55)   Steffensen, M. B., Simanek, E. E. *Org. Lett.* **2003**, *5*, 2359-2361.

(56)   Ringsdorf, H. *J. Polym. Sci. Polym. Symp.* **1975**, *51*, 135-153.

(57)   Zhang, K., Wu, X. Y. *Biomaterials* **2003**, *25*, 5281-5291.

(58)   Edelman, E. R., Langer R. *Biomaterials* **1993**, *14*, 621-626.

(59)   Creque, M., Langer, R., Folkman, J. *Diabetes* **1980**, *29*, 37-41.

(60)   Kost, J., Langer, R. *Advanced Drug Delivery Reviews* **1991**, *6*, 19-50.

(61)   Hunter, A. C., Moghimi, S. M. *Drug Discovery Today* **2002**, *7*, 998-1001.

(62)   Breslow, D. S. *Pure Appl. Chem.* **1976**, *46*, 103-113.

(63)   Wang, X. S., Armes, S. P. *Macromolecules* **2000**, *33*, 6640-6647.

(64)   Moghimi, S. M., Hunter, A. C. *Trends Biotechnol.* **2001**, *18*, 412-420.

(65)   Szebeni, J. *Crit. Rev. Ther. Drug Carrier Syst.* **2001**, *18*, 567-606.

(66)   Maeda, H. *Adv. Enzyme Regul.* **2001**, *41*, 189–207.

(67)   Duncan, R. *Pharmaceutical Science & Technology Today* **1999**, *2*, 441-449.

(68)   Lu, Y., Philip S. L. *Advanced Drug Delivery Reviews* **2002**, *54*, 675-693.

(69)   Broxterman, H. J., Georgopapadakou, N. H. *Drug Resistance Updates* **2004**, *7*, 79-87.

(70)   Malik, N., Wiwattanapatapee, R., Klopsch, R., Lorenz, K., Frey, H., Weener, J.-W., Meijer, E. W., Paulus, W., Duncan, R. *J. Controlled Release* **2000**, *65*, 133-148.

(71)   Stevelmans, S., van Hest, J. C., M., Jansen, J., F., G., A., van Boxtel, D., A., F., J., de Brabander-van den Berg, E. M., M., Meijer, E., W. *J. Am. Chem. Soc.* **1996**, *118*, 7398-7399.

(72)   Hawker, C. J., Wooley, K. L., Frechet, J. M. J. *J. Chem. Soc., Perkin. Trans. I* **1993**, 1287-1297.

(73)   Liu, M., Kono, K., Frechet, J. M. J. *J. Controlled Release* **2000**, *65*, 121-131.

(74)   Jansen, J. F. G. A., de Brabander-van den Berg, E. M. M., Meijer, E. W. *Science* **1994**, *266*, 1226-1229.

(75)   Jansen, J. F. G. A., Meijer, E. W., de Brabander-van den Berg, E. M. M. *J. Am. Chem. Soc.* **1995**, *117*, 4417-4418.

(76)   Haensler, J., Szoka, F. C. Jr. *Bioconjugate Chem.* **1993**, *4*, 372-379.

(77)   Seeman, N. C. *Nano Letters* **2001**, *1*, 22-26.

(78)   Frutos, A. G.; Smith, L. M.; Corn, R. M. *J. Am. Chem. Soc.* **1998**, *120*, 10277-10282.

(79)   Frutos, A. G.; Liu, Q.; Thiel, A. J.; Sanner, A. M. W.; Condon, A. E.; Smith, L. M.; Corn, R. M. *Nucleic Acids Res.* **1997**, *25*, 4748-4757.

(80)   Liu, F.; Sha, R.; Seeman, N. C. *J. Am. Chem. Soc.* **1999**, *121*, 917-922.

(81)   Winfree, E.; Liu, F.; Wenzler, L. A.; Seeman, N. C. *Nature* **1998**, *394*, 539-544.

(82)   Seeman, N. C. *Annu. Rev. Biophys. Biomol. Struct.* **1998**, *27*, 225-248.

(83)   Yan, H.; Zhang, X.; Shen, Z.; Seeman, N. C. *Nature* **2002**, *415*, 62-65.

(84)   Mao, C.; Sun, W.; Shen, Z.; Seeman, N. C. *Nature* **1999**, *397*, 144-146.

(85)   Turberfield, A. J.; Mitchell, J. C.; Yurke, B.; Mills, A. P., Jr.; Blakey, M. I.; Simmel, F. C. *Phys. Rev. Lett.* **2003**, *90*, 118102/118101-118102/118104.

(86)   Yurke, B. *Polymeric Materials Science and Engineering* **2003**, *89*, 127.

(87)   Yurke, B.; Turberfield, A. J.; Mills, A. P., Jr.; Simmel, F. C.; Neumann, J. L. *Nature* **2000**, *406*, 605-608.

(88)   Park, S.-J.; Taton, T. A.; Mirkin Chad, A. *Science* **2002**, *295*, 1503-1506.

(89)   Porath, D., Bezryadin, A., de Vries, S., Dekker, C. *Nature* **2000**, *403*, 635-637.

(90)   Carbone, A.; Seeman, N. C. *Proc. Natl. Acad. Sci.* **2002**, *99*, 12577-12582.

(91)   Shchepinov, M. S. M., K. U.; Elder, J. K.; Frank-Kamenetskii, M. D.; Southern, E. M. *Nucl. Acid. Res.* **1999**, *54*, 3035-3041.

(92)   Benters, R., Niemeyer, C. M., Wohrle D. *Chem. Bio. Chem.* **2001**, *2*, 686-694.

(93)   Lysik, M. A.; Wu-Pong, S. *J. Pharm. Sci.* **2003**, *92*, 1559-1573.

(94)   Morgan, R. A., Anderson, W. F. *Annu. Rev. Biochem.* **1993**, *62*, 191-217.

(95)   Houk, B. E., Martin, R., Hochhaus, G., Hughes, J. A. *Pharm. Res.* **2001**, *18*, 67-74.

(96)   Houk, B. E., Hochhaus, G., Hughes, J. A. *AAPS Pharm. Sci.* **1999**, *1*, E9.

(97)   Eichman, J. D., Bielinska, A. U., Latallo, J. F. K., Baker, J. R. Jr. *Pharmaceut. Sci. Technol. Today* **2000**, *3*, 232-245.

(98)   Sadler, K., Tam, J. P. *Rev. Mol. Biotech.* **2002**, *90*, 195-229.

(99)   Wu, X., Zhao, R., Li, Z., Yao, M., Wang, H.,; Han, J., Qu, S., Chen, X., Qian, L., Sun, Y.,; Xu, Y., Gu, J. *Biochem. Biophys. Res. Commun.* **2004**, *315*, 1004-1010.

(100)   Langer, M., Beck-Sickinger, A. G. *Curr. Med. Chem. Anti-Cancer Agents* **2001**, *1*, 71–93.

(101)   Tomalia, D. A., Huang, B., Swanson, D. R., Brothers, H. M., Klimash, J. W. *Tetrahedron* **2003**, *59*, 3799-3813.

(102)   Zeng, F., Zimmerman, S. C., Kolotuchin, S. V., Reichert, D. E. C., Ma, Y. *Tetrahedron* **2002**, *58*, 825-843.

(103)   Percec, V.; Glodde, M.; Bera, T. K.; Miura, Y.; Shiyanovskaya, I.; Singer, K. D.; Balagurusamy, V. S. K.; Heiney, P. A.; Schnell, I.; Rapp, A.; Spiess, H.-W.; Hudson, S. D.; Duan, H. *Nature* **2002**, *419*, 384-387.

(104)   Uyemura, M., Aida, T. *J. Am. Chem. Soc.* **2002**, *124*, 11392-11403.

(105)   Denti, G., Campagna, S., Serroni, S., Ciano, M., and Balzani, V. *J. Am. Chem. Soc.* **1992**, *114*, 2944-2950.

(106)   Balzani, V., Juris, A., Venturi, M., Campagna, S., Serroni, S. *Chem. Rev.* **1996**, *96*, 759-833.

(107)   Zimmerman, S. C.; Zeng, F.; Reichert, D. E. C.; Kolotuchin, S. V. *Science* **1996**, *271*, 1095-1098.

(108)   Newkome, G. R., Woosley, B. D., He, E., Moorefield, C. N., Güther, R., Baker, G. R., Escamilla, G. H., Merrill, J., Luftmann, H. *J. Chem. Soc. Chem. Commun.* **1996**, 2737-2738.

(109)   Corbin, P. S.; Lawless, L. J.; Li, Z.; Ma, Y.; Witmer, M. J.; Zimmerman, S. C. *Proc. Natl. Acad. Sci. USA* **2002**, *99*, 5099-5104.

(110)   Seeman, N. C. *Chemistry and Biology* **2003**, *10*, 1151-1159.

(111)   Yang, J. G., I.; Krishnamurthy, V. M.; Vazquez, J. A.; Costello, C. E.; Whitesides, G. M. *J. Am. Chem. Soc.* **2003**, *125*, 12392-12393.

(112)   Padilla, J. E., Colovos, C., Yeates, T. O. *Proc. Natl. Acad. Sci. USA* **2001**, *98*, 2217-2221.

(113)   Bell, S. A., McLean, M. E., Oh, S.-K., Tichy, S. E., Zhang, W., Corn, R. M., Crooks, R. M., Simanek, E. E. *Bioconjugate Chem.* **2003**, *14*, 488-493.

(114)   Zhang, W.; Nowlan, D. T., III; Thomson, L. M.; Lackowski, W. M.; Simanek, E. E. *J. Am. Chem. Soc.* **2001**, *123*, 8914-8922.

(115)   Brothers, H. M., Piehler, L. T., Tomalia, D. A. *J. Chromatogr. A* **1998**, *814*, 233-246.

(116)   Sambrook, J., Fristch, E. F., Maniatis, T. *Molecular Cloning: A Laboratory Manual; 2nd ed*; Cold Spring Harbor Laboratory: Plainview, NY, 1989; Vol. 1.

(117)   Brockman, J. M., Corn, R. M. *J. Am. Chem. Soc.* **1999**, *121*, 8044-8051.

(118)   Shimomura, M., Nomura, Y., Zhang, W., Sakino, M., Lee, K-H., Ikebukuro, K., Karube, I. *Analytica. Chimica. Acta.* **2001**, *434*, 223-230.

(119) Wink, T., Van Zuilen, S. J., Bult, A., Van Bennekom, W. P. *Anal. Chem.* **1998**, *70*, 827-832.

(120) Severs, A. H., Schasfoort, R. B. M. *Biosens. Bioelectron.* **1993**, *8*, 365-370.

(121) Bianchi, N., Rutigliano, C., Tomassetti, M., Feriotto, G., Zorzato, F., Gambari, R. *Clinic. Diag. Virol.* **1997**, *8*, 199-208.

(122) Nallur, G., Luo, C., Fang, L., Cooley, S., Dave, V., Lambert, J., Kukanskis, K., Kingsmore, S., Lasken, R., Schweitzer, B. *Nucleic Acids Res.* **2001**, *29*, e118.

(123) Leung, P. T., Pollard-Knight, D., Malan, G. P., Finlan, M. F. *Sens. Actuators* **1994**, *22*, 175-180.

(124) Chah, S., Hutter, E, Roy, D., Fendler, J. H., Yi, J. *Chem. Phys.* **2001**, *272*, 127-136.

(125) de Vries, E. F. A., Schasfoort, R. B. M., van der Plas, J. Greve, J. *Biosens. Bioelectron.* **1994**, *9*, 509-514.

(126) Frutos, A. G., Smith, L. M., Corn, R. M. *J. Am. Chem. Soc.* **1998**, *120*, 10277.

(127) Park, S.-J., Taton, T. A., Mirkin, C. A. *Science* **2002**, *295*, 1503-1505.

(128) Capaldi, S., Getts, R. C., Jayasena, S. D. *Nucleic Acids Res.* **2000**, *28*, e21.

(129) Wallace, R. B., Shaffer, J., Murphy, R. F., Bonner, J., Hirose, T., Itakura, K. *Nucleic Acids Res.* **1979**, *6*, 3543.

(130) Breslauer, K. J., Frank, R., Blšcker, H., Marky, L. A. *Proc. Natl. Acad. Sci. USA* **1986**, *83*, 3746-3750.

(131) Howley, P. M., Israel, M. F., Law, M-F., Martin, M. A. *J. Biol. Chem.* **1979**, *254*, 4876-4883.

(132) Koomen, J. M., Russell, W. K., Hettick, J. M., Russell, D. H. *Anal. Chem.* **2000**, *72*, 3860-3866.

(133) Green, N. M. *Methods Enzymol.* **1970**, *56*, 418-424.

(134) Zhang, W., Nowlan, D. T. III., Thomson, L. M., Lackowski, W. M., Simanek, E. E. *J. Am. Chem. Soc.* **2001**, *123*, 8914-8922.

(135) Saga, T., Sakahara, H. *Adv. Drug Deliv. Rev.* **1999**, *37*, 89-101.

(136) Wender, P. A., Mitchell, D. J., Pattabiraman, K., Pelkey, E. T., Steinman, L., Rothbard, J. B. *Proc. Natl. Acad. Sci. USA* **2000**, *97*, 13003-13008.

(137) Mie, M., Takahashi, F., Funabashi, H., Yanagida, Y., Aizawa, M., Kobatake, E. *Biochem. Biophys. Res. Commun.* **2003**, *310*, 730-734.

(138) Nori, A., Jensen, K. D., Tijerina, M., Kopeckova, P., Kopecek, J. *J. Control. Release* **2003**, *91*, 53-59.

(139) Schwarze, S. R., Ho, A., Vocero-Akbani, A., Dowdy, S. F. *Science* **1999**, *285*, 1569-1572.

APPENDIX A

List of abbreviations

A	adenine, (purine base in DNA)
BAM HI	sequence specific enzyme that cleaves double-stranded DNA (endonuclease)
Boc	butoxycarbonyl (amine protecting group)
C	cytosine (pyrimidine base in DNA)
DIPEA	*N,N*-diisopropyl ethylamine (Hunig's base)
DMT	dimethoxy trityl protecting group
DMF	*N,N*-dimethylformamide
DTT	dithiothreitol
EDTA	ethylenediaminetetra acetic acid
EMCS	*N*-(6-maleimidocaproxy)succinimide
EPR	enhanced permeability and retention
EXO III	enzyme that cleaves double-stranded DNA from the 3' terminus (exonuclease)
Fmoc	fluorinylmethoxycarbonyl (amine protecting group)
FTIR	fourier transform infrared
G	guanine (purine base in DNA)
GMBS	*N*-(4-maleimidobutyryloxy)succinimide
HABA	2-(4'-hydroxyazobenzene) benzoic acid
HPLC	high performance liquid chromatography
m/z	mass-to-charge ratio
MALDI-TOF	matrix-assisted laser desorption ionization time-of-flight
MWCO	molecular weight cutoff
NMR	nuclear magnetic resonance
PAGE	polyacrylamide gel electrophoresis
PAMAM	polyamidoamine
PEG	polyethylene glycol
SDS-PAGE	sodium dodecyl sulfate polyacrylamide gel electrophoresis
SPDP	succinimidyl 3-(2-pyridylthio)propionate
SPPS	solid-phase peptide synthesis
SPRi	surface plasmon resonance imaging
SSMCC	sulfosuccinimidyl 4-(*N*-maleimidomethyl)cyclohexane-1-carboxylate
T	thymine (pyrimidine base in DNA)
TAT	transactivator of transcription (peptide sequence from the TAT protein)
TBE	tris(hydroxymethyl) aminomethane-borate ethylenediaminetetra acetic acid buffer
TCEP	2-carboxyethylphosphine
TEAA	triethylamine acetate
TEMED	*N,N,N',N'*-tetramethylethylenediamine
TFA	trifloroascetic acid
THAP	2,4,6-trihydroxyacetophenone
THF	tetrahydrofuran
Tris-HCl	tris(hydroxymethyl) aminomethane-hydrochloric acid buffer
Tween-20	surfactant, sorbitan mono-9octadecenoate poly(oxy-1,1-ethanedlyl)

APPENDIX B

Letter of permission to reproduce Scheme 3-2

UCI: DEPARTMENT OF CHEMISTRY

UNIVERSITY OF CALIFORNIA, IRVINE

BERKELEY · DAVIS · IRVINE · LOS ANGELES · RIVERSIDE · SAN DIEGO · SAN FRANCISCO   SANTA BARBARA · SANTA CRUZ

Prof. Robert M. Corn
Department of Chemistry
University of California, Irvine
Irvine, CA 92697-2025

Tel: 949-824-4097
Fax: 949-824-8571
rmcorn@chem..ps.uci.edu
http://corninfo.ps.uci.edu

July 13, 2004
Thesis Office
Texas A&M University

To Whom It May Concern:

I have granted Ms. Megan McLean permission to reproduce, within her doctoral dissertation, a graphic originally created for publication in the *Annual Review of Physical Chemistry*. It was published in 2000, volume 51, pages 41-63 with co-authors Brockman and Nelson. The graphic, labeled Figure 4, illustrates the surface plasmon resonance (SPR) imaging experimental setup. If there are any questions regarding this matter please contact me at 949-824-1746 or email me at rcorn@uci.edu.

Thank you,

Robert M. Corn
Professor of Chemistry

VITA

Megan E. McLean   1010 Autumn Circle Apt B
(979) 260-9613   College Station, TX 77840

Education
    Ph.D. Chemistry - August 2004
    Texas A&M University, College Station, TX
    Research advisor: Dr. Eric Simanek

    B.S. Chemistry - May 1999
    State University of New York (SUNY) College at Fredonia, Fredonia, NY
    Research advisor: Dr. Konrad Kabza

Experience
    Department of Chemistry, Texas A&M University
    Research assistant (1999-2004)
    Teaching assistant (1999-2001)
    Undergraduate Organic Chemistry and General Chemistry laboratory instructor

    Department of Chemistry, SUNY Fredonia
    Independent lab research student (1997-1999)

Selected Oral Presentations
    2003 - 226th National ACS symposium, New York City "Solution-phase synthesis
        of DNA-dendrimers for use as antisense agents"
    2002 - Southwest Regional ACS Meeting, Austin "Synthesis and characterization of
        covalently linked DNA-dendrimers"

Publications
    Bell, S. A., McLean, M. E., Oh, S-K., Tichy, S. E., Zhang, W., Corn, R. M., Crooks,
    R. M., Simanek, E. E., Synthesis and characterization of covalently linked single-
    stranded DNA oligonucleotide-dendrimer conjugates. *Bioconjugate Chem.* **2003**, *14,*
    488-493

Volunteer Positions
    2004 - Regional Science Bowl, scientific judge; Jr. Regional Science Bowl,
        moderator; Texas Jr. Academy of Science, judge
    2003 - Regional Science Fair, judge
    2003 - National Science Olympiad, practical data gathering event coordinator
    2000, 2002, 2003, 2004 - Graduate Visitation Weekend (GVW), mentor

Honors
    A. E. Martell Travel Award, **2003** - $250 for national ACS conference in NY
    Susan M. Arseven Make-A-Difference Memorial Award, **2003** - $1,000 award
    Dean's Graduate Scholar Award, **2000** - outstanding qualification for graduate study